Experimental Investigations of Slider-Lubricant Interactions in Hard Disk Drives

by

Sean N. Moseley

B.S. (Georgia Institute of Technology) 2004
M.S. (University of California, Berkeley) 2008

A dissertation submitted in partial satisfaction

of the requirements for the degree of

Doctor of Philosophy

in

Mechanical Engineering

in the

Graduate Division

of the

University of California, Berkeley

Committee in charge:

Professor David B. Bogy, chair
Professor Kyriakos Komvopoulos
Professor Thomas Devine

Spring 2009

The dissertation of Sean N. Moseley is approved:

Chair _____ Date _____

_____ Date _____

_____ Date _____

University of California, Berkeley

Experimental Investigations of Slider-Lubricant Interactions in Hard Disk Drives

by Sean N. Moseley

Abstract

Experimental Investigations of Slider-Lubricant Interactions in Hard Disk Drives

by

Sean N. Moseley

Doctor of Philosophy in Mechanical Engineering

University of California, Berkeley

Professor David B. Bogy, chair

To achieve the ever smaller slider-disk spacing that is required for the continual increase in data storage density of hard disk drives, it is necessary to understand the interaction between the slider and the lubricant layer. As the lubricant layer has been used in the hard drive industry for many years, the general properties of the lubricant have been well-studied. However, a focus in the literature has been on theoretical and simulation-based studies. This dissertation focuses on experimental studies of the behavior of the lubricant occurring in the slider-disk interface *while the slider is flying*. General experimental observations seen across many experimental studies are given. Experimental investigations on the influence of various experimental parameters on the lubricant modulation are detailed. The recovery of the lubricant after the experiment has stopped is explored. A unique experimental observation of droplets of lubricant suddenly appearing in the slider-disk interface is detailed. Finally, studies on how the latest hard-drive technology, thermal fly-height control (TFC), changes the slider-lubricant interactions as compared to traditional slider designs are given.

To my wife.

Table of Contents

1 INTRODUCTION 1

1.1 HISTORICAL BACKGROUND 1
1.2 PARTS AND OPERATION OF A HARD DRIVE 2
1.3 BEHAVIOR OF THE LUBRICANT LAYER 5
1.4 DISSERTATION OUTLINE 6

2 EXPERIMENTAL SETUP AND DATA ANALYSIS 8

2.1 INTRODUCTION 8
2.2 APPARATUS SETUP 8
2.3 CANDELA OSA 10
2.4 POLYTEC LDV 11
2.5 LOADING STAGE AND ACOUSTIC EMISSION SENSOR 12
2.6 OTHER EQUIPMENT 14
2.7 GENERAL EXPERIMENT WORKFLOW 14
2.8 MATLAB PROCESSING WORKFLOW 16
2.9 DATA ANALYSIS TECHNIQUES 18
2.9.1 Lubricant Modulation Profile 18
2.9.2 Lubricant Modulation Area 21
2.9.3 Lubricant Modulation Frequencies 22
2.9.4 Incremental Change in Lubricant 23
2.10 CONCLUSION 24

3 GENERAL EXPERIMENTAL OBSERVATIONS 25

3.1 INTRODUCTION 25
3.2 CHANGE IN LUBRICANT MODULATION PROFILE WITH TIME 25
3.3 LUBRICANT RECOVERY WITH TIME 29
3.4 EFFECT OF SLIDER UNLOADING 33
3.5 EVOLUTION OF LOCAL MODULATION PEAKS AND TROUGHS 34
3.6 LOCAL REPEATABILITY OF LUBRICANT PEAKS AND TROUGHS 36
3.7 CONCLUSION 42

4 LUBRICANT PARAMETRIC STUDIES ON MODULATION AREA 44

4.1 INTRODUCTION 44
4.2 SLIDER FORM-FACTOR 44
4.3 LUBRICANT THICKNESS 46
4.4 MOLECULAR WEIGHT 47
4.5 LUBRICANT ADDITIVES 48
4.6 MODULATION FREQUENCIES 50
4.7 CONCLUSION 54

5 LUBRICANT RELAXATION AND RECOVERY 55

5.1 INTRODUCTION 55
5.2 EXPERIMENTAL TRENDS IN RELAXATION RATE 56
5.2.1 Calculation of relaxation rate 56
5.2.2 Predictive ability of relaxation rate 61
5.2.3 Effect of lubricant properties on relaxation rate 62

5.2.4 Frequency effect on relaxation rate *68*
5.3 EXPERIMENTAL ESTIMATION OF LUBRICANT DIFFUSION CONSTANT 77
5.3.1 Finite-Difference Simulations of Point-by-Point Lubricant Relaxation *78*
5.3.2 Numerical Implementation *79*
5.3.3 Simulation Results *83*
5.4 CONCLUSION 88

6 LUBRICANT DROPLETS 91

6.1 INTRODUCTION 91
6.2 EXPERIMENTAL SETUP 92
6.3 EXPERIMENTAL RESULTS 94
6.3.1 AE/LDV sensor *94*
6.3.2 OSA scans *99*
6.3.3 Lubricant dragging *105*
6.4 REPEATABILITY OF DROPLETS 107
6.5 RADIAL REPEATABILITY OF LOCATION 108
6.6 CIRCUMFERENTIAL REPEATABILITY OF LOCATION 112
6.7 EXPLANATION 113
6.8 ANALYTICAL PREDICTION 114
6.9 SIMULATION RESULTS OF SLIDER-DROPLET INTERACTION 117
6.10 CONCLUSION 123

7 EFFECT OF THERMAL FLY-HEIGHT CONTROL ON LUBRICANT 125

7.1 INTRODUCTION 125
7.2 REPEATABILITY OF TOUCHDOWN 126
7.3 EFFECT OF TFC ON LUBRICANT 130
7.3.1 Lubricant buildup/depletion *130*
7.3.2 Lubricant modulation profile *132*
7.3.3 Lubricant modulation frequencies *134*
7.4 BACK-OFF STUDIES 135
7.4.1 Minimum back-off for negligible change to mean lubricant thickness *137*
7.4.2 Minimum back-off for negligible change to lubricant modulation *139*
7.4.3 Minimum back-off for negligible change to modulation frequency *141*
7.4.4 Relationship of lubricant changes to slider features *144*
7.4.5 Lubricant recovery after back-off tests and conclusion *146*
7.5 CONCLUSION 148

8 CONCLUSION AND FUTURE WORK 151

8.1 SUMMARY 151
8.2 FUTURE WORK 157

REFERENCES 159

APPENDIX A 168

APPENDIX B 171

List of Figures

FIGURE 1-1. HISTORICAL INCREASE IN AREAL DATA DENSITY WITH TIME. FROM HTTP://WWW.HITACHIGST.COM/MEDIA/TIMELINE/ZOOM/ERA3_7.HTML RETRIEVED 3-05-2009. 2
FIGURE 1-2. PARTS OF A MODERN HARD DRIVE (FROM STORAGEREVIEW.COM) 3
FIGURE 1-3. SCHEMATIC OF THE SLIDER-DISK INTERACTION AREA. DISK LAYERS AND SLIDER BODY ARE NOT TO SCALE. 4
FIGURE 2-1. EXPERIMENTAL SETUP WITH (A) CANDELA OSA, (B) POLYTEC LDV, (C) AIR SPINDLE WITH DISK, (D) MICROMETER LOADING STAGE WITH AE SENSOR. 10
FIGURE 2-2. DETAILS OF THE LOADING STAGE WITH POSITIONING CONTROLS (RADIAL AND VERTICAL), SUSPENSION HOLDER, AND AE SENSOR INDICATED. THE SUSPENSION BASEPLATE ATTACHES TO THE BOTTOM OF THE HOLDER WITH A SCREW WHERE INDICATED, WITH THE SLIDER FACING DOWN TOWARDS THE DISK. 13
FIGURE 2-3. OSA SUBTRACTION METHOD ILLUSTRATION. TOP: DISK SURFACE BEFORE SLIDER FLYING. MIDDLE: DISK SURFACE AFTER 45 MINUTES OF SLIDER FLYING. BOTTOM: CHANGE IN DISK SURFACE (DURING – BEFORE = NET CHANGE). ALL THREE IMAGES ARE OF SIZE 360 DEGREES BY 1 MM (X-AXIS BY Y-AXIS). 17
FIGURE 2-4. MAGNITUDE RESPONSE OF 10KHZ HIGH-PASS FILTER. NYQUIST FREQUENCY FOR THIS TEST WAS 681.8 KHZ, SO THE FILTER REACHES 0 DB AT (0.016*681.8 = 10.9 KHZ). 18
FIGURE 2-5. LUBRICANT PROFILE ABOVE 10KHZ AT TWO LOCATIONS IN THE SCAN AREA: INSIDE SLIDER'S PATH AND OUTSIDE SLIDER'S PATH. X- AND Y-SCALES ARE IDENTICAL BETWEEN PLOTS. 19
FIGURE 2-6. MODULATION PROFILE AFTER 45 MINUTES OF ON-TRACK FLIGHT. ARROWS INDICATE LOCATION OF DATA POINTS CORRESPONDING TO THE TWO LUBRICANT PROFILES SHOWN IN FIGURE 2-5. 20
FIGURE 2-7. LUBRICANT MODULATION FREQUENCIES FOR THE DATA SHOWN IN FIGURE 2-6. 22
FIGURE 2-8. ILLUSTRATION OF THE DIFFERENCE BETWEEN A "NET CHANGE" SUBTRACTION AND AN "INCREMENTAL CHANGE" SUBTRACTION. 24
FIGURE 3-1. OSA IMAGES DURING A 45 MINUTE FLYING TEST, SHOWING THE EVOLUTION OF THE LUBRICANT DISTURBANCE WITH TIME. 26
FIGURE 3-2. LUBRICANT MODULATION PROFILE (BASED ON STANDARD DEVIATION) SHOWING INCREASING MODULATION WITH CONTINUED FLYING TIME. 27
FIGURE 3-3. AVERAGE LUBRICANT THICKNESS SHOWING INCREASED DEPLETION WITH FLYING TIME. 27
FIGURE 3-4. MODULATION AREA VERSUS TIME CURVE SHOWING LOGARITHMIC SHAPE. 28
FIGURE 3-5. OSA SCANS OF A MODULATED LUBRICANT TRACK RECOVERING WITH INCREASED RELAXATION TIME. 29
FIGURE 3-6. LUBRICANT MODULATION PROFILES TAKEN FROM FIGURE 3-5. 30
FIGURE 3-7. ADJUSTED LUBRICANT MODULATION AREA VERSUS TIME FOR SEVEN INDIVIDUAL TRIALS. 31
FIGURE 3-8. AVERAGE LUBRICANT RELAXATION TREND AND BEST-FIT LOGARITHMIC CURVE FOR DATA IN FIGURE 3-7. 32

FIGURE 3-9. 3D LUBRICANT HEIGHT AFTER 45 MINUTES OF ON-TRACK FLIGHT (JUST BEFORE UNLOADING). 33
FIGURE 3-10. 3D LUBRICANT HEIGHT AFTER 45 MINUTES OF ON-TRACK FLIGHT (JUST AFTER UNLOADING). 34
FIGURE 3-11. ILLUSTRATION OF LOCALIZED LUBRICANT HEIGHT EVOLUTION WITH TIME. AXES IN ALL FOUR QUADRANTS ARE IDENTICAL. 35
FIGURE 3-12. ILLUSTRATION OF LOGARITHMIC TREND IN LOCAL LUBRICANT PEAK HEIGHTS VERSUS TIME. 36
FIGURE 3-13. MODULATION PROFILES FOR THREE REPEATED TESTS ON THE SAME DISK TRACK. 38
FIGURE 3-14. BAR GRAPH OF MODULATION AREAS FOR THREE REPEATED TESTS ON THE SAME DISK TRACK. 39
FIGURE 3-15. OSA SCREENSHOT (1 MM X ~100 DEG) FOR THREE REPEATED TESTS ON THE SAME DISK TRACK. 40
FIGURE 3-16. VISUALIZATION OF LUBRICANT THICKNESS OVER 1MM X 4.5 DEG SECTION FOR A) TEST 1, B) TEST 4, AND C) TEST 7. DASHED BOXES MARK REGIONS OF HIGH AND LOW CORRESPONDENCE BETWEEN IMAGES. 41
FIGURE 4-1. MODULATION AREA AVERAGE FOR FIVE SLIDER DESIGNS AFTER ADJUSTING FOR THE BASELINE MODULATION. 45
FIGURE 4-2. MODULATION AREA AVERAGE FOR TWO SLIDER FORM FACTORS. 46
FIGURE 4-3. AVERAGE MODULATION AREA VERSUS TIME FOR DIFFERING ZDOL LUBRICANT THICKNESSES. 47
FIGURE 4-4. AVERAGE MODULATION AREA VERSUS TIME FOR DIFFERING ZDOL LUBRICANT MOLECULAR WEIGHTS. 48
FIGURE 4-5. EFFECT OF ADDITIVES ON LUBRICANT MODULATION. 49
FIGURE 4-6. LUBRICANT MODULATION PROFILE AND AVERAGE LUBRICANT THICKNESS VERSUS RADIUS. 50
FIGURE 4-7. EXAMPLE PLOT SHOWING THE DISTRIBUTION OF MODULATION FREQUENCIES ACROSS THE SLIDER WIDTH DIRECTION AFTER 45 MINUTES OF FLIGHT. 51
FIGURE 4-8. SIDE VIEW OF MODULATION FREQUENCY PLOTS AT (A) 15 MIN, (B) 30 MIN, AND (C) 45MIN SHOWING TIME EVOLUTION OF MODULATION POWER OCCURRING BELOW 100 KHZ WITH A STRONG PEAK AROUND 25 KHZ. 52
FIGURE 4-9. LUBRICANT MODULATION FREQUENCY RESULTS FOR 10K G/MOL 10.7 ANGSTROM DISK (SLD17-2 AT 45 MIN) SHOWING STRONG FREQUENCY PEAKS AT APPROXIMATELY 50 AND 265 KHZ. 53
FIGURE 5-1. OSA SCANS OF A MODULATED LUBRICANT TRACK RECOVERING WITH INCREASED RELAXATION TIME. 57
FIGURE 5-2. LUBRICANT MODULATION PROFILES TAKEN FROM FIGURE 5-1. LARGEST PROFILE IS ASSOCIATED WITH THE DATA TAKEN IMMEDIATELY AFTER SLIDER UNLOAD, WITH THE PROFILE REDUCING IN MAGNITUDE WITH INCREASING RELAXATION TIME. 57
FIGURE 5-3. RELAXATION OF LUBRICANT MODULATION AREA, BEFORE ZEROING AND SCALING. 58
FIGURE 5-4. ADJUSTED LUBRICANT MODULATION AREA VERSUS TIME FOR SEVEN INDIVIDUAL TRIALS. 59

FIGURE 5-5. AVERAGE LUBRICANT RELAXATION TREND AND BEST-FIT LOGARITHMIC CURVE FOR DATA IN FIGURE 5-4. 60
FIGURE 5-6. BEST-FIT PREDICTION (SOLID BLUE) AND EXPERIMENTAL DATA (RED ASTERISKS) OF LUBRICANT MODULATION AREA RELAXATION VS. TIME FOR ZDOL + X1P. 62
FIGURE 5-7. EXPERIMENTAL MODULATION AREA VS. TIME FOR 15 ANGSTROMS ZTETRAOL, WITH BEST-FIT LOGARITHMIC LINE. 64
FIGURE 5-8. BEST-FIT LOGARITHMIC PREDICTIONS FOR ZDOL + X1P (20 ANG) AND ZTETRAOL (15 ANG) WITH EQUATIONS. 64
FIGURE 5-9. RELAXATION OF LUBRICANT MODULATION AREA, BY LUBRICANT MOLECULAR WEIGHT. 65
FIGURE 5-10. FITTING EQUATION 5.4 TO AVERAGE RELAXATION TRENDS FOR 10K AND 2K G/MOL ZDOL. 67
FIGURE 5-11. VARIATION IN PRE-LOGARITHMIC FIT PARAMETER WITH LUBRICANT MOLECULAR WEIGHT. 68
FIGURE 5-12. EXAMPLE OF LUBRICANT MODULATION ASSOCIATED WITH 10 KHZ FREQUENCY RANGES FROM 10 TO 100 KHZ FOR A RANDOMLY CHOSEN SECTION OF ONE EXPERIMENT. X-AXIS (ANGLE) IS APPROXIMATELY 22 DEGREES LONG, Y-AXIS (RADIUS) IS 1 MM WIDE, AND Z-AXIS (LUBE HEIGHT) IS FROM -1.2 TO +1.2 NM. 69
FIGURE 5-13. LUBRICANT MODULATION PROFILE AT SLIDER UNLOADING, BY FREQUENCY BAND. LOWER FREQUENCIES ARE ASSOCIATED WITH HIGHER LUBRICANT MODULATION. 70
FIGURE 5-14. LUBRICANT MODULATION PROFILE AFTER 10 MINUTES OF RELAXATION, BY FREQUENCY BAND. SAME Y-SCALE AS FIGURE 5-13. 71
FIGURE 5-15. AVERAGE MODULATION AREA VERSUS TIME, SORTED BY FREQUENCY BAND. 72
FIGURE 5-16. EXAMPLE OF THREE BEST-FIT EQUATIONS, AS FITTED TO (A) 10 – 20 KHZ BAND, (B) 30 – 40 KHZ BAND, (C) 60 – 70 KHZ BAND, (D) 90 – 100 KHZ BAND. EXPERIMENTAL DATA (SOLID, ASTERISKS), 2-PARAMETER LN FIT (SOLID), 2-PARAMETER EXP FIT (DASHED), 1-PARAMETER EXP FIT (DOTTED) 73
FIGURE 5-17. R^2 FIT VALUE FOR THREE CURVE FIT EQUATIONS VERSUS FREQUENCY BAND. 74
FIGURE 5-18. VARIATION OF THE EXPONENTIAL PARAMETER "A" VERSUS FREQUENCY BAND (SOLID RED LINE WITH ASTERISKS) AND LINEAR TRENDLINE OF THIS VARIATION (BLACK DOTTED LINE). 76
FIGURE 5-19. LUBRICANT HEIGHT FOR EXPERIMENTAL DATA, (A) BEFORE RADIAL FILTERING AND (B) AFTER RADIAL FILTERING AT ~40 UM. X-AXIS IS THE ANGULAR DATA POINT (0 TO 600), Y-AXIS IS THE RADIAL DATA POINT (0 TO 500), AND Z-AXIS IS LUBRICANT THICKNESS [NM] (-1.5 TO 1.5). 81
FIGURE 5-20. MODULATION PROFILES FOR EXPERIMENTAL DATA, WITHOUT RADIAL FILTERING (SOLID) AND WITH RADIAL FILTERING AT ~40 UM (DASHED). 82
FIGURE 5-21. COMPARISON OF ACTUAL AND SIMULATED RELAXATION OF LUBRICANT MODULATION AT 20 MINUTES: A) ACTUAL LUBRICANT HEIGHT DATA B) SIMULATED LUBRICANT HEIGHT DATA C) ERROR (SIMULATED – ACTUAL) D) MODULATION

profiles for actual (red, solid) and simulated (blue, dashed) lubricant modulation. 84
Figure 5-22. Modulation profile comparison between experiments (solid) and simulation (dashed). 85
Figure 5-23. Comparison of actual modulation area (black, asterisks) and three simulated modulation areas (dashed) for $D = 5.0x10^{-12}$ (red), $5.5x10^{-12}$ (green), and $6.0x10^{-12}$ (blue) m^2/s. 86
Figure 5-24. Comparison of actual modulation area (black, asterisks) and simulated modulation area for five different diffusion constants, D = 2.5 through $5.0x10^{-13}$ m^2/s. 87
Figure 6-1. ABS geometry. 93
Figure 6-2. AE (top) and LDV (bottom) data showing intermittent spikes during a 20-minute flying test at approximately 30m/s linear speed. 95
Figure 6-3. Example AE sensor spike (x-axis length is 2 seconds). 96
Figure 6-4. Example AE and LDV sensor spike (x-axis length is 2 seconds). 97
Figure 6-5. Example AE and LDV sensor spike (x-axis length is 0.5 seconds). Same data as in Figure 6-4. 97
Figure 6-6 Example AE and LDV sensor spike (x-axis length is 0.1 seconds). Same data as in Figure 6-4. 98
Figure 6-7 Example AE and LDV sensor spike (x-axis length is 1 millisecond). Same data as in Figure 6-4. 98
Figure 6-8. OSA screenshot showing lubricant thickness over 500 μm x 54 degree area (darker = thicker) showing an interval with no lubricant droplets or AE/LDV spikes (a) 9 minute – base (b) 8 minute – base (c) 9 minute – 8 minute. 101
Figure 6-9. OSA screenshot showing lubricant thickness over 500 μm x 54 degree area (darker = thicker) showing a lubricant droplet (a) 15 minute – base (b) 16 minute – base (c) 16 minute – 15 minute. 102
Figure 6-10. Lubricant height from 16 minute – 15 minute data showing 1 mm x 25 degree area around lubricant droplet (oblique view). 103
Figure 6-11. Lubricant height from 16 minute – 15 minute data showing 1 mm x 25 degree area around lubricant droplet (angular view). 103
Figure 6-12. Microscope pictures of lubricant pickup at TEC (a) after a 20 minute on-track flying test with lubricant pickup area outlined (b) after cleaning with HFE ultrasonic bath. The width of the TEC rail is approximately 0.15 mm. 104
Figure 6-13. LDV sensor data from lubricant dragging result, zoomed view of 4 to 14 minutes with broadened region bracketed. Inset shows the entire 20 minute test data with the 4 to 14 minute region outlined. 105
Figure 6-14. OSA screenshot of changes in lubricant thickness between scans over 350 μm x 27 degree area (darker = thicker) showing down-track motion of a large lubricant droplet (down-track is to the right of each frame). 106

FIGURE 6-15. ANGULAR VIEW OF LUBRICANT DROPLET HEIGHT DATA AS IT MOVES DOWN-TRACK WITH SUCCESSIVE OSA SCANS (6 MIN TO 13 MIN) WITH CMLAIR SIMULATION MINIMUM FH MARKED. 107
FIGURE 6-16. LUBRICANT NET CHANGE AT 20 MINUTES OF ON-TRACK FLYING (20MIN – BASE). DARK REGIONS REPRESENT THICKER LUBRICANT AND LIGHT REGIONS REPRESENT THINNER LUBRICANT. THE ENTIRE IMAGE IS 360 DEGREES IN THE X-AXIS AND 1 MM IN THE Y-AXIS. 110
FIGURE 6-17. LUBRICANT NET CHANGE AT 20 MINUTES OF ON-TRACK FLYING (20MIN – BASE). DARK REGIONS REPRESENT THICKER LUBRICANT AND LIGHT REGIONS REPRESENT THINNER LUBRICANT. THE ENTIRE IMAGE IS 37 DEGREES IN THE X-AXIS AND 1 MM IN THE Y-AXIS. THE SUPERIMPOSED ABS PICTURE IS SCALED CORRECTLY IN THE RADIAL DIRECTION (Y-AXIS), BUT THE CIRCUMFERENTIAL LENGTH (X-AXIS) IS EXAGGERATED BY A FACTOR OF 21. 111
FIGURE 6-18. LUBRICANT INCREMENTAL CHANGE IMAGE (20 MIN – 19 MIN) OF THE SAME OSA DATA AS FIGURE 6-17. THE DARK REGION ON THE RIGHT OF THE IMAGE IS A LUBRICANT DROPLET. 112
FIGURE 6-19. LOCATION REPEATABILITY OF LUBRICANT DROPLETS. THE COLORED BOXES (RED, BLUE, AND GREEN) REPRESENT SEPARATE SUCCESSIVE TESTS ON THE SAME TRACK. NOTE THAT THE Y-AXIS IS 0.4 MM WIDE. 113
FIGURE 6-20. POINT-BY-POINT DISK TRACK PROFILE USED IN THE CMLAIR DYNAMIC SIMULATOR TO MODEL THE EFFECT OF A LARGE LUBRICANT DROPLET ON THE FLYABILITY OF THE SLIDER. 118
FIGURE 6-21. DYNAMIC SIMULATION RESULT (MINIMUM FH VS. TIME) FROM SLIDER ENCOUNTERING THE LUBRICANT DROPLET. 119
FIGURE 6-22. DISTURBANCE PROFILE (PEAK-TO-PEAK DISTURBANCE [NM] VS. OFFSET FROM CENTER [MM]) OF SLIDER'S RESPONSE TO THE 7 MINUTE LUBRICANT DROPLET. NOTE THE LOG SCALE ON THE Y-AXIS. 120
FIGURE 6-23. DISTURBANCE PROFILES FOR DROPLET HEIGHT DATA TAKEN FROM 7 THROUGH 12 MINUTES. NOTE THE LOG SCALE ON THE Y-AXIS. 121
FIGURE 6-24. COMPARISON BETWEEN DROPLET RADIAL LOCATION, SIZE OF MINIMUM FH DISTURBANCE, AND SLIDER RAIL GEOMETRY. 122
FIGURE 7-1. EXAMPLES OF INDICATION OF SLIDER TOUCH-DOWN. A) SUDDEN AE SPIKE CORRESPONDING TO A PARTICULAR LOCATION ON THE DISK. B) SUDDEN CHANGE IN PEAK-TO-PEAK AE SIGNAL. IN BOTH PLOTS, THE TOP TRACE IS THE ONCE-AROUND TRIGGER SIGNAL, SHOWING THE DISK ROTATION RATE. 128
FIGURE 7-2. VARIATION OF EXPERIMENTAL TDP VERSUS TEST NUMBER. 129
FIGURE 7-3. EXAMPLE OF LUBRICANT BUILDUP/DEPLETION PROFILES FOR UN-ACTUATED (1-5 MIN) AND FULLY-ACTUATED (6-10 MIN) TFC SLIDER FLIGHT. 131
FIGURE 7-4. LUBRICANT MODULATION PROFILES FOR UN-ACTUATED (1-5 MIN) AND FULLY-ACTUATED (6-10 MIN) TFC SLIDER FLIGHT. 133
FIGURE 7-5. LUBRICANT MODULATION FREQUENCIES FOR A) UN-ACTUATED (5 MIN) TFC SLIDER FLIGHT AND B) ACTUATED (6 MIN) TFC SLIDER FLIGHT. 134
FIGURE 7-6. MEAN LUBRICANT THICKNESS VS. RADIUS BEFORE HEATER ACTUATION (RED) AND AFTER BACK-OFF (BLUE) FOR A) 50 MW BACK-OFF, B) 30 MW BACK-

OFF, C) 20 MW BACK-OFF, D) 10 MW BACK-OFF, E) 0 MW BACK-OFF, AND F) 0 MW BACK-OFF. 138
FIGURE 7-7. LUBRICANT MODULATION PROFILE VS. RADIUS BEFORE HEATER ACTUATION (RED) AND AFTER BACK-OFF (BLUE) FOR A) 50 MW BACK-OFF, B) 30 MW BACK-OFF, C) 20 MW BACK-OFF, D) 10 MW BACK-OFF, E) 0 MW BACK-OFF, AND F) 0 MW BACK-OFF. 140
FIGURE 7-8. LUBRICANT MODULATION FREQUENCIES BEFORE HEATER ACTUATION (RED) AND AFTER BACK-OFF (BLUE) FOR A) 10 MW BACK-OFF AND B) 0 MW BACK-OFF. 142
FIGURE 7-9. VARIATION OF LUBRICANT MODULATION FREQUENCY ACROSS SLIDER WIDTH A) BEFORE HEATER ACTUATION AND B) AFTER 0 MW BACK-OFF. X-AXIS IS THE RADIAL INCREMENT IN 2 MM STEPS, Y-AXIS IS THE MODULATION FREQUENCY [KHZ], AND Z-AXIS IS THE ARBITRARY MODULATION POWER, WITH BOTH SUBPLOTS USING THE SAME SCALING. 143
FIGURE 7-10. RELATIONSHIP OF LUBRICANT FEATURES TO ABS GEOMETRY AT 0 MW BACK-OFF. 146
FIGURE 7-11. LUBRICANT THICKNESS A) AFTER 3 MINUTES OF 0 MW BACK-OFF FLIGHT AND B) AFTER ~20 HOURS OF RECOVERY TIME. 147

1 Introduction

1.1 Historical Background

IBM introduced the first hard disk drive in 1956 [1]. It was part of an accounting system called RAMAC for Random Access Method of Accounting and Control. The system weighed 2,140 pounds and had a total storage capacity of 5 MB (1 MB = $1x10^6$ bytes) at a yearly leasing cost of $35,000. The initial application of the system was for businesses needing to record transactions in real-time. Over the years, the hard drive changed from a niche business product to something versatile enough to be used in computing systems from portable music players to massively parallel supercomputers conducting university research.

The history of hard drives is interesting in that the basic idea of storing data as magnetic "bits" on a rotating disk has not changed. However, the storage capacity, access speed, and durability have increased many orders of magnitude while the physical size and cost have decreased similarly. The RAMAC system mentioned was leased at a cost of $7 million/GB in 1956. Modern consumer hard drives are now available at a cost of around $100 for 1 TB (1 TB = $1x10^{12}$ bytes), yielding a cost of 10 cents/GB. This dramatic evolution of the hard drive is seen in Figure 1-1, showing the increase in storage capacity (in units of GB/in^2) versus year.

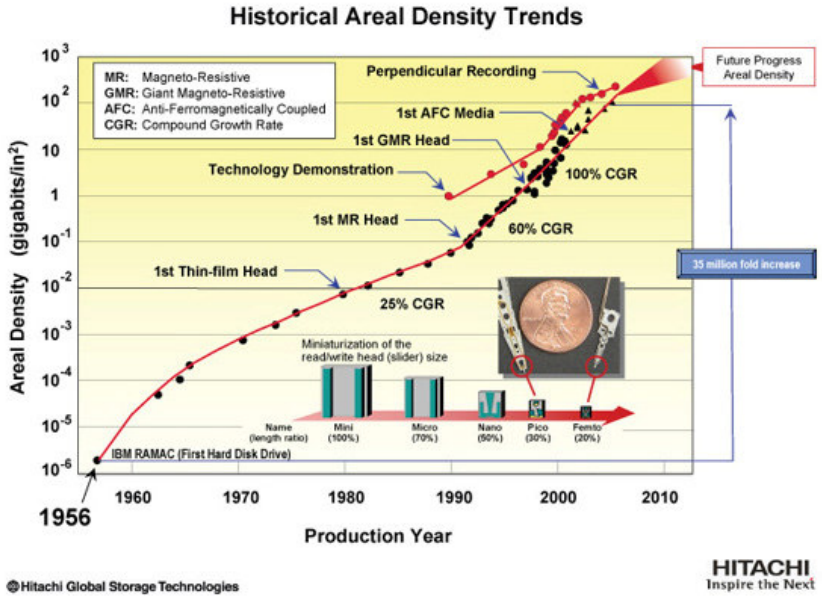

Figure 1-1. Historical increase in areal data density with time. From http://www.hitachigst.com/media/timeline/zoom/era3_7.html retrieved 3-05-2009.

1.2 Parts and Operation of a Hard Drive

A hard drive consists of many interacting mechanical devices and parts. They all work together to store information as magnetic "bits" on a rotating disk. A device called a "slider" contains the sensors that read and write the bits of data. The slider flies over the rotating disk supported by a cushion of air between the slider and the disk. Features on the slider called "rails" form the "air-bearing surface" or ABS that determines the air pressure underneath the slider. The specifics of this pressure distribution determine the separation between the read/write sensors and the magnetic information on the disk, which directly influences the capacity of the hard drive. One of the primary enablers for increasing storage capacity over the years has been the reduction of the separation between the sensors and the disk. Figure 1-2 shows what a

modern hard drive looks like with the cover removed, showing most of the mechanical parts discussed here.

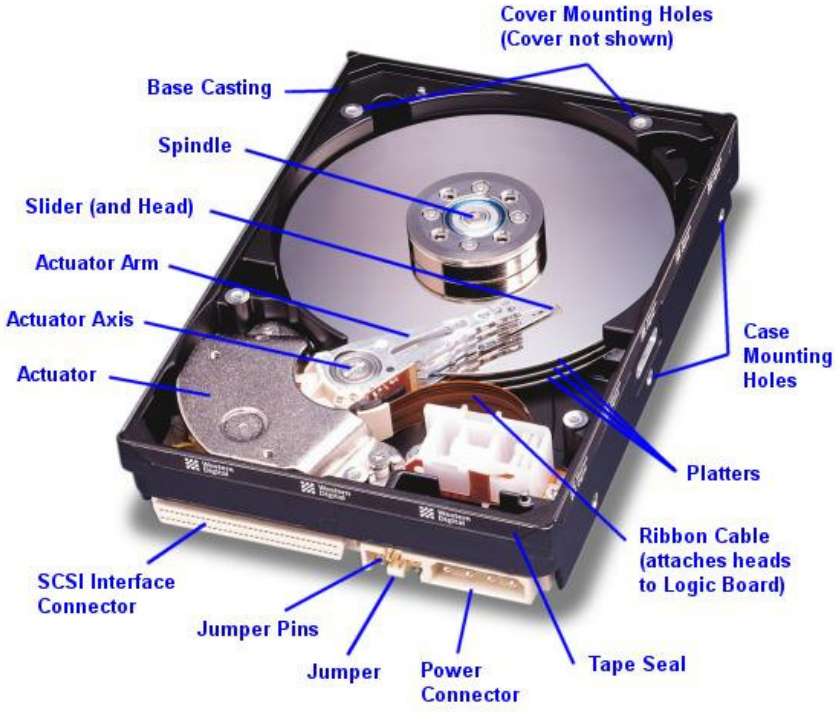

Figure 1-2. Parts of a modern hard drive (from storagereview.com)

The disk that contains the magnetic data is the large circular part at the top of the drive. The slider is located at the end of a supportive structure called the actuator or suspension. The suspension serves to locate the slider radially on the disk as well as to support the wires that carry the read/write information from the disk to the operating system of the computer. During operation, the slider appears to be touching the disk, but it is actually separated by a small gap called the "fly-height" or FH. Figure 1-3 shows a schematic of the slider and a small section of the disk.

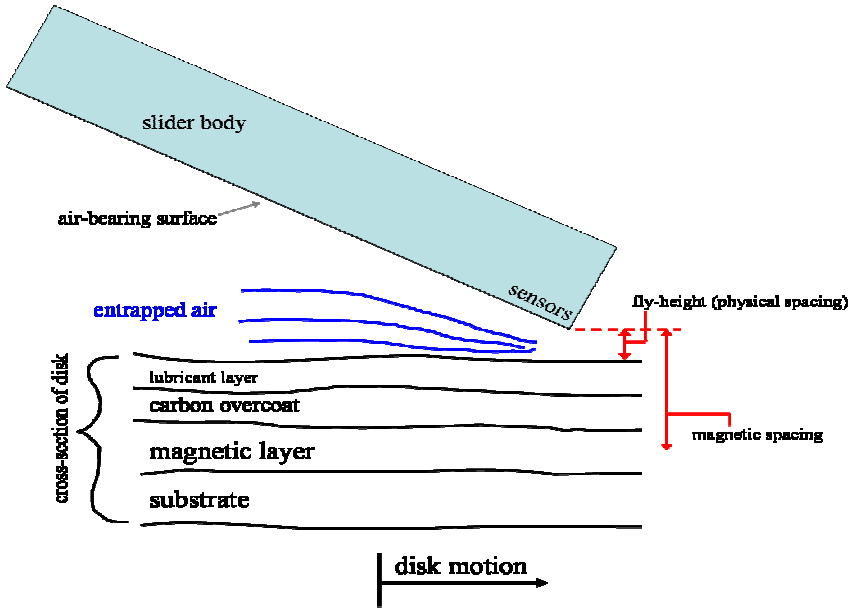

Figure 1-3. Schematic of the slider-disk interaction area. Disk layers and slider body are not to scale.

The main layers of a hard drive disk are the lubricant layer, carbon overcoat, magnetic layer, and the substrate. The substrate provides the structure of the disk, making it stiff and giving it shape. The magnetic layer consists of small magnetic domains that store the data. The carbon overcoat serves to protect the soft magnetic layer from corrosion and physical damage. The lubricant layer lowers friction between the slider and disk in the event of physical contact and provides additional protection for the magnetic layer against corrosion in the case of defects in the carbon layer [2].

As the disk rotates at high speed (usually between 5,200 to 10,000 rpm), a layer of air is "pulled along" with the disk. The presence of the slider body forces the air to be compressed between the slider and the disk. With this compression comes

higher air pressure. The higher air pressure creates an upward force on the slider, which must be counteracted by the downward suspension load at the design fly-height. The design of the ABS determines how the air is compressed in the interface, and thus the fly-height. As the read/write sensors are located in the slider body, the magnetic spacing is determined by the fly-height and the other parameters of the slider's orientation (pitch and roll). The magnetic spacing is what determines the ability of the read/write sensors to read and write data. Any significant disturbance of the magnetic spacing will degrade the performance of the system.

1.3 Behavior of the Lubricant Layer

The lubricant layer of the hard drive serves the mechanical purpose of reducing friction and wear in the case of unintended slider-disk contact [3-6]. It also protects the magnetic layer from corrosion in case there are defects in the carbon layer [2]. The lubricant itself is often a PFPE long-chain polymer [5] with thickness between 0.5 and 2 nm and molecular weight between 1,000-10,000 g/mol. Commonly used lubricants in the hard drive industry include Zdol and Ztetraol [6, 7]. These lubricants share the same main chain, but differ in the endgroups. Zdol has two endgoups while Ztetraol has four endgroups per chain [7, 8]. The endgroups help the lubricant adhere to the carbon layer and resist being displaced by the high air pressure and air shear in the slider-disk interface [9]. The lubricants used in this dissertation are Zdol and Ztetraol.

1.4 Dissertation Outline

As the lubricant layer has been used in the hard drive industry for many years, the general properties of the lubricant have been well-studied. However, a focus in the literature has been on theoretical and simulation-based studies. The experimental studies that are available tend to measure the lubricant distribution on the disk only after a slider has been unloaded and the test is finished [10, 11]. The delay between the slider flight and measurement of the lubricant layer, as well as the ex-situ nature of the measurement, limits the phenomena that can be studied. Khurshudov et al. have made in-situ optical surface analyzer (OSA) measurements of the effect of a flying slider on lubricant behavior, but their focus was on tens of hours of flying and track average measurements [12]. This dissertation focuses on the behavior of the lubricant occurring in the slider-disk interface in the time scale of a few to tens of minutes *while the slider is flying*. This is achieved by conducting flyability tests where the test spindle and measurement spindle are the same. Chapter 2 introduces the experimental equipment required for this type of measurement as well as some of the data analysis methods used throughout the studies. The data analysis methods are sometimes slightly altered to accommodate a specific analytical need, with the specific details given in the corresponding section. Chapter 3 focuses on general experimental observations seen across many experimental studies, regardless of the specific experimental parameters studied. Despite the strong influence of slider design, lubricant type, and other experimental parameters on the quantitative outcome of the experiment, many general qualitative observations hold for almost all tests.

Acknowledging this "common ground" gives a backdrop upon which future differences are made more obvious.

Chapter 4 presents experimental results on the influence of various experimental parameters on the modulation area of the lubricant layer. This chapter focuses on the influence of slider design, slider form factor, lubricant thickness, lubricant molecular weight, and lubricant additives on the slider-induced lubricant modulation. Chapter 5 explores the recovery of the lubricant after the experiment has stopped, giving experimental results as well as simulation models. Lubricant recovery after slider flight is a much simpler system than lubricant disturbance under a flying slider. Therefore, understanding the lubricant relaxation behavior is an important step in understanding the lubricant behavior as a whole. Chapter 6 presents an unique experimental observation of droplets of lubricant suddenly appearing in the slider-disk interface. This phenomenon occurs during "normal" slider flight and does not appear to have any external triggers. All three data measurement techniques (acoustic emission, laser Doppler velocimeter, and lubricant thickness) are used to explore and explain the phenomenon. Chapter 7 introduces studies on how the latest hard-drive technology, thermal fly-height control (TFC), changes the slider-lubricant interactions as compared to traditional slider designs. In this technology, a locally heated zone undergoes thermal expansion and moves towards the disk with the remainder of the slider body relatively unchanged. This is in contrast to traditional un-actuated slider designs where the slider moves essentially as a rigid body. Finally, Chapter 8 draws some conclusions and makes suggestions for future work.

2 Experimental Setup and Data Analysis

2.1 Introduction

The types of analyses and conclusions possible in any experimental investigation are strongly influenced by the experimental equipment available. Understanding the experimental apparatus and experimental techniques is important in understanding the experimental results. In this dissertation, a specific experimental apparatus is used in many different ways to investigate the slider-lubricant interactions that occur in a computer hard drive. The components of this experimental apparatus are explained in relation to their intended measurement purpose. Also, some of the basic analytical methods and tools are detailed here as they are used throughout the rest of the dissertation.

2.2 Apparatus Setup

All experiments discussed in this work were performed on a multi-instrument test stand (Figure 2-1) consisting of a Candela Optical Surface Analyzer (OSA) system (a), a Polytec Laser Doppler Velocimeter (LDV) (b), a speed-controlled air-bearing spindle (c), and a manual micrometer-based vertical loading stage with acoustic emission (AE) sensor attached (d). This multi-instrument test stand is an integral part of the data collection process. By conducting the flying tests on the same spindle as the OSA measurement system, in-situ lubricant measurements are possible. This setup enables specific data analysis methods to be used that are not possible if the OSA measurement takes place on a spindle that is different from the one on which the

flying tests are conducted. Data collection was performed on a PC equipped with TTi Ultrafast ADC software version 5NT b1 interfaced with a TTi data acquisition card with sampling rates from 10 kHz to 100 MHz. The TTi card can sample up to four input signals and the associated software contains simple analysis and plotting abilities. Most signal captures with time as the x-axis are taken directly from the TTi software. A Lecroy digital oscilloscope, usually sampling at $1x10^6$ samples/sec, was used to monitor the sensor signals in real time but did not perform any data acquisition. The experimental apparatus was supported by a vibration isolation table located under a laminar flow clean-air bench. As the slider-disk interface involves nanometer-scale clearance, dust and other airborne contamination falling on a spinning disk could easily become entrapped in the interface, causing a slider-disk crash or scratch. The laminar flow clean-air bench was used to minimize the chance of such contamination.

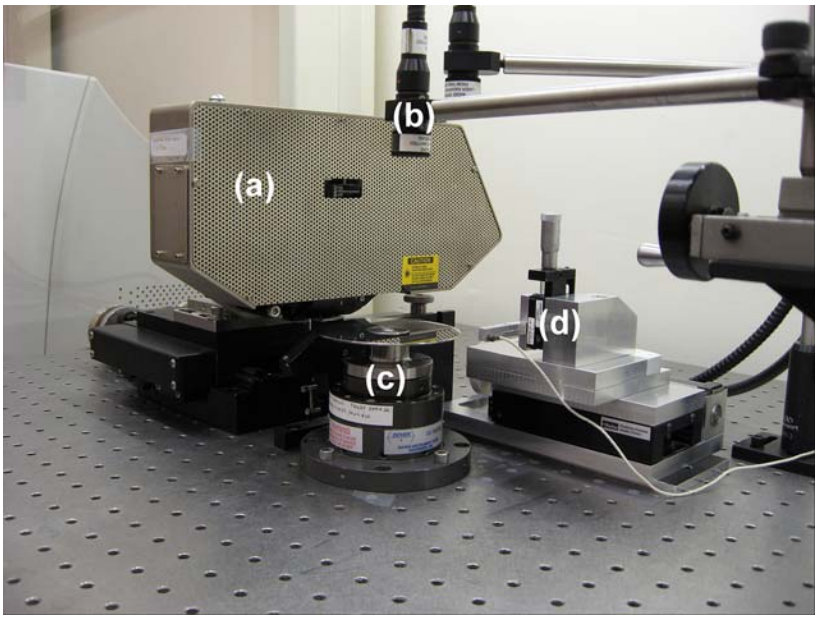

Figure 2-1. Experimental setup with (a) Candela OSA, (b) Polytec LDV, (c) air spindle with disk, (d) micrometer loading stage with AE sensor.

2.3 Candela OSA

The Candela OSA has hardware number 5100 and software version 3.5.7. In the experiments presented here, the OSA uses the Q phase channel to monitor sub angstrom-level thickness changes in a one to two nanometer thick lubricant layer. The operating principle is based on ellipsometry [1, 2]. A diode laser emits an optical wave that is polarized in a particular combination of P (parallel to the incident plane) and S (perpendicular to the incident plane) polarizations. The incoming wave reflects off the disk surface and is measured by a detector. The specific material properties and film thicknesses of the lubricant and carbon layers determines the changes in the reflected wave. When the OSA is calibrated, the changes in the reflected wave

(compared to the incident wave) can be converted into data about the thickness of the lubricant and carbon layers.

The OSA is used to measure thickness changes in the lubricant layer by comparing a disk scan taken during or after slider flight to a disk scan taken before said slider flight. Since the carbon layer has not changed while the slider is flying (unless *severe* contact occurs), any changes in the measurement correspond to changes in the lubricant thickness (which does change while the slider is flying). In this way, the Candela OSA is used to measure the thickness changes of the thin lubricant layer induced by slider flight during operation of a hard disk drive. Specifics of the data analysis and conversion process are discussed in Section 2.9.

2.4 Polytec LDV

The Polytec LDV consists of hardware version OFV 518 laser RVA sensor connected to an OFV 2802i electronics unit. The LDV is used to qualitatively measure the fly-height variation of a slider during operation, specifically to detect "normal" versus "disturbed" flight patterns. The operating principle is based on detecting changes in the reflected frequency of a laser beam induced by the vibrations of the target surface [3]. When the reflected wave is compared to the incident wave, the frequency shift corresponds to the velocity of the target surface. A perfectly stationary target surface will induce no frequency shift in the reflected wave. A target surface moving away from the laser source will reflect the incoming wave at a lower frequency than it arrives, while a target surface moving towards the laser source will reflect the incoming wave at a higher frequency than it arrives. In the experiments, the

LDV laser spot was focused on either the back of the slider or the suspension flexure, depending on the specifics of the suspension design. Some suspension designs allow clear view of the back side of the slider body when viewed from above. Other suspension designs obscure the back side of the slider body. LDV sensors are sometimes used to monitor the quantitative fly-height modulation (FHM) of the slider by measuring the slider velocity and numerically integrating to find the actual slider motion. In the experiments detailed here, the LDV is used to detect a qualitative change in "normal" slider flying to "disturbed" slider flying, usually indicated by a large change in the RMS value of the LDV signal. This type of change is indicative of strong slider-disk interaction due to loss of flyability or other severe event.

2.5 Loading Stage and Acoustic Emission Sensor

The loading and positioning stage consists of two micrometers, one for vertical loading (0.0001" resolution analog display) and one for radial positioning (0.01mm resolution digital display) of the slider/HGA assembly. Figure 2-2 shows a closer view of the loading stage indicated in Figure 2-1(d) with the disk spindle clearly visible. These positioning micrometers were supported on an aluminum fixture that rotated to allow for skew changes. Unless otherwise specified, the skew for all tests was approximately zero degrees throughout the entire radial range. The skew error is estimated as within 0.5 degrees. The aluminum fixture is a custom design that allows adjustment of the slider flying radius and z-height while the slider is flying. The skew must be set before the slider flight as it is not adjustable in-situ.

An acoustic emission (AE) sensor was mounted on the aluminum arm to which the suspension baseplate was attached using a single screw. The operating principle of the AE sensor is based on piezo-electric crystals. The AE sensor consists of a small piezo-electric crystal that converts physical strain into small electrical signals. In the event of slider-disk contact, the sudden vibration of the slider sends vibrations up the suspension and into the aluminum arm. The vibration is picked up by the AE sensor which converts compressive waves into electrical signals. These electrical signals were amplified by a pre-amp box from Acoustic Emission Technology Corporation and captured by the TTi data acquisition system. AE sensors are routinely used in the hard drive industry to monitor slider flyability [4].

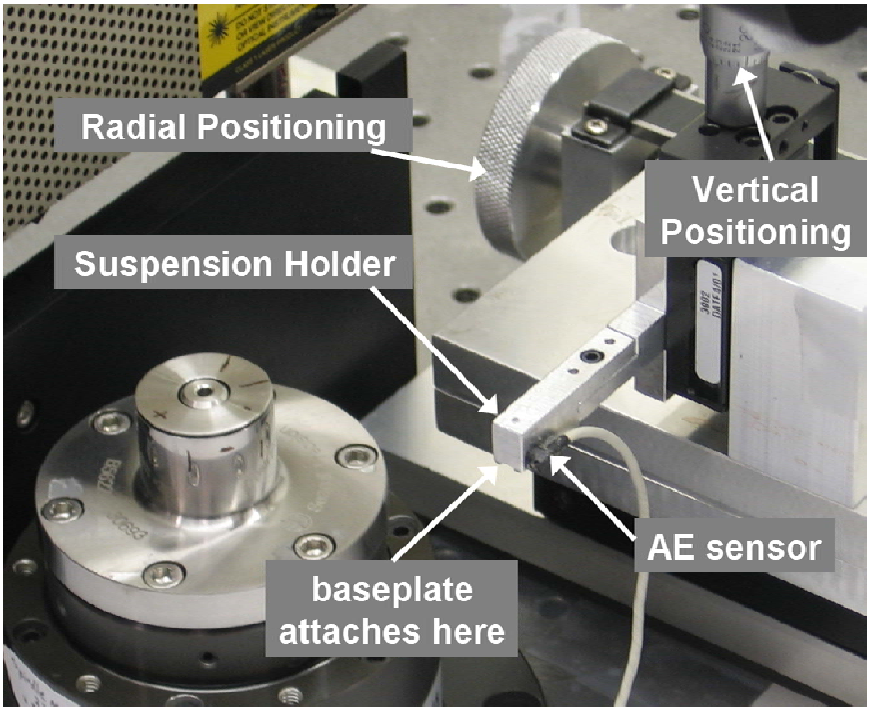

Figure 2-2. Details of the loading stage with positioning controls (radial and vertical), suspension holder, and AE sensor indicated. The suspension baseplate attaches to the bottom of the holder with a screw where indicated, with the slider facing down towards the disk.

2.6 Other Equipment

Other equipment used during these experiments include two Krohn-Hite solid-state filters, model 3202; an Olympus VANOX microscope with 5-100x lenses; an Olympus DP10 digital camera with microscope mount; and 3M Novec HFE-7100 solvent. The Krohn-Hite filters were used to high-pass the LDV signal at 2 kHz before data capture. When a "trigger" signal was required to detect the once-around disk frequency, the second LDV channel was focused on a scratch at the edge of the disk. This signal was then high-pass filtered at 300 kHz using a second Krohn-Hite filter. The Olympus microscope with a digital camera was used to inspect the slider ABS surface before and after tests, specifically to check for lubricant that would have transferred from the disk. Finally, the HFE solvent was used in an ultrasonic bath to remove lubricant from the slider after tests. The HFE solvent is used in the hard drive industry as a lubricant solvent [5]. Uses of the HFE solvent included removing lubricant from disks (in half-delubed experiments) as well as from sliders after contamination.

2.7 General Experiment workflow

While the specifics of each investigation are discussed in the applicable section, the general experiment workflow was the following. The slider-suspension assembly to be tested, sometimes called the head-gimble assembly (HGA), was removed from the storage container and secured to the suspension holder using a single screw through the suspension baseplate. The suspension holder was then secured to the loading and positioning stage. Next, the test disk was removed from the storage

container and placed on the air spindle where it was clamped into place. Immediately after being clamped, the Candela software was used to start the disk spinning in an effort to further minimize the chance of dust contamination.

The radial positioning of the slider was zeroed by using the vertical LDV laser to align the center of the slider with the edge of the disk. Using this technique, the radial position of the slider can be easily related to the disk outer diameter (OD). The vertical positioning (z-height) system was zeroed by slowly lowering the suspension holder towards a stationary disk and using an indicator gauge to detect first interference. When the suspension holder first interferes with the stationary disk, the z-height is exactly zero. In this way, the z-height of the suspension is related to the location of the top surface of the disk. After establishing the zero z-height in this way before the experiment, the slider can be loaded at the designed z-height by using the vertical positioning system.

During a typical on-track test procedure, the OSA was used to measure the lubricant thickness on the disk over a 2 mm range around the test radius at the test rpm (the “base” scan). Second, the slider was loaded manually onto the disk at the load radius and then moved to the test radius (usually 1 mm inwards from the load radius). Once at the test radius, the vertical LDV was focused on the back of the slider or flexure to maximize the reflected signal. The loading, positioning, and focusing procedure usually took between twenty and sixty seconds. Once loaded this way, the slider remained on-track at the test radius for the duration of the test. At predetermined times, OSA scans were taken over the entire disk circumference at a resolution of 2 μm in the radial direction and approximately 0.044 degrees (20 to 30

μm) circumferentially. At the end of the test, the slider was unloaded manually from the test track and then inspected for lubricant pick-up using a microscope. Various magnification levels were used to inspect the trailing edge side pads, the center trailing pad, and four quadrants of the slider for lubricant pick-up and contamination.

2.8 Matlab processing workflow

The OSA data were converted to lubricant thickness change data by subtracting the before-test "base" scan from the in-situ scans (Figure 2-3) using the Candela OSA software. In this figure, the top and middle images show a very strong light region in the middle and dark region on the sides that appears as a variation in the lubricant thickness but in fact corresponds to the non-flatness of the disk. Because of the resolution of the OSA system, small offsets of the spindle axis and clamping distortions show up as low-frequency variations in the lubricant thickness. By taking a base scan and subtracting it from the in-situ scans, this non-physical effect is eliminated and the actual slider-induced changes in the lubricant layer can be isolated. This type of "net change" analysis is only possible on a system with a shared disk spindle for both conducting the test and making OSA scans. A separate OSA scanning system will not be able to easily remove this non-physical background disturbance from the scanned image.

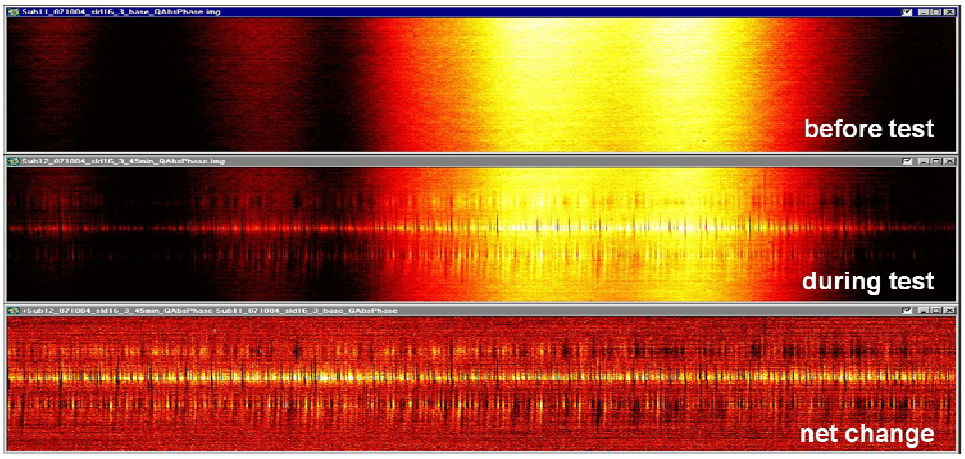

Figure 2-3. OSA subtraction method illustration. Top: disk surface before slider flying. Middle: disk surface after 45 minutes of slider flying. Bottom: Change in disk surface (during – before = net change). All three images are of size 360 degrees by 1 mm (x-axis by y-axis).

The OSA software was again used to reduce the scan area width from the original 2 mm to 1 mm to reduce the size of the data to analyze, but care was taken to ensure that the entire flying track was still covered. Most sliders studied here were of 0.7 mm width so a 1 mm wide scan would fully capture the slider-induced disturbance, but a few were 1 mm wide. The OSA scans corresponding to 1 mm wide sliders were analyzed at the full 2 mm width. The reflectivity data was saved as a text file by using the "control + shift + mouse select" keyboard command in the Candela software. The text file was imported using a Matlab program where a custom data processing code [appendix A] converted the reflectivity measurements into lubricant thickness changes after high-pass filtering at 10 kHz. Figure 2-4 shows the magnitude response of the 10 kHz filter used during one particular experimental analysis. Other experiments used similar filters, with the specific shape of the filter being determined

essentially by the disk rotation speed which determines the sampling rate of the experimental data. The magnitude response plots were virtually identical across all tests.

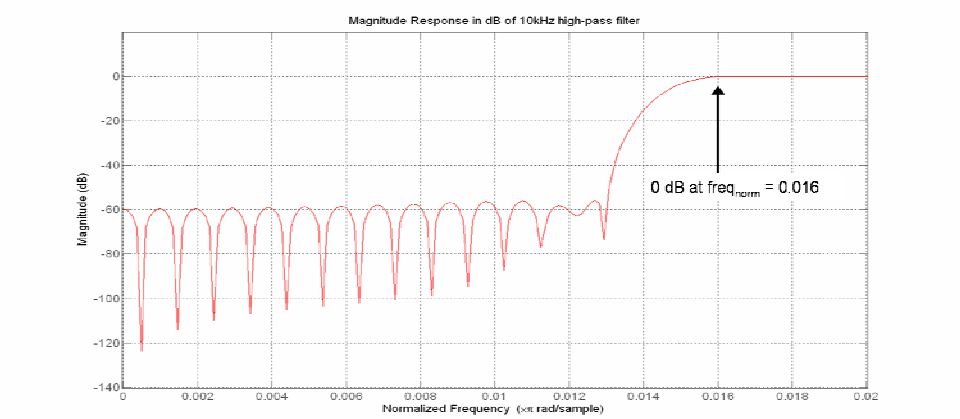

Figure 2-4. Magnitude Response of 10kHz high-pass filter. Nyquist frequency for this test was 681.8 kHz, so the filter reaches 0 dB at (0.016*681.8 = 10.9 kHz).

2.9 Data Analysis Techniques

After the data was converted from reflectivity percentage into lubricant thickness and high-pass filtered to get the lubricant variation using Matlab, the data analysis technique varied. Specific techniques are outlined below.

2.9.1 Lubricant Modulation Profile

Using the Matlab workspace described in Secion 2.8, further data analysis can be performed. To illustrate the change in lubricant induced by the action of a flying slider, Figure 2-5 shows the variation in lubricant thickness for a location outside the slider's path and for a location inside the slider's path. As seen in the figure there is more modulation of the lubricant thickness inside the slider path than outside the slider

path. This is a normal result, as most experiments showed some disturbance of the lubricant layer along the slider path and no disturbance outside the slider path. These plots are based on the "variation" matrix in the Matlab workspace, reflecting the results after high-pass filtering at 10 kHz.

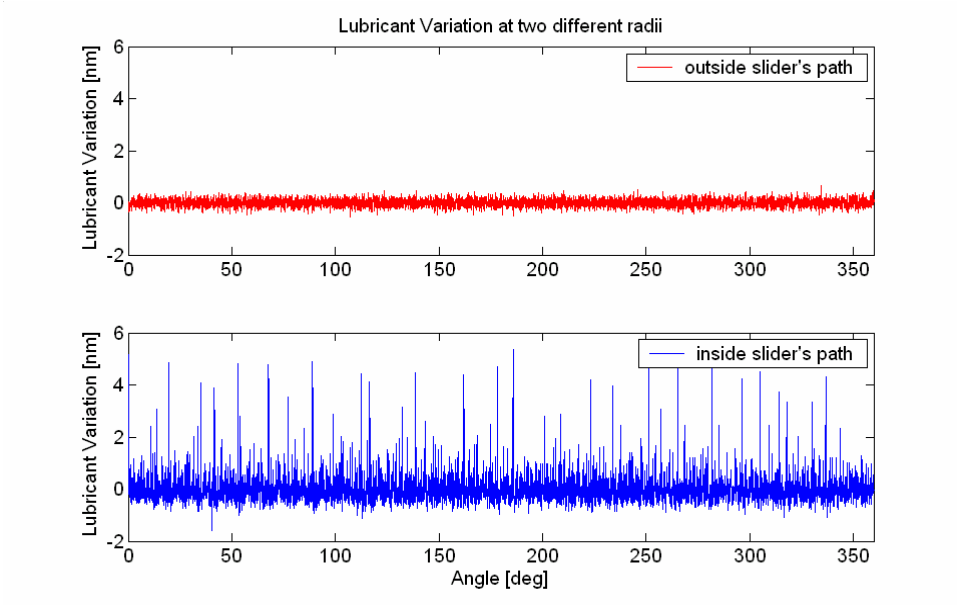

Figure 2-5. Lubricant profile above 10kHz at two locations in the scan area: inside slider's path and outside slider's path. X- and Y-scales are identical between plots.

The Matlab workspace contains information about the standard deviation of the lubricant thickness at each measurement radius. Specifically, the vector "sig3" contains three times the standard deviation of the variation data at each measurement radius. Using Figure 2-5 as an example, 3 sigma outside the slider's path is much lower than 3 sigma inside the slider's path. These "3 sigma" levels can be plotted at each radius to show the "lubricant modulation profile" after the outlier data points are numerically removed. Figure 2-6 shows the lubricant modulation profile after 45

minutes of on-track slider flying with the colored arrows indicating the points corresponding to the "inside" and "outside" slider's path data from Figure 2-5. Each point in Figure 2-6 is found by calculating three times the standard deviation of the lubricant modulation at each of the 501 measurement radii. The standard deviation is chosen as a representative measure of the variation in lubricant height at each measurement radius. This method takes the modulation data from a 501 by 8192 element matrix into a 501 element vector. The 501 elements represent the 1 mm wide measurement band at 2 μm sampling.

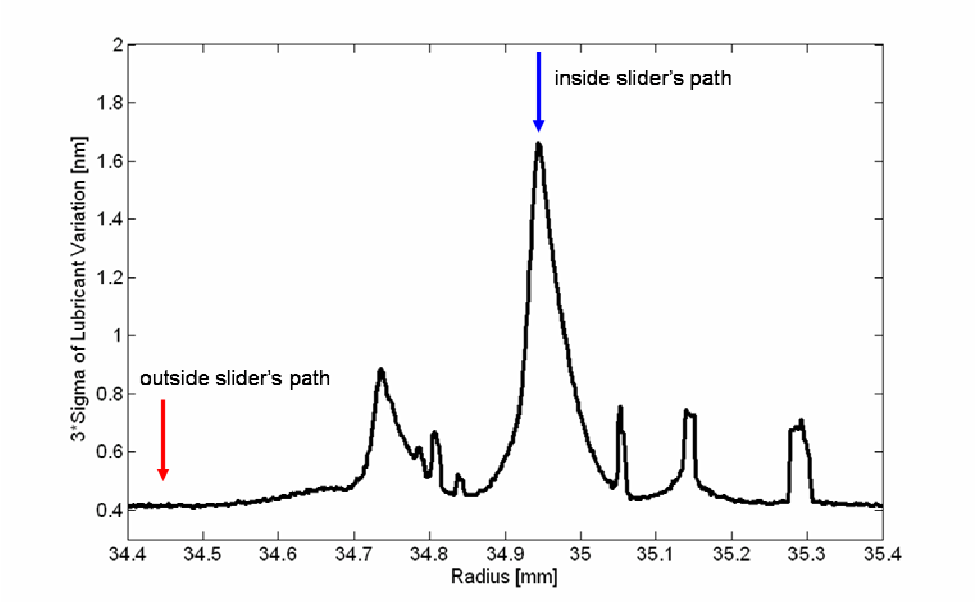

Figure 2-6. Modulation profile after 45 minutes of on-track flight. Arrows indicate location of data points corresponding to the two lubricant profiles shown in Figure 2-5.

From this figure, it is clear that the lubricant modulation occurs in distinct peaks at certain radial positions. The edge-to-edge width of the slider in this test was 0.7 mm, so the approximately 600 μm width of the modulation area helps to locate the

exact center of the slider even though the slider's radial positioning system was independent of the OSA stage control. Experiments with a very narrow modulation pattern cause difficulty in locating the slider over the modulation.

2.9.2 Lubricant Modulation Area

This calculation of the lubricant modulation profile was repeated for each measurement time during the tests. One further analysis method, calculating the "lubricant modulation area", was used to quantify the amount of lubricant modulation under a flying slider. To perform this analysis, the area under the lubricant modulation profile was calculated. The modulation profile presented in Figure 2-6 has a modulation area of 274 units. A track where the slider did not fly would have a modulation area around 200 units (baseline 3*sigma of 0.4 times 501 tracks = 200 units). While not directly related to any physical area, the modulation area provides a convenient single parameter to quantify the strength of the slider-lubricant interaction that allows easy comparison between experimental results with different slider designs and lubricant properties. A large modulation area can be caused by moderate lubricant modulation over the entire slider width or severe lubricant modulation over a small portion of the slider width. Either situation indicates strong slider-induced lubricant modulation. In Section 3.1 the lubricant modulation area is used to illustrate the evolution of the slider-lubricant interactions with time.

2.9.3 Lubricant Modulation Frequencies

In addition to the spatial calculations from the OSA lubricant measurements, one can analyze the data in the frequency spectrum. With the disk rpm known, the angularly indexed OSA data can be converted to time-indexed data. The Matlab workspace described in Section 2.8 includes the power spectrum of the modulation above the 10 kHz high-pass cutoff. Figure 2-7 shows an example of the frequency content of lubricant modulation after 45 minutes of on-track flight. Note that the frequency content is strongest at low frequencies and occurs in specific radial locations as does the modulation profile peaks from Figure 2-6. Frequency results like this are discussed in the appropriate sections in later chapters.

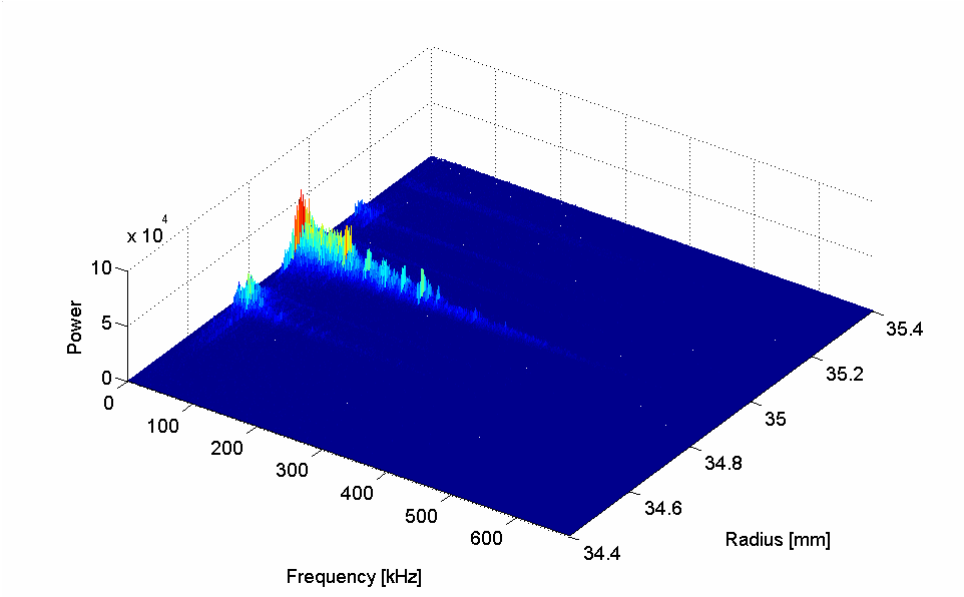

Figure 2-7. Lubricant Modulation Frequencies for the data shown in Figure 2-6.

2.9.4 Incremental Change in Lubricant

While most analysis in this work is performed using the analysis techniques listed above, some results in Chapter 6 require the more advanced analysis technique of the "incremental change" in lubricant. Instead of subtracting the "base" OSA scan from a particular in-situ OSA scan, the incremental change is found by subtracting the *previous* in-situ scan from a particular scan. Figure 2-8 shows the difference between a "net change" subtraction and an "incremental change" subtraction as performed on a result taken after 10 minutes of slider flight. The right side of the figure shows the net change analysis discussed in Section 2.8. The left side of the figure shows the result from subtracting the 9 minute OSA scan from the 10 minute OSA scan, giving the "incremental change" of the lubricant. It is clear that even though the net change image shows definite lubricant modulation in three distinct bands under the slider's path, there is very little change in the lubricant modulation between 9 and 10 minutes of slider flight. In this way, the incremental change in the lubricant can show different results from the net change result. The incremental change analysis is only possible on an in-situ test stand where the same disk spindle is used for conducting the test and conducting the OSA scan. Reproduction of some results presented in this work will not be possible without such an in-situ OSA scanning setup.

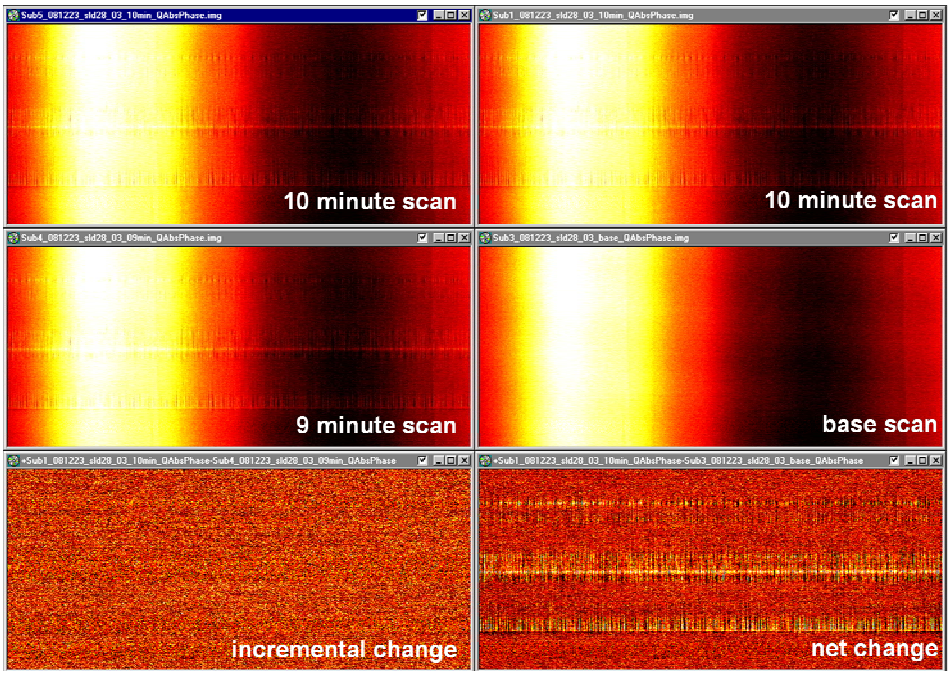

Figure 2-8. Illustration of the difference between a "net change" subtraction and an "incremental change" subtraction.

2.10 Conclusion

The experimental apparatus used in this dissertation has been introduced. The component measurement systems have been detailed along with the general experimental procedure. Basic analysis techniques have been introduced and explained and the Matlab code used for the basic analysis has been discussed. With the types of measurement systems detailed here, later discussion can focus on the results instead of the procedure required to arrive at the results. Where not explicitly noted, the experimental procedures and analytical methods used are implied to be those detailed here. While the basic experimental procedure and analytical method given here forms a basis for most of the experiments in this work, specific modifications of these procedures and methods are given in the particular sections.

3 General Experimental Observations

3.1 Introduction

While the purpose of this work is in part to investigate the influence of various parameters on the slider-lubricant interactions, some observations can be made that apply generally to all results, regardless of the specific slider-lubricant interface. These general observations are qualitative and based on hundreds of flyability tests performed with a range of slider designs, lubricant types, disk speeds, and flying times. With these general trends established, the influence of various interface parameters on the slider-lubricant interactions will be more obvious.

3.2 Change in Lubricant Modulation Profile with Time

The OSA scans of the lubricant thickness at every measurement time show how the lubricant disturbance evolves with time. In general, the shape of the modulation profile tends to stay the same while the magnitude of the profile increases as the flying time increases. Figure 3-1 shows the OSA scanned images at various flying times from 1 minute through 45 minutes, illustrating how the continued slider flight modifies the lubricant distribution on the disk surface. Of note is that the general disturbance pattern of the lubricant remains qualitatively constant. As the slider continues to fly over the same track, the magnitude of the lubricant modulation increases. Fortunately, this increasing modulation tends to level off after a certain initial period. This implies that the most easily removed lubricant has been affected.

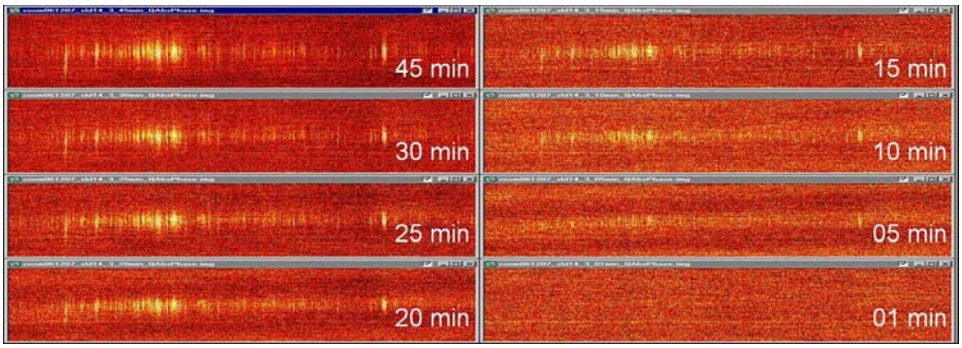

Figure 3-1. OSA images during a 45 minute flying test, showing the evolution of the lubricant disturbance with time.

Figure 3-2 shows the amount of lubricant modulation versus radius at each measurement time using the "lubricant modulation profile" analysis discussed in Section 2.8.1. As seen in Figure 3-1, the qualitative disturbance does not change appreciably with increased flying time. The shape of the disturbance remains qualitatively consistent and simply increases in magnitude with increased flying time. Figure 3-3 shows the average lubricant thickness versus radius at each measurement time. As with the modulation profile, the shape of the average lubricant thickness profile is constant and simply changes in magnitude with increased flying time. The modulation band in the middle of the track increases in height and the depletion band deepens with flying time. During this experiment, the modulation band coincides with the depletion band, but this is not always the case. Other results commonly show strong modulation at the sides of the slider without associated depletion in those regions.

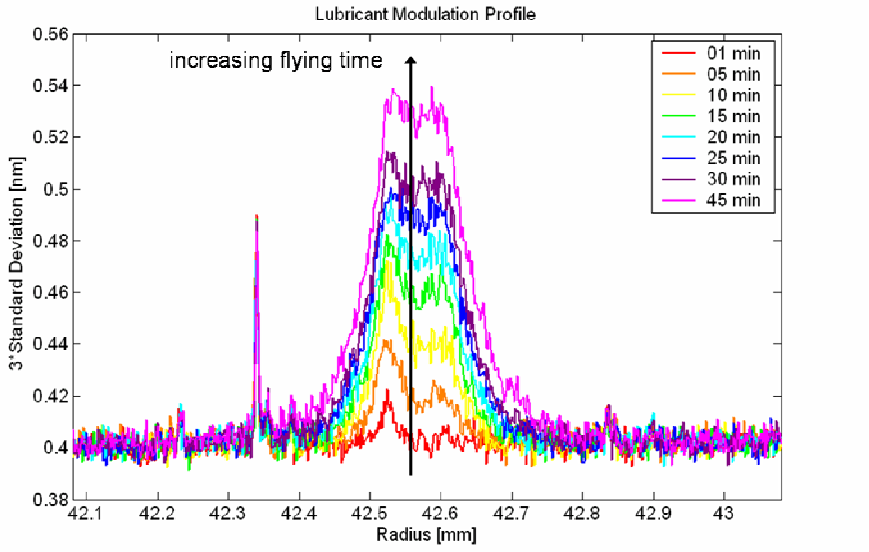

Figure 3-2. Lubricant modulation profile (based on standard deviation) showing increasing modulation with continued flying time.

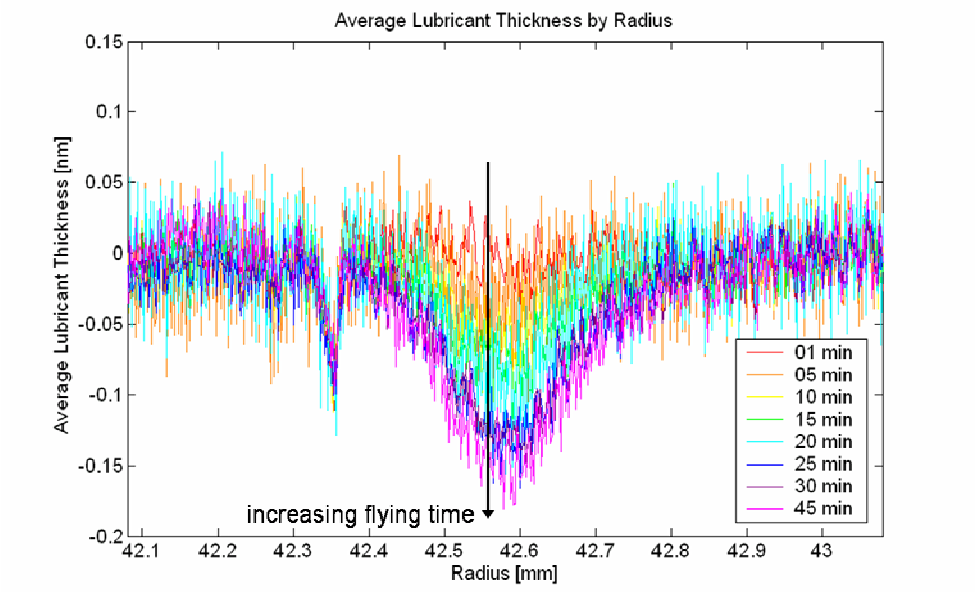

Figure 3-3. Average lubricant thickness showing increased depletion with flying time.

The “modulation area” plot associated with this data is presented in Figure 3-4, showing the modulation area (introduced in Section 2.8.2) monotonically increasing with flying time. Also of note is that the modulation area tends to decrease in slope with flying time, giving a logarithmic-like profile. There are always outlier results, but the general modulation trend in most experiments is towards a logarithmic slope in the modulation area vs. time data. Long on-track flying-time modulation levels are not expected to be substantially higher than levels seen after the modulation area vs. time plot levels off, a consequence of the logarithmic trend. The modulation area starts out with a value above 200 units. Because even an undisturbed lubricant track has some variation in thickness, the “baseline” modulation area is about 200 units (from 501 radial points and 0.40 nm baseline 3*sigma). Some modulation area results presented later are given with the baseline modulation area already subtracted so that the trend begins near zero units.

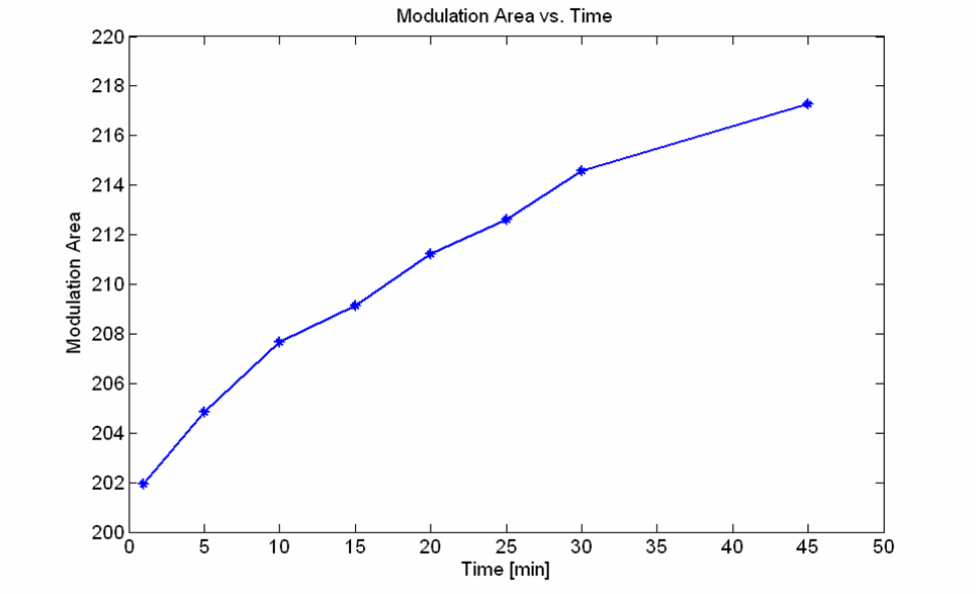

Figure 3-4. Modulation area versus time curve showing logarithmic shape.

3.3 Lubricant Recovery with Time

While most results show the lubricant modulation profile growing in a logarithmic shape in time, the same can be said about the lubricant recovery with time. In a series of experiments, sliders were flown for 20 minutes and then unloaded. After slider unloading, the lubricant layer was monitored by OSA scans with the disk still spinning. An example plot of a lubricant modulation profile versus relaxation time is shown in Figure 3-5. The modulation pattern after slider unloading is shown in the lower right of the figure. This strong modulation pattern "softens" with increasing relaxation time but the general shape remains. The modulation profiles associated with this figure are shown in Figure 3-6

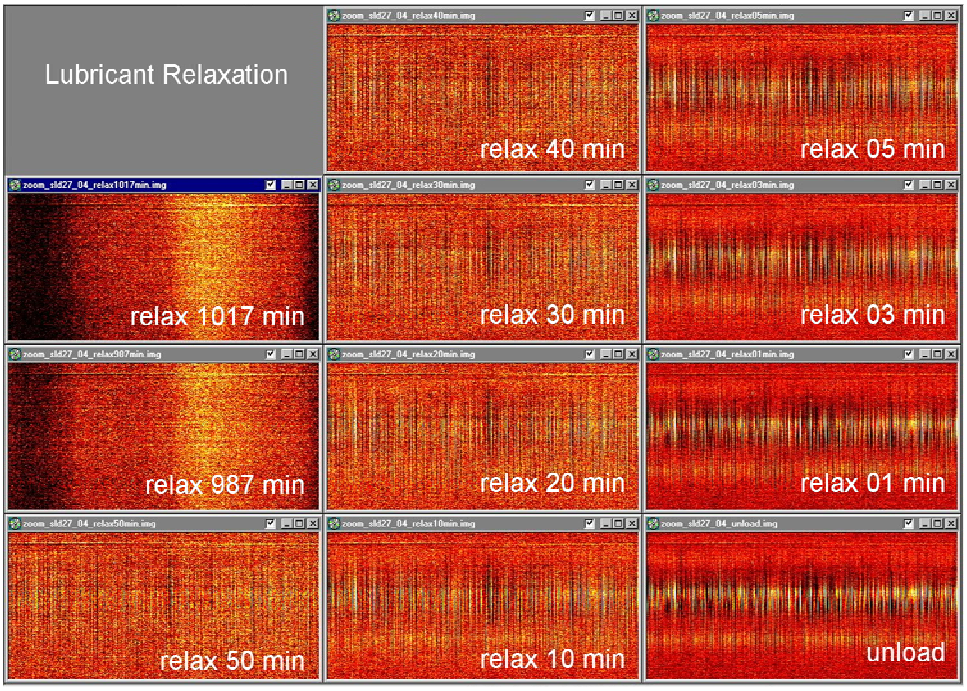

Figure 3-5. OSA scans of a modulated lubricant track recovering with increased relaxation time.

.

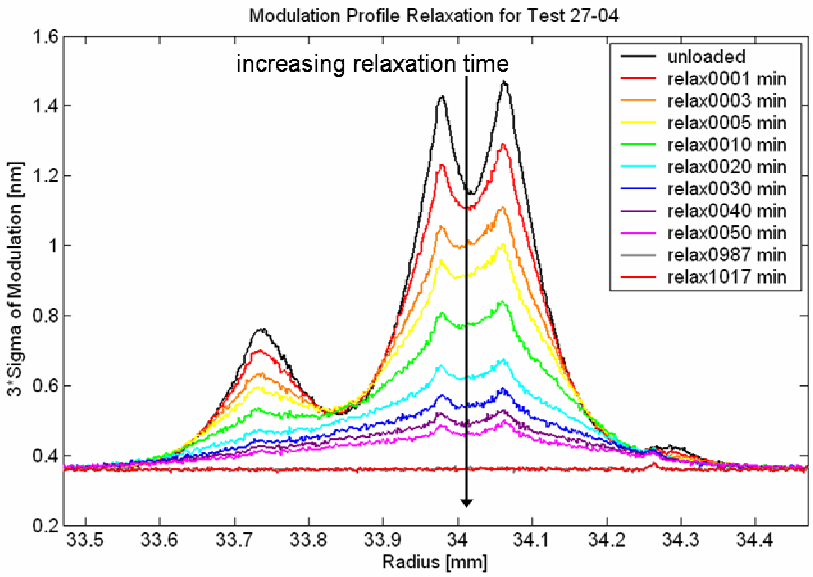

Figure 3-6. Lubricant modulation profiles taken from Figure 3-5.

Immediately after slider unloading, the modulation profile has three distinct peaks (black line). Until about 30 minutes of relaxation, the three peaks are diminished in magnitude, but still visible. Beyond 30 minutes of relaxation, the smallest peak is not clear and only the two highest peaks are visible.

The modulation area of the profiles depicted in Figure 3-6 can be plotted versus relaxation time. Instead of plotting the straight modulation area, two analysis steps are taken. First, the modulation area is "zeroed" so that a perfectly flat modulation profile (no modulation peaks) will produce a modulation area of zero units. This zeroing is identical to shifting the profiles in Figure 3-6 so that the 3*sigma value is zero at the edge of the data (instead of 0.37 nm). Second, the zeroed data is scaled such that the modulation area at slider unloading is exactly one unit. This is done by dividing all the results by the modulation area at slider unloading. This scaling is done so that

comparisons can be made between results with different initial modulation levels. Without this scaling, a test with very strong modulation would not be easily comparable to a test with moderate modulation. Equation 3.1 shows how these two analysis steps would be implemented in a data processing code, where Y is the unadjusted modulation area, Y_{base} is the modulation area associated with a flat modulation profile, Y_{unload} is the modulation area at the unload scan, and Y_{new} is the adjusted modulation area.

$$Y_{new} = (Y - Y_{base})/(Y_{unload} - Y_{base}) \quad (3.1)$$

The modulation area resulting from applying Equation 3.1 to seven individual trials is shown in Figure 3-7. The data presented in Figure 3-6 represents one of these seven trials. From these results, the average trend and error bars are found and plotted with the best-fit logarithmic curve in Figure 3-8.

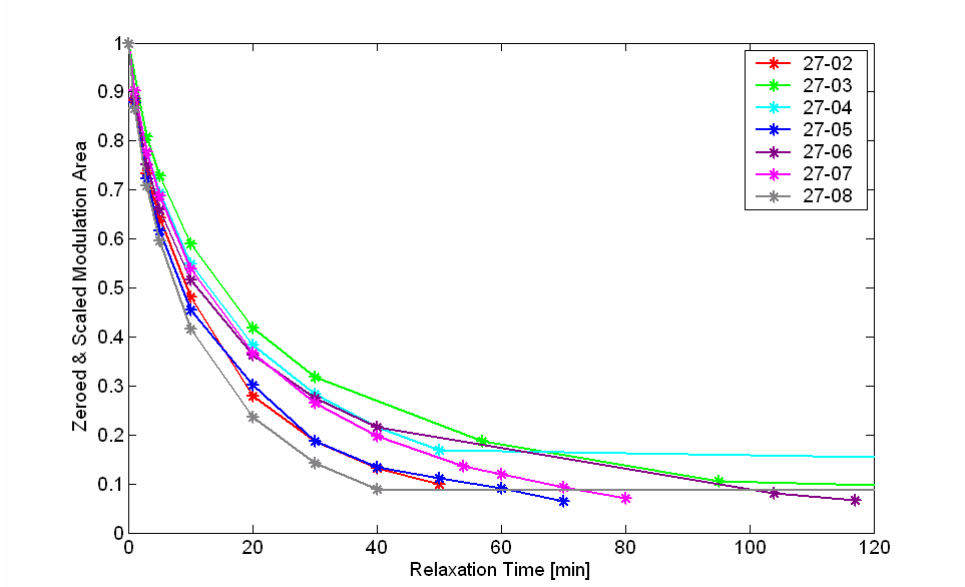

Figure 3-7. Adjusted lubricant modulation area versus time for seven individual trials.

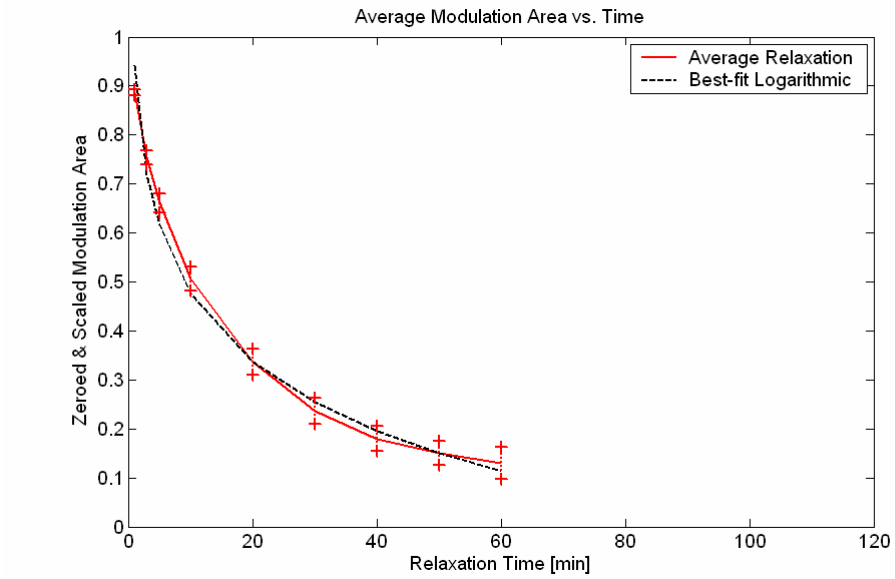

Figure 3-8. Average lubricant relaxation trend and best-fit logarithmic curve for data in Figure 3-7.

Figure 3-8 makes clear that the lubricant relaxes very quickly upon removal of the slider for this particular lubricant type. After one hour of relaxation, the modulation area is approximately 15% of the original level. Even after a relatively short time of 10 minutes, the modulation area has reduced to 50% of the original level. While the specifics of the slider-lubricant interface are expected to strongly influence the speed of this reduction, it is clear that measurements of the lubricant modulation made after a slider has been removed must be taken quickly to capture as much of the original modulation as possible. More detailed analysis of the effect of lubricant type on relaxation rate is given in Section 5.2.3.

3.4 Effect of Slider Unloading

Another general trend is the sometimes dramatic change in lubricant modulation and thickness profile introduced by unloading the slider. The OSA scan of the lubricant thickness at the end of a 45 minute test (before unloading) and the OSA scan of the lubricant just after unloading can be quite different despite being taken only one minute apart. By comparing Figure 3-9 and Figure 3-10, it is clear that there is evidence of changed lubricant height such as lubricant depletion tracks, in the 50 degree area shown due to the unloading process. Notice that both the lubricant modulation and mean lubricant thickness have been affected by the unloading process. For this reason, it is important to make lubricant modulation measurements while the slider is still flying on the disk since scanning the disk after unloading may reflect the specifics of the unloading process instead of the steady-state flying conditions.

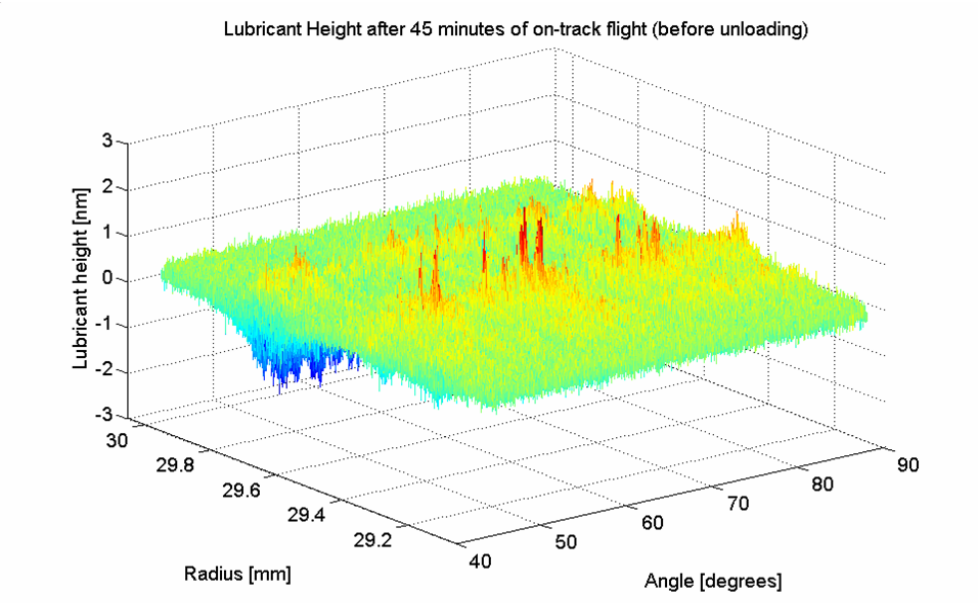

Figure 3-9. 3D lubricant height after 45 minutes of on-track flight (just before unloading).

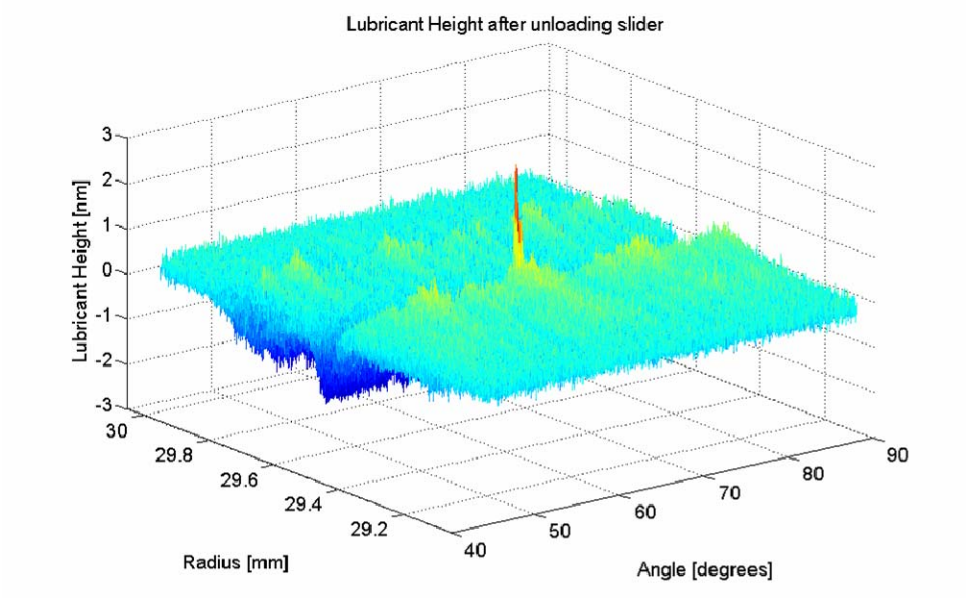

Figure 3-10. 3D lubricant height after 45 minutes of on-track flight (just after unloading).

3.5 Evolution of Local Modulation Peaks and Troughs

To investigate the evolution of local modulation peaks and troughs, experimental results were analyzed at specific locations under the slider's path. In this experiment, a slider was flown on-track for 20 minutes using the procedure described in Section 2.6. OSA scans were taken of the disk in one minute increments, beginning at one minute of slider flight. From each OSA scan, a small area that contained a single lubricant peak was isolated. The area was 0.4 deg (0.25 mm) x 0.09 mm. Figure 3-11 shows a 3D image of the area at 1, 5, 10, and 15 minutes of flight.

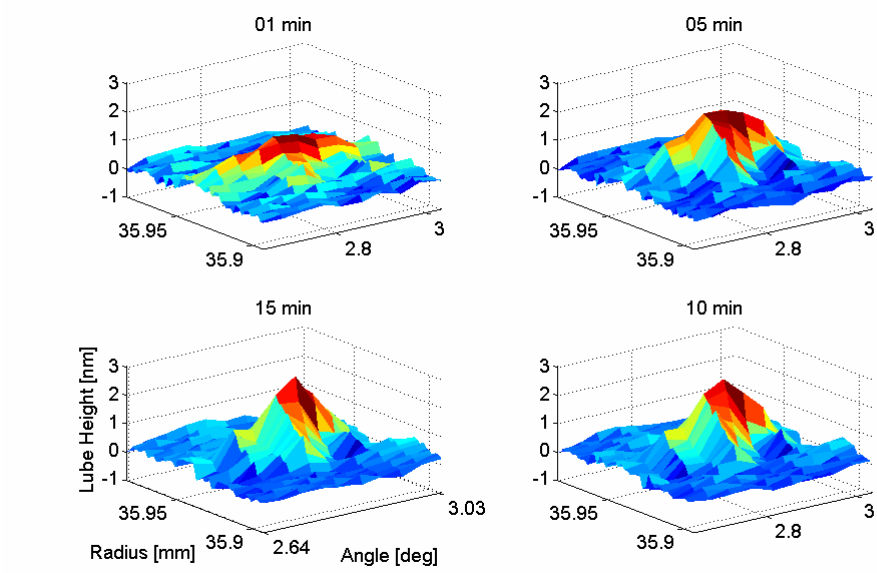

Figure 3-11. Illustration of localized lubricant height evolution with time. Axes in all four quadrants are identical.

From this figure it is clear that the local lubricant peak becomes higher with increasing slider flying time. Further analysis is performed by finding the peak lubricant height in this small region and plotting it versus time in Figure 3-12. The dotted line is the best-fit logarithmic trendline, showing very good agreement with the experimental results. The standard deviation of the lubricant modulation over the entire disk circumference is composed of many individual lubricant peaks. Thus, the global logarithmic trend is understood as being based on this kind of localized lubricant height evolution. For this particular location, the local lubricant peak height seems to be approaching 3 nm asymptotically. Similar plots at different locations on the disk show a similar trend in both lubricant peaks and troughs.

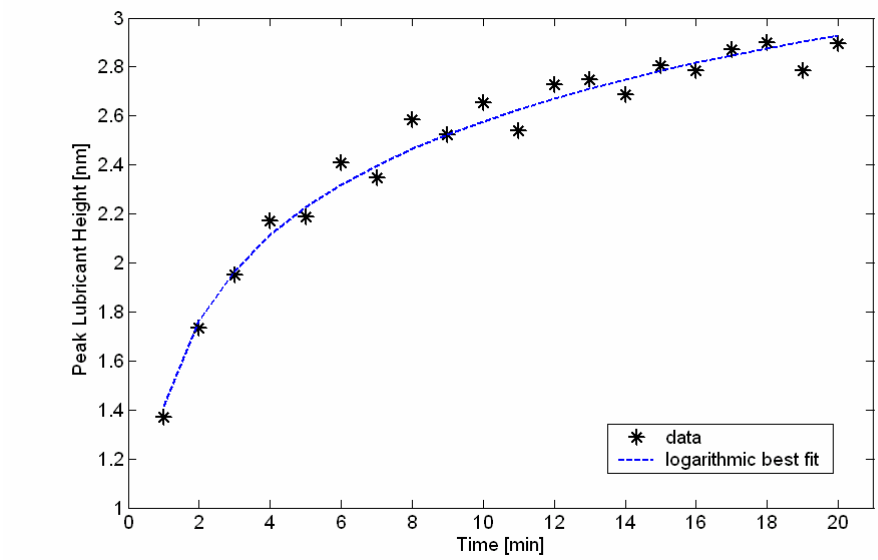

Figure 3-12. Illustration of logarithmic trend in local lubricant peak heights versus time.

3.6 Local Repeatability of Lubricant Peaks and Troughs

Previous research by Pit et al. has indicated that modulation of lubricant is influenced by the underlying carbon layer [1]. In their results, repeatable lubricant modulations related to the underlying layer are called moguls. Based on this idea, repeated experiments on the same disk track should give similar lubricant moguls. These results were tested in a series of experiments, with the same slider being flown on the exact same track multiple times in a row with identical experimental parameters.

The experimental setup was as follows. The slider was a femto design being flown at 34 mm radius on a disk spinning at 5620 rpm to give a linear speed of 20 m/s. The disk was coated with 20 angstroms of Zdol + X1P lubricant at 2000 g/mol. The

slider flew on-track for 20 minutes with OSA scans taken at one-minute intervals during this time. Between tests, the slider was unloaded and inspected for lubricant pickup, but the disk was not removed from the spindle. Since the disk was not removed, the angular and radial position of the disk remains constant in the OSA scan. This correspondence allows localized comparison of the lubricant modulation pattern. Sufficient time was given between tests to allow the lubricant to recover, giving each test a "fresh" lubricant distribution.

The lubricant modulation profiles for three consecutive tests are given in Figure 3-13. This figure shows that the modulation profile has some strongly repeated features, but varies somewhat between repeated tests. The most striking feature is the "double-peak" observed on the right side of the profile, clearly visible on two of the three profiles (test 4 and 7). Also, there is a region of small modulation between two regions of high modulation near the middle of the profile, visible in all three profiles. If these features were solely influenced by the substrate, they would occur at exactly the same radius. The slight shifting of the modulation profile in the radial direction suggests that the slider plays a strong role in the creation of these features.

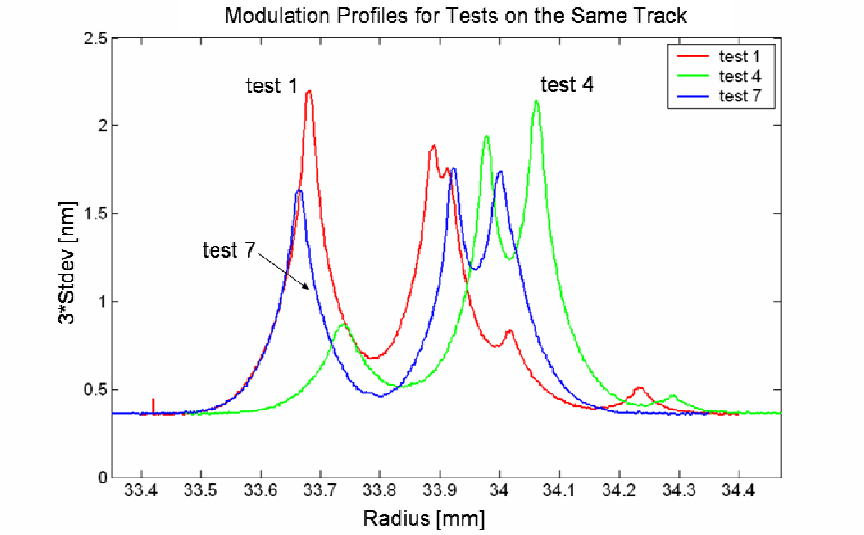

Figure 3-13. Modulation Profiles for three repeated tests on the same disk track.

The modulation area associated with these three profiles can be easily calculated. Figure 3-14 shows a bar graph comparing the modulation areas with the y-axis beginning at the "base modulation area" of 200 units. The modulation areas vary by 14%, showing that the modulation area is repeatable between these three tests even when the modulation profiles do not correspond exactly in the radial direction.

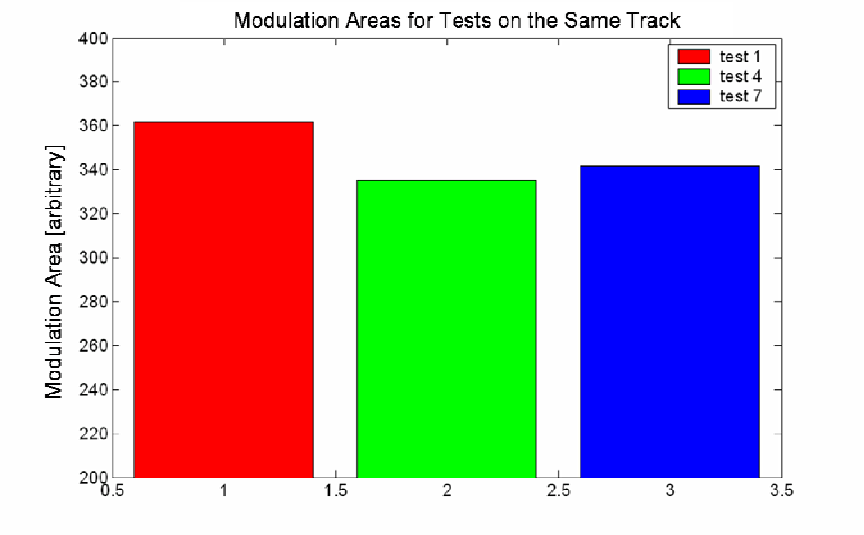

Figure 3-14. Bar graph of modulation areas for three repeated tests on the same disk track.

With the qualitative modulation repeatability established, local repeatability of modulation is explored. OSA scans are available at one-minute intervals for each of the three tests. Figure 3-15 presents the OSA screenshots of a section 1 mm x ~100 deg for all three tests. Visual inspection of these screenshots shows that there are regions where the lubricant buildup or depletion corresponds in two or more of the tests. Equally visible are regions where the lubricant thickness features do not correspond.

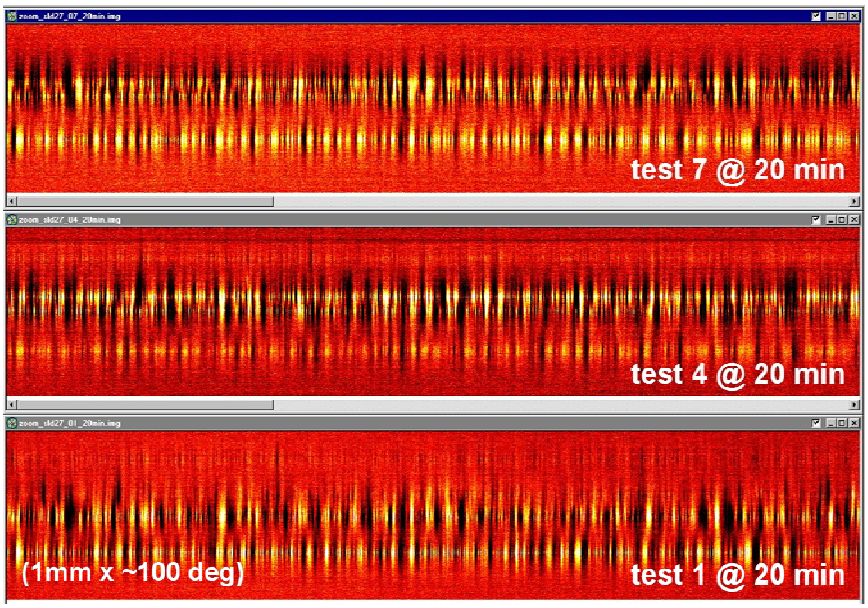

Figure 3-15. OSA screenshot (1 mm x ~100 deg) for three repeated tests on the same disk track.

While the scaling of this figure makes it difficult to make close comparisons, the eye can easily pick out some areas of the disk where the thick (dark) or thin (light) regions seem to be repeated. Examination of smaller regions at higher magnification further illustrates these observations.

Figure 3-16 shows a smaller, 1 mm x 4.5 deg band across all three tests as plotted after data analysis in Matlab. In this figure, lubricant thickness is plotted using a "thermal" color scale where thicker lubricant is "hot"/red and thinner lubricant is "cool"/blue. The radial and angular positions correspond to the same points on the disk across all three tests.

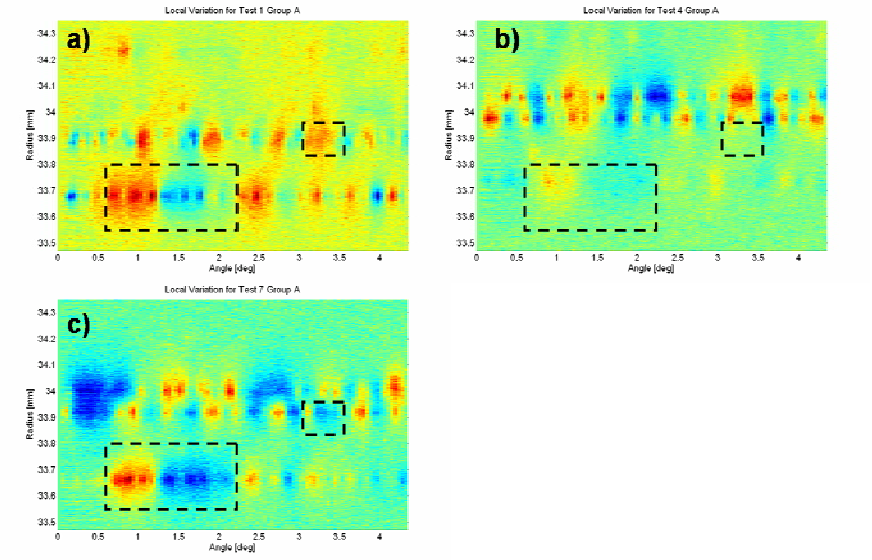

Figure 3-16. Visualization of lubricant thickness over 1mm x 4.5 deg section for a) test 1, b) test 4, and c) test 7. Dashed boxes mark regions of high and low correspondence between images.

A region of corresponding lubricant thickness is clear in the lower left corner, marked out with a dashed box as an aid to the eye. In this region all three tests show thicker lubricant with an adjacent region of thinner lubricant. The strongest correspondence occurs between subplots a) and c). In the smaller dashed box, there is a region of thicker lubricant in subplot a) while subplot c) shows thinner lubricant. Quantitative comparison of the regions shows that positively correlated regions occur about three times more often than negatively correlated regions. Clearly, while some regions on the disk show repetition of high or low lubricant thickness across multiple tests, there is not perfect correlation between different tests. Thus, the disk substrate is not entirely responsible for the location and magnitude of the lubricant modulation features.

3.7 Conclusion

In this chapter, some general experimental observations were made that apply across a variety of slider-disk conditions. Emphasis was placed on those observations that occur commonly so that later discussion can focus on those observations that are different. Specifically, the slider-induced lubricant modulation profile is well-established by one minute of on-track flying. The magnitude of the modulation profile increases with increased flying time, but the general shape undergoes only small changes with increasing time. A plot of the modulation area shows that the modulation area increases in a roughly logarithmic shape, with large increases at early times and small changes at later times. Based on this trend, it is expected that the modulation area will level off after a long time and not increase any further. Similarly, relaxation of the slider-induced lubricant modulation follows a trend with large decrease in modulation area at short relaxation times and smaller decreases in the modulation area at longer relaxation times. Any measurements of the slider-induced lubricant modulation should be taken as soon as possible after the flying test to minimize the loss of information due to this lubricant relaxation. Additionally, it was shown that the slider unloading process introduces significant changes in the lubricant modulation and mean thickness profiles. Because of this influence, the lubricant profile under a flying slider will be different from the lubricant profile as measured after slider unloading, independent of the lubricant relaxation effect just discussed. Next, the growth of local lubricant peaks was undertaken to show that the height of individual peaks follow a logarithmic growth trend. This was taken as an explanation

for the logarithmic growth trend in modulation area, a global measure of lubricant modulation. Finally, the repeatability of lubricant peaks and troughs was undertaken to explore the influence of the disk substrate on the modulation profile. While the modulation area was repeatable, the local modulation peaks and troughs were only partially repeatable in location and the modulation profile shifted in radius along with the slider location. The disk substrate is not entirely responsible for the location and magnitude of the lubricant modulation features, the slider is responsible for some. With this influence established, later chapters focus on the influence of the slider and lubricant properties on the modulation of the lubricant.

4 Lubricant Parametric studies on modulation area

4.1 Introduction

One useful method to analyze the effect of lubricant parameters on the slider-induced lubricant modulation is the idea of modulation area discussed in Section 2.8.2. If the same slider design is used to fly on identically lubricated disks with only one parameter varying between disks, the differences in lubricant modulation area can be attributed to the single parameter that was varied.

4.2 Slider form-factor

In testing the effect of slider form-factor (slider size), disks of the same lubricant type and thickness were used with differing slider form-factors. For these tests, two pico form-factor designs of size 1.0 x 1.25 x 0.3 mm (known as CML 7nm and CML 5nm) were compared with three femto form-factor designs of size 0.83 x 0.67 x 0.20 mm (known as CML Femto, DSI Panda 2, and DSI Panda 3) in Figure 4-1. Using the modulation area analysis method described above, it was found that the modulation area was larger for the pico-size sliders than the femto-size sliders. This agrees well with the work by Marchon et. al. [1] that found more low-frequency modulation (moguls) for wider sliders. As the moguls have some component above 10kHz (our high-pass filter cutoff), more moguls means more lubricant modulation.

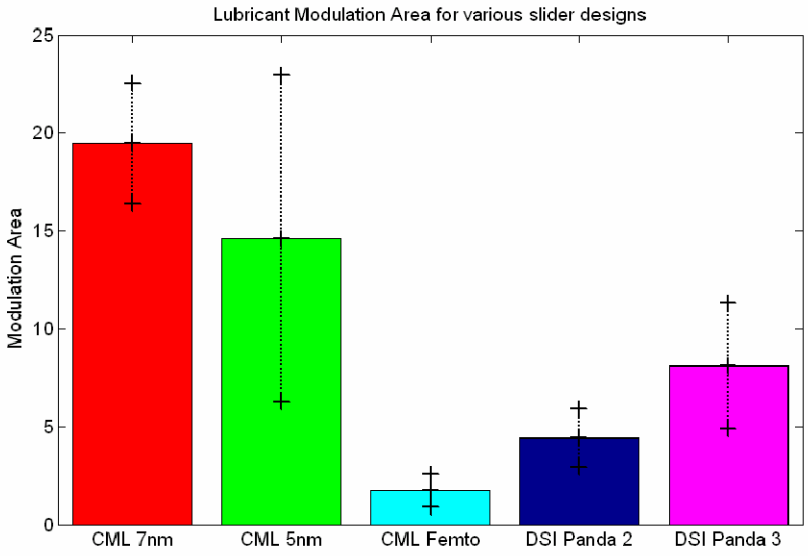

Figure 4-1. Modulation area average for five slider designs after adjusting for the baseline modulation.

The CML 7nm and CML 5nm sliders are both pico designs. The CML Femto, DSI Panda 2, and DSI Panda 3 sliders are femto designs. Thus, one can see that the smaller slider designs tend to give less lubricant modulation as compared to larger form factors (Figure 4-2). Simulations of the CML 7nm and CML Femto designs show similar minimum fly-heights. Figure 4-1 shows the CML Femto design giving the lowest lubricant modulation area and the CML 7nm design giving the highest. This comparison shows that at similar flying heights, a larger form-factor modulates the lubricant more strongly than a smaller form-factor.

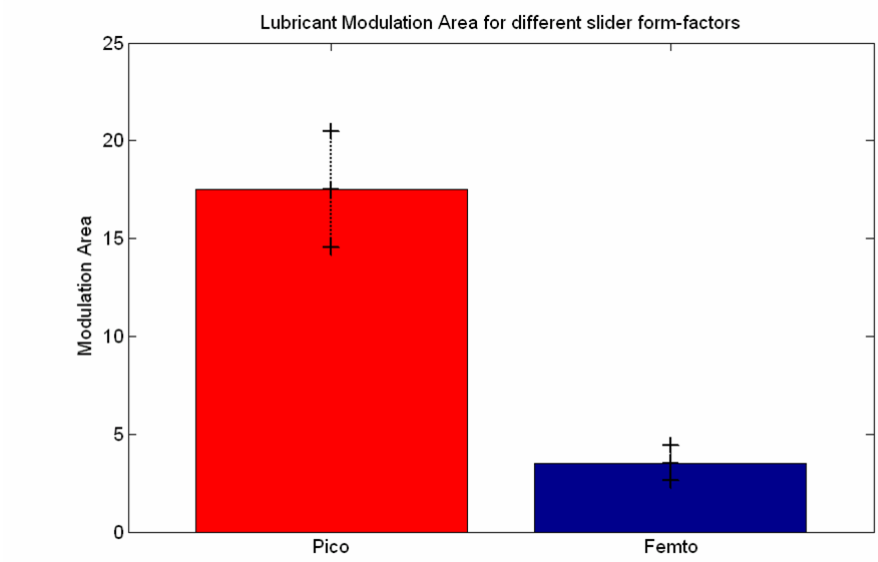

Figure 4-2. Modulation area average for two slider form factors.

4.3 Lubricant Thickness

In testing the effect of lubricant thickness, disks of the same lubricant type were used with differing lubricant thickness. For these tests, Zdol lubricated disks were used with lube thicknesses 10.4, 12.4, and 17.0 angstroms. Using the modulation area analysis method just described, it was found that the modulation area increased with increasing lubricant thickness (Figure 4-3) in agreement with Marchon et al. [1] and Dai et al. [2]. It is understood that a thicker lubricant layer has more lubricant available for modulation. Also, the lubricant at the top of the layer is less strongly bound to the disk surface, so it should modulate easier than the lubricant next to the disk surface. In this way, a thicker lubricant layer is expected to modulate more easily.

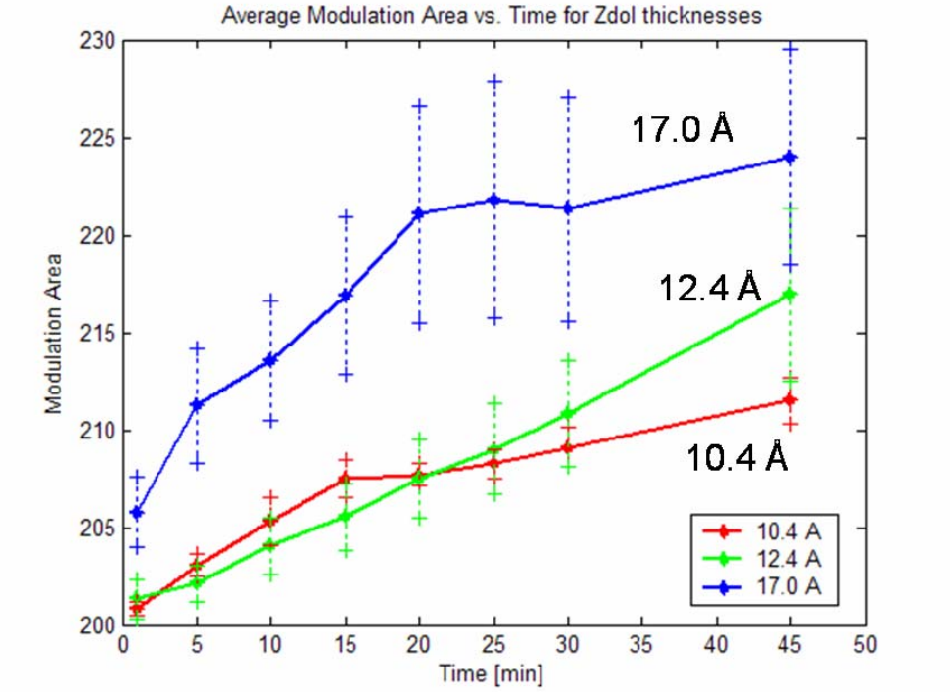

Figure 4-3. Average modulation area versus time for differing Zdol lubricant thicknesses.

4.4 Molecular weight

To investigate the effect of lubricant molecular weight, we studied disks with similar Zdol lubricant thicknesses and different molecular weights. One set of disks had lube thickness just under 11 angstroms and molecular weights of 5700 and 10,000 g/mol. Another set of disks had thicknesses in the 16 angstroms range and molecular weights of 3500 and 10,000 g/mol. By performing multiple experiments with the same slider design on each disk, we found that the modulation area was increased for the higher molecular weight (Figure 4-4). This can be seen by comparing the ~11 angstrom lubricant thickness results for 5700 g/mol (green x's) vs. 10k g/mol (blue

circles) and the ~16.5 angstrom lubricant thickness results for 3500 g/mol (red asterisks) vs. 10k g/mol (purple squares).

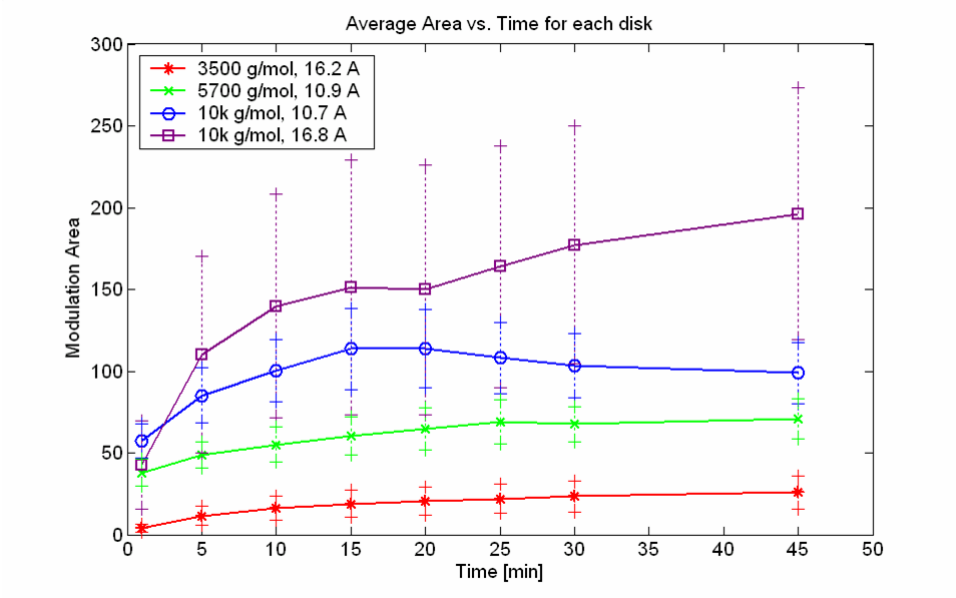

Figure 4-4. Average modulation area versus time for differing Zdol lubricant molecular weights.

Comparing in Figure 4-4 the 10.7 angstroms and 16.8 angstroms disks of the same 10k g/mol molecular weight we see that the thicker lubricant showed higher modulation. This supports the conclusion presented in Section 4.3 that higher lubricant thickness leads to higher lubricant modulation.

4.5 Lubricant additives

To study the effect of lubricant additives, disks were studied with similar Zdol lubricant thicknesses but different additives. One disk had A20H as an additive and the other disk had X1P as an additive. By performing multiple experiments with the

same slider design on each disk, it was found that the modulation area was increased for Zdol + A20H as compared to Zdol + X1P.

The X1P molecule preferentially bonds to the carbon overcoat, increasing the mobility of the Zdol lubricant by preventing it from adhering to the disk [3]. In contrast, the A20H additive is created by chemically reacting Zdol with the X1P molecule. The result is that the A20H additive helps the lubricant bond more strongly to the disk in contrast to the X1P additive (anchoring instead of displacement) [4, 5]. As the slider flies over the disk, the air-bearing shear forces tend to move around the lubricant chains. Because the A20H lubricant is more strongly bonded to the disk at the ends of the chains, the middle of the chain can withstand more modulation before the endgroups release from the carbon layer and the lubricant transfers to the slider. In this way, the X1P lubricant is expected to show less modulation than the A20H lubricant, as seen in Figure 4-5.

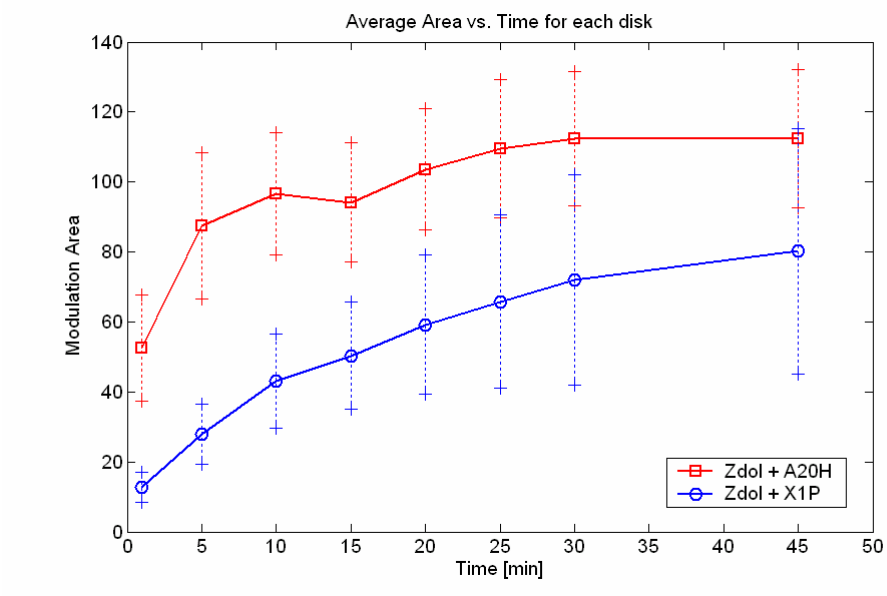

Figure 4-5. Effect of additives on lubricant modulation.

4.6 Modulation Frequencies

In the above studies we analyzed the lubricant modulation data in time and space. The same data can be analyzed in frequency and space. Using numerical Fourier Transforms in Matlab, we can analyze the modulation frequencies for previously presented results. Since the lubricant thickness data is available at each scan radius, the modulation frequencies are presented in 3D form. Figure 4-6 shows the lubricant modulation profile and average lubricant thickness versus radius for the test sld14-6 at 45 minutes. For this test, the peak of the lubricant modulation coincides with the highest lubricant depletion.

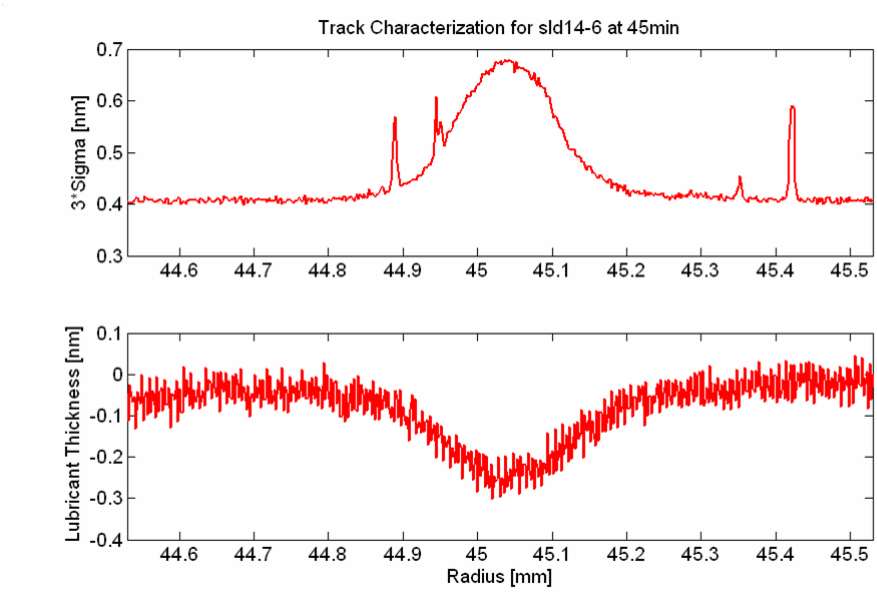

Figure 4-6. Lubricant modulation profile and average lubricant thickness versus radius.

Figure 4-7 shows that the lubricant modulation frequencies are strongest below about 100 kHz and the modulation changes in strength across the width of the slider track. The shape of the change of modulation frequencies mimics the modulation

profile seen in Figure 4-6. The same data is presented in Figure 4-8 with a different view that emphasizes the modulation power at different frequencies in addition to showing how the modulation power changes with time. The majority of changes in modulation frequency occur below about 100 kHz with a strong peak occurring around 25 kHz.

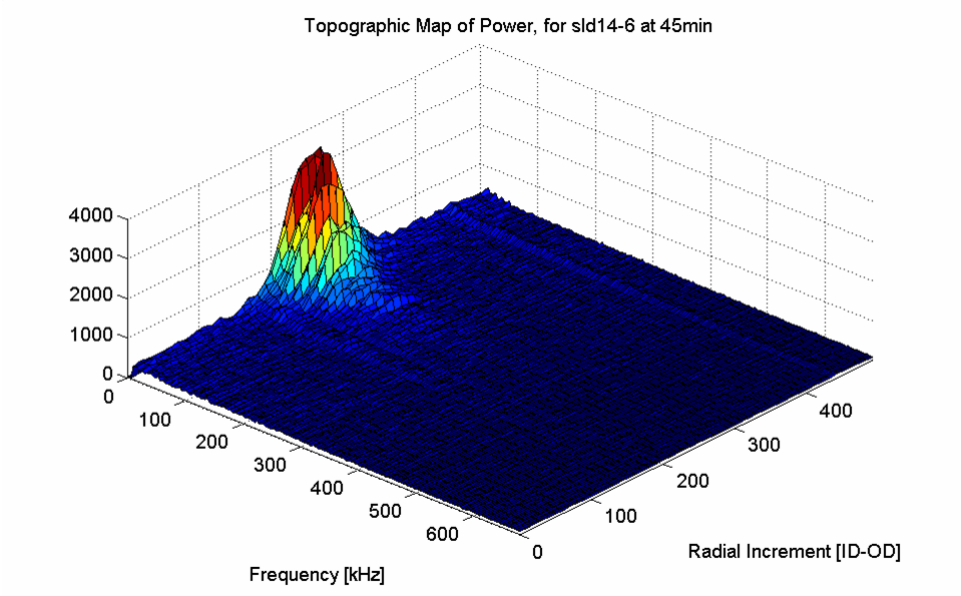

Figure 4-7. Example plot showing the distribution of modulation frequencies across the slider width direction after 45 minutes of flight.

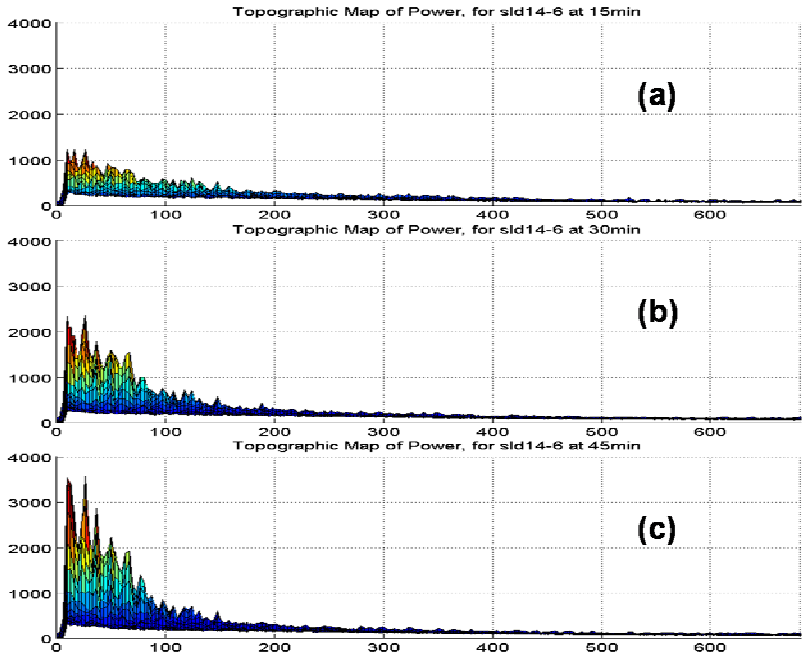

Figure 4-8. Side view of modulation frequency plots at (a) 15 min, (b) 30 min, and (c) 45min showing time evolution of modulation power occurring below 100 kHz with a strong peak around 25 kHz.

While the majority of lubricant modulation frequencies occur below 100 kHz with a strong peak appearing in the 20-30 kHz range, some experiments showed higher frequency lubricant modulation. While testing the effect of lubricant molecular weight, some tests of the 10k g/mol 10.7 angstrom disk showed strong modulation frequency peaks at 50 and 265 kHz (Figure 4-9).

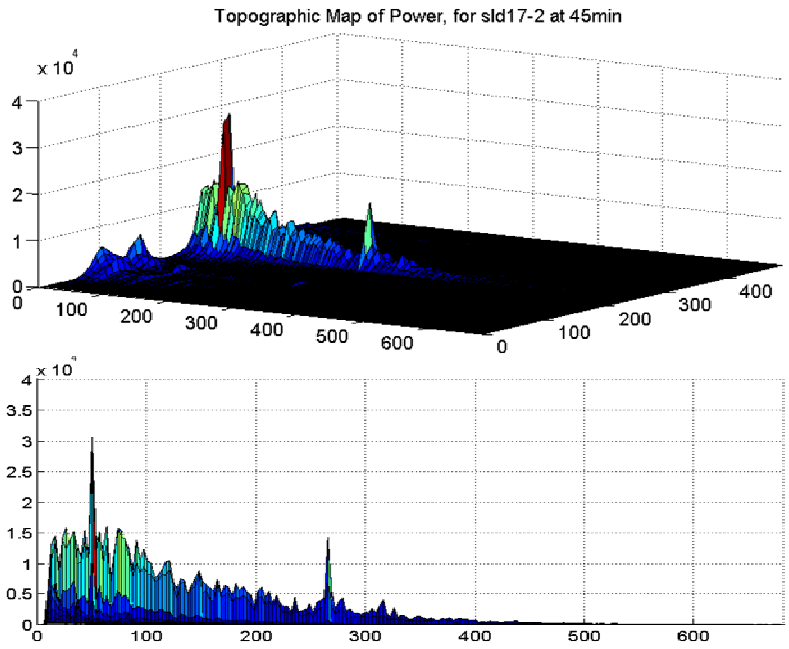

Figure 4-9. Lubricant modulation frequency results for 10k g/mol 10.7 angstrom disk (sld17-2 at 45 min) showing strong frequency peaks at approximately 50 and 265 kHz.

The third highest natural frequency of the ABS is usually the "2nd pitch" mode. This mode corresponds to slider pitch rotation about the middle of the slider in comparison to the "1st pitch" mode which corresponds to slider pitch rotation about the slider trailing edge. While the CMLAir design file is not available for this particular slider, the 2nd pitch frequency is known to be in the 250 kHz range for contemporary femto slider designs. So the lubricant modulation frequency peak seen here at 265 kHz is in the correct range. In this way, it is shown that while the lubricant modulates most strongly at sub-100 kHz frequencies, it can modulate at the ABS natural frequencies.

4.7 Conclusion

Parametric studies of various interface parameters on the lubricant modulation area were performed. The slider form-factor results showed that the modulation area was increased for larger sliders (pico versus femto). This comparison held for slider designs with similar minimum fly-heights and different form factors. The lubricant thickness results showed that modulation area increased for higher lubricant thickness. Similarly, the lubricant molecular weight results showed that modulation area was increased for higher molecular weight. Comparison of Zdol with additives A20H and X1P showed that Zdol + A20H had higher lubricant modulation than Zdol + X1P. Finally, the lubricant modulation frequencies were analyzed with generally strong modulation below 100 kHz. The only strong influence seen was that the high molecular weight disk (Zdol 10.7 Å 10k g/mol) showed strong modulation peaks at 50 and 265 kHz. These peaks are in the range of suspension modes (50 kHz) and pitch modes (265 kHz).

5 Lubricant Relaxation and Recovery

5.1 Introduction

After a slider flies on-track for more than a few seconds, the lubricant profile becomes modulated. After removal of the forces related to the slider's motion, the lubricant will re-flow away from the modulated state towards a uniform undisturbed distribution [1, 2]. The lubricant properties are expected to play a key role in the speed of this recovery, with more mobile lubricant recovering faster. Section 5.2 introduces experimental trends in the relaxation of slider-induced modulation.

Section 5.3 attempts to numerically model the lubricant relaxation. Previous researchers have studied the diffusion of lubricant layers by analyzing the lubricant recovery motion of an artificially introduced step-change in lubricant thickness observed on a half de-lubed disk [3-5]. The analytical simplicity of a step-change in lubricant thickness simplifies their data analysis. In contrast, a straightforward method of studying the recovery of the lubricant after experimental slider-induced modulation is introduced, a scenario that actually occurs in hard disk drives. This method is used to estimate the lubricant diffusion constant based on experimental lubricant modulation.

5.2 Experimental Trends in Relaxation Rate

5.2.1 Calculation of relaxation rate

In a series of experiments, sliders were flown on-track for 20 minutes over a lubricated disk and then unloaded. After slider unloading, the lubricant layer was monitored by OSA scans with the disk still spinning to elucidate the recovery behavior of the lubricant. Experimental conditions were as follows. The 3.5" disk had a 20 angstrom thick lubricant layer (Zdol + X1P, 2000 g/mol). The slider was the WD Femto TFC #1 design, but flew without TFC actuation. Disk rotation and slider radius combined to create a linear speed of 20 to 30 m/s at a skew of 0 deg.

An example plot of a lubricant modulation profile versus relaxation time is shown in Figure 5-1. The modulation pattern after slider unloading is shown in the lower right of the figure. This strong modulation pattern "softens" with increasing relaxation time but the general shape remains. The modulation profiles associated with this figure are shown in Figure 5-2

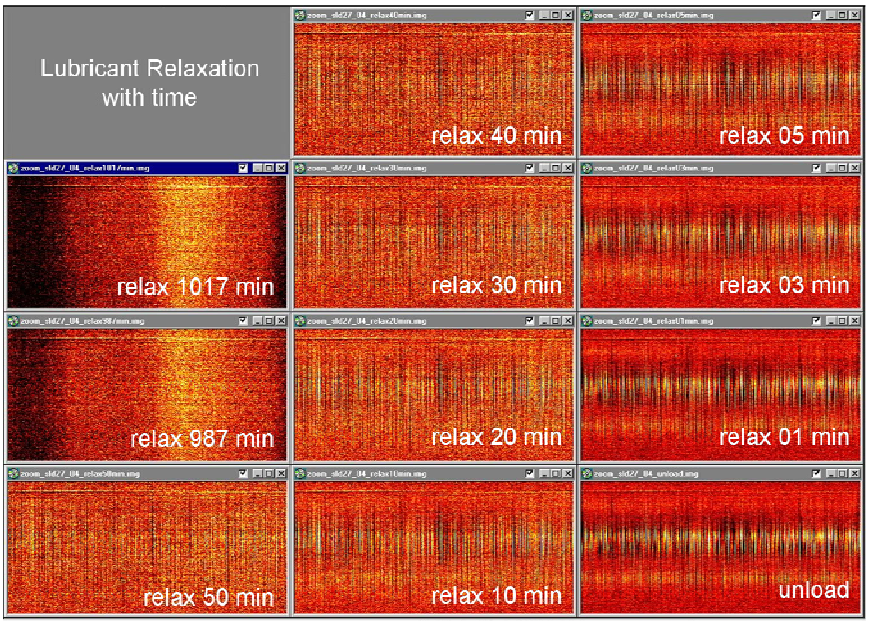

Figure 5-1. OSA scans of a modulated lubricant track recovering with increased relaxation time.

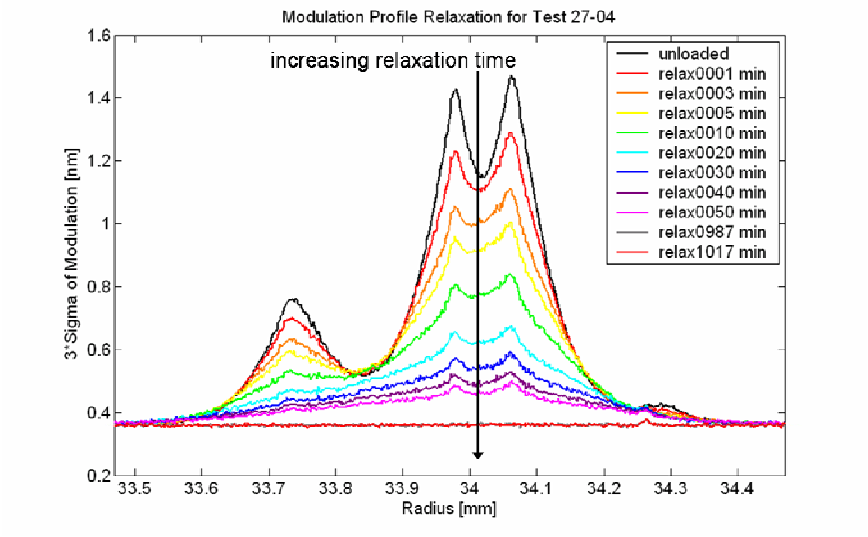

Figure 5-2. Lubricant modulation profiles taken from Figure 5-1. Largest profile is associated with the data taken immediately after slider unload, with the profile reducing in magnitude with increasing relaxation time.

Figure 5-2 shows that during the first 10 minutes of relaxation, the triple-peak modulation profile is visible. Beyond 30 minutes of relaxation, the profile has changed to the point that the third modulation peak is no longer visible.

Seven repeated tests on the same disk were conducted and the modulation profiles were calculated. The modulation areas of these profiles are shown in Figure 5-3, plotted versus relaxation time.

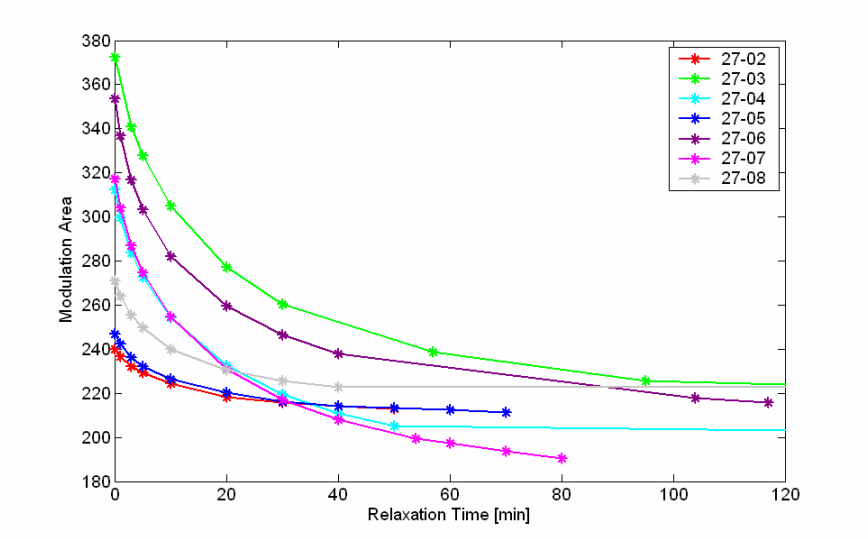

Figure 5-3. Relaxation of lubricant modulation area, before zeroing and scaling.

This figure makes it appear that the lubricant relaxation is not repeatable between repeated experiments. Instead of plotting the straight modulation area, two analysis steps are taken. First, the modulation area is "zeroed" so that a perfectly flat modulation profile (no modulation peaks) will produce a modulation area of zero units. This zeroing is identical to shifting the modulation profiles (not shown) so that the 3*sigma value of each test is zero at the edge of the data. Second, the zeroed data is scaled such that the modulation area at slider unloading is exactly one unit. This is

done by dividing all the results by the modulation area at slider unloading. This scaling is done so that comparisons can be made between results with different initial modulation levels as seen in Figure 5-3. Equation 5.1 shows how these two analysis steps would be implemented in a data processing code, where Y is the unadjusted modulation area, Y_{base} is the modulation area associated with a flat modulation profile, Y_{unload} is the modulation area at the unload scan, and Y_{new} is the adjusted modulation area. Each experiment will have unique values of the scaling parameters Y_{base}, Y_{unload}.

$$Y_{new} = (Y - Y_{base})/(Y_{unload} - Y_{base}) \quad (5.1)$$

The modulation area resulting from applying Equation 5.1 to seven individual trials is shown in Figure 5-4. It is clear that this zeroing and scaling method is useful for collapsing seemingly different relaxation results into a tighter curve (compare Figure 5-3 to Figure 5-4). From these results, the average trend and error bars are found and plotted with the best-fit logarithmic curve in Figure 5-5.

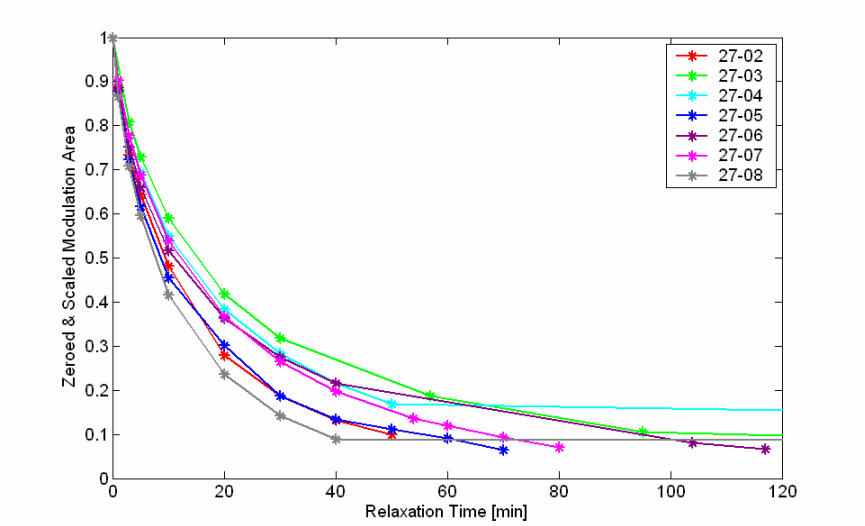

Figure 5-4. Adjusted lubricant modulation area versus time for seven individual trials.

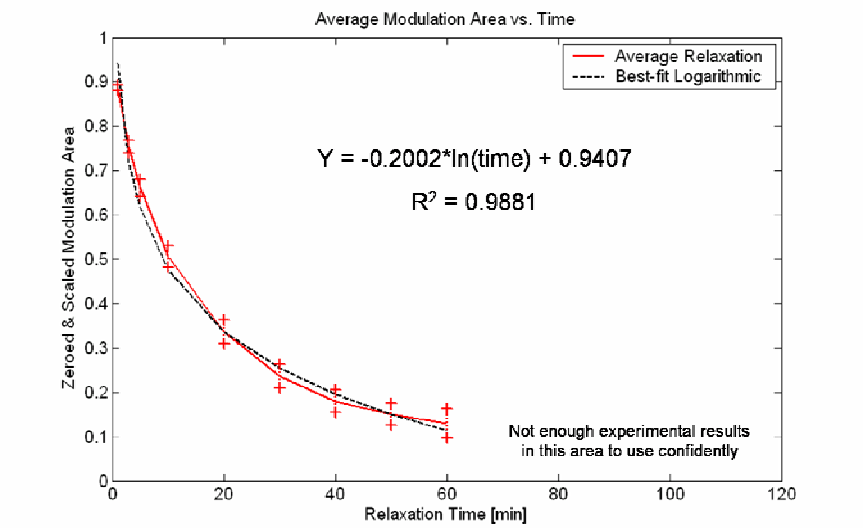

Figure 5-5. Average lubricant relaxation trend and best-fit logarithmic curve for data in Figure 5-4.

The average trend was only calculated out till 60 minutes of relaxation, as the number of relaxation scans beyond 60 minutes was too low for confidence in the average. The logarithmic best-fit line is given by Equation 5.2

$$Y = -0.2002 * \ln(\text{time}) + 0.9407, \qquad \text{for } 0 \leq \text{time} \leq 60 \text{ min} \qquad (5.2)$$

with an R^2 value of 0.9881, showing very good fit to the experimental data. Before exploring the predictive ability of this equation, an observation can be made about the relaxation trend. Notice the extreme changes that occur during the first few minutes of relaxation. After only 10 minutes of lubricant relaxation, the modulation area is approximately half as large as it was at slider unloading (0 minutes relaxation). This is a significant observation, as it highlights the importance of controlling the time delay between any experiment and the scanning of the disk to measure the lubricant response. In labs where in-situ experiments are not feasible, the delay between the

end of an experiment and the scanning of the disk should be very closely noted when comparing results. Any experiments with a large delay before disk scanning may show an artificially low lubricant disturbance, more indicative of the scanning delay than the conditions at the slider-disk interface.

5.2.2 Predictive ability of relaxation rate

With the best-fit logarithmic line introduced in Section 5.2.1, its use as a predictive tool is explored. Since this best-fit line was calculated using a set of experiments with similar interface conditions, it is expected to have predictive ability in regards to another experiment conducted in the same conditions. One such experiment exists, where the interface conditions were similar to those used to create the best-fit line. However, this experimental data was not used in finding the average trend, so it had no influence on the best-fit line.

Experimental conditions were as follows. The 3.5" disk had a 20 angstrom thick lubricant layer (Zdol + X1P, 2000 g/mol). The slider was the WD Femto TFC #1 design, but flew without TFC actuation. Disk rotation and slider radius combined to create a linear speed of 20 m/s at a skew of 0 deg. The slider was loaded on an adjacent track, moved radially onto the test track, and remained for 20 minutes at which time the slider was unloaded directly from the test track. The OSA scans examined here were taken after slider unloading, and after relaxation of 37, 50, and 60 minutes.

Because the lubricant modulation at slider unloading is known, the zeroing and scaling is possible, as described above. The prediction of the best-fit line, along with the data points, is given in Figure 5-6.

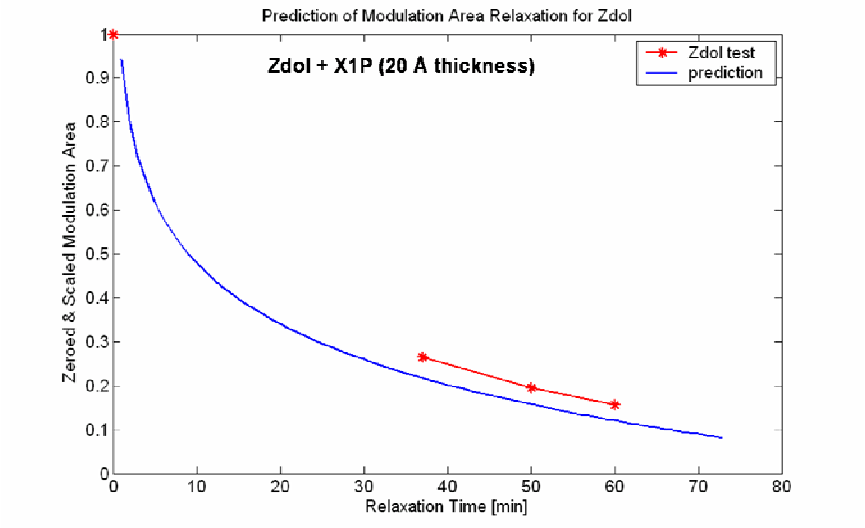

Figure 5-6. Best-fit prediction (solid blue) and experimental data (red asterisks) of lubricant modulation area relaxation vs. time for Zdol + X1P.

At these three data points, the prediction error is around 20%. This is not a superb prediction, but it gives a ballpark estimation of the actual lubricant modulation area at these later times, based solely on the modulation at slider unloading. Thus, the usefulness of the best-fit logarithmic line is shown in predicting the relaxation of lubricant modulation induced at similar slider-disk interfaces.

5.2.3 Effect of lubricant properties on relaxation rate

As the lubricant relaxation rate is intimately related to the lubricant properties, it is expected that a substantial change in lubricant will produce a similarly substantial

change in the equation of the best-fit logarithmic relaxation line. To study the effect of lubricant properties on the modulation relaxation rate, an experiment was performed using Ztetraol and compared to the results just presented using Zdol + X1P.

Experimental conditions were as follows. The 3.5" disk had a 15 angstrom thick lubricant layer (Ztetraol, 3000 g/mol). The slider was the WD Femto TFC #1 design, but flew without TFC actuation. Disk rotation and slider radius combined to create a linear speed of 20 m/s at a skew of 0 deg. The slider was loaded on an adjacent track, moved radially onto the test track, and remained for 20 minutes at which time the slider was unloaded directly from the test track. The OSA scans examined here were taken after slider unloading, and after relaxation of 1, 3, 5, 10, 20, 30, 40, 50, and 63, and 73 minutes.

Figure 5-7 presents the experimental measurements of lubricant modulation area, after zeroing and scaling, versus time. The best-fit logarithmic line is also presented. Again, the logarithmic trend describes the data very well, with an R^2 value of 0.9922. The equation of this logarithmic best-fit line is given by Equation 5.3

$$Y = -0.12*\ln(\text{time}) + 0.9368, \qquad \text{for } 0 \leq \text{time} \leq 72 \text{ min.} \qquad (5.3)$$

In 10 minutes, this equation predicts a modulation area approximately 66% of the original value. This value is larger than the 50% predicted by the Zdol + X1P curve, but is still a substantial change in lubricant modulation from the original value (at slider unload). These two best-fit logarithmic equations can be compared in Figure 5-8, extended to 70 minutes.

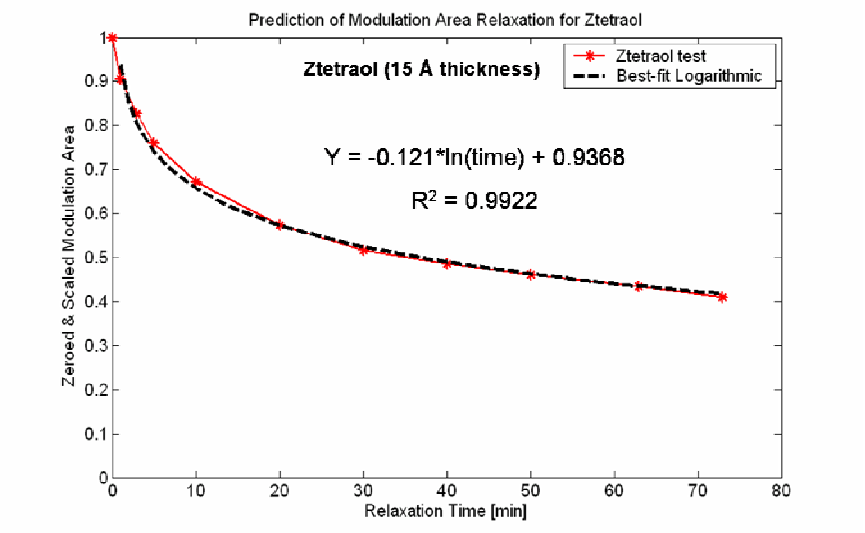

Figure 5-7. Experimental modulation area vs. time for 15 angstroms Ztetraol, with best-fit logarithmic line.

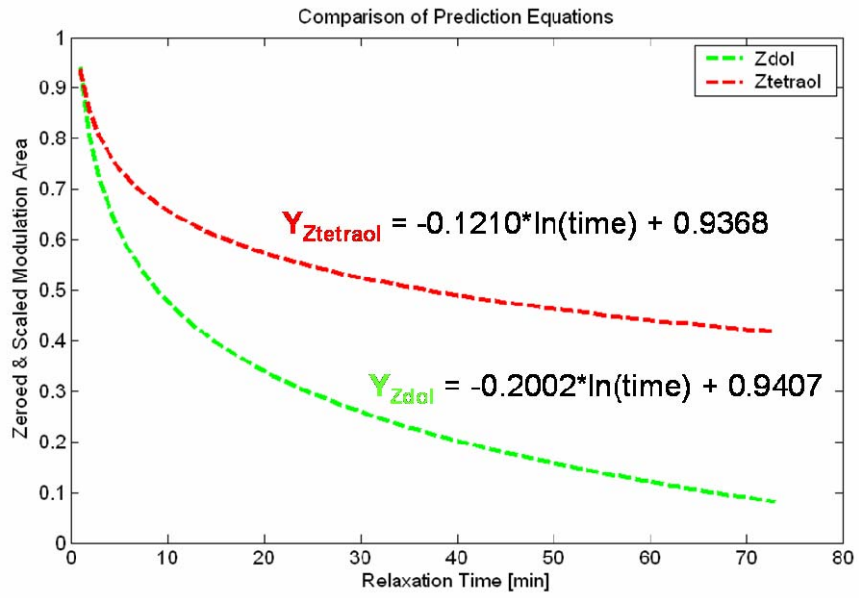

Figure 5-8. Best-fit logarithmic predictions for Zdol + X1P (20 ang) and Ztetraol (15 ang) with equations.

In comparing the best-fit equations, it appears that the offset does not vary much between the two equations. However, the coefficient of the ln term changes drastically. Qualitatively, Ztetraol is less mobile and more highly bonded to the carbon layer than Zdol. This lower mobility is due to Ztetraol's two polar endgroups as compared to Zdol's single polar endgroups. This difference in mobility could explain why the Ztetraol results relax at a slower rate than the Zdol results.

Further relaxation experiments were conducted using disks of identical lubricant type (Zdol) and similar lubricant thicknesses (10.1 and 10.7 Å), but significantly different molecular weight (2000 vs. 10,000 g/mol). After a 20 minute on-track flyability test, the relaxation of the lubricant modulation area was monitored. Averaging over multiple attempts, the average relaxation of lubricant modulation area is given in Figure 5-9.

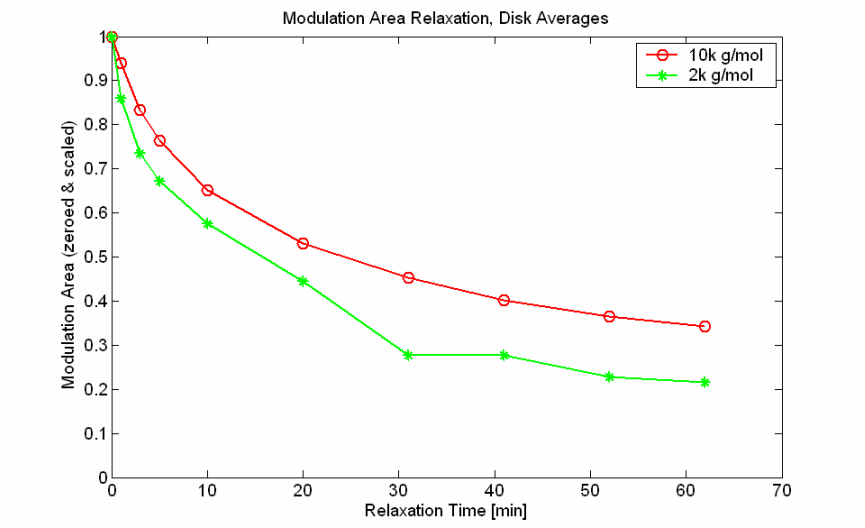

Figure 5-9. Relaxation of Lubricant Modulation Area, by lubricant molecular weight.

Relaxation equations can also be fitted to these results. In this case, a slightly modified form of the relaxation equation will be used. Considering that the previous offset values did not change much between two very different lubricants, one can modify the relaxation equation to be

$$Y = 1 - \text{alpha}*\ln(\text{time}+1). \quad (5.4)$$

Modifying the argument of the logarithm is done to allow the equation to have a value at the unload scan (relaxation time of 0 minutes) since the logarithm of zero is undefined. Also, the offset is no longer a separate parameter; instead it is set to exactly unity. At the unload scan, the argument of the logarithm is one, so the second term is zero. The zeroing and scaling method described earlier ensures that the modulation area at the unload scan is always one. Thus, these two changes allow the fitted equation to be used over the entire range of times as well as reduce the fit parameters from two to one.

The results of using this new fit equation on the molecular weight results shown in Figure 5-9 is shown in Figure 5-10 with both average trends and a series of fit equations with different pre-logarithmic parameters.

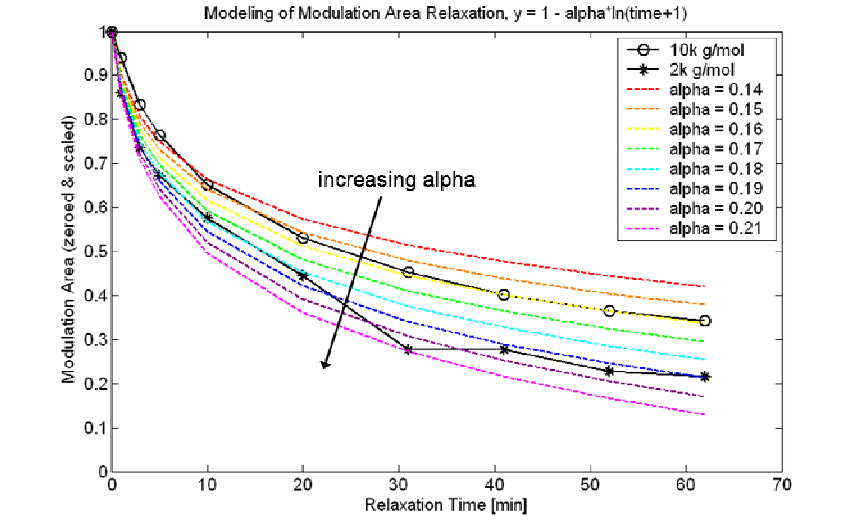

Figure 5-10. Fitting Equation 5.4 to average relaxation trends for 10k and 2k g/mol Zdol.

From these fitting equations, it appears that the pre-logarithmic parameters are approximately 0.16 for the 10k g/mol average and 0.19 for the 2k g/mol average. Again, it is clear that one trend relaxes slower than the other. In this case, the higher molecular weight lubricant relaxes slower than the lower molecular weight. It is known that higher molecular weight lubricant has a smaller diffusion coefficient, causing it to recover more slowly than lower molecular weight lubricant [5].

Plotting the change of pre-logarithmic fit parameter against the molecular weight of the lubricant tested yields the trend in Figure 5-11. While only two data points does not make a robust trend, it is clear that a decrease in lubricant molecular weight is associated with an increase in the pre-logarithmic fit coefficient.

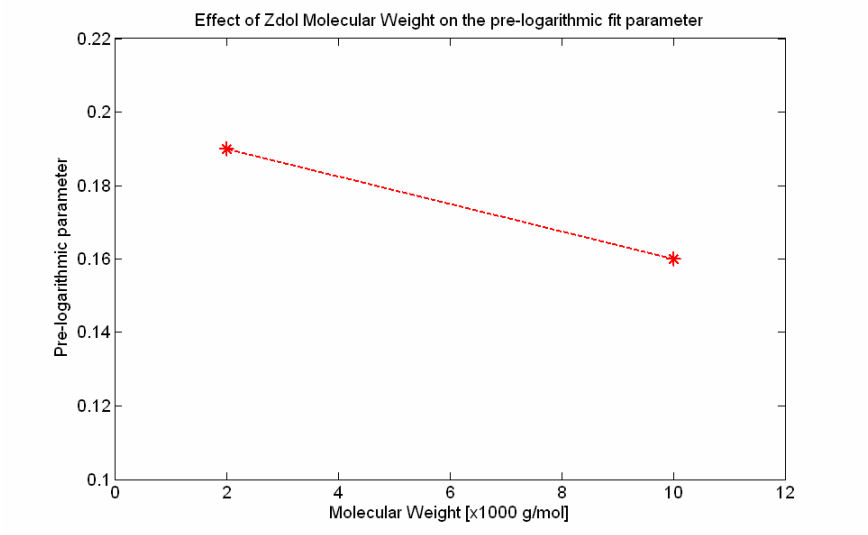

Figure 5-11. Variation in pre-logarithmic fit parameter with lubricant molecular weight.

5.2.4 Frequency effect on relaxation rate

The analysis presented in Section 5.2.3 considered the lubricant modulation at all frequencies above 10 kHz. Further analysis is possible, focusing on the lubricant relaxation rate in terms of modulation frequency. The same data from the previous section can be band-pass filtered at the following frequency ranges (Table 3-1).

Table 3-1. Frequency ranges for relaxation rate analysis

Group #	Frequency Range [kHz]
1	10 and above
2	10 – 20
3	20 – 30
4	30 – 40
5	40 – 50
6	50 – 60
7	60 – 70
8	70 – 80
9	80 - 90

10	90 - 100

Figure 5-12 shows an example of the lubricant modulation associated with these frequency ranges, taken from the unload scan of one experiment. The y-scale is shared between all nine plots, so it becomes clear that lower frequencies have much larger modulation than higher frequencies. Other experiments show similar results. With the data bandpass filtered into the frequency bands detailed in Table 3-1, the modulation area of each frequency band can be found. The averaging over all experiments is done after calculation of the modulation area.

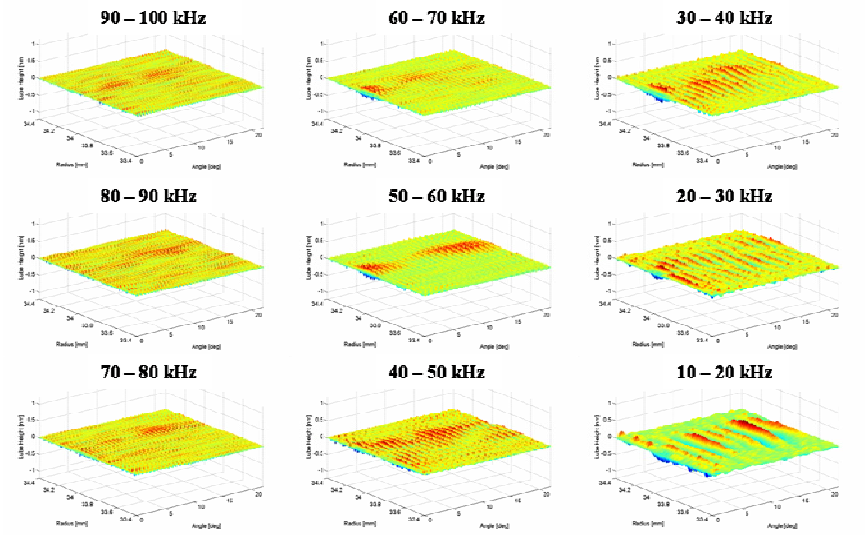

Figure 5-12. Example of lubricant modulation associated with 10 kHz frequency ranges from 10 to 100 kHz for a randomly chosen section of one experiment. X-axis (angle) is approximately 22 degrees long, Y-axis (radius) is 1 mm wide, and Z-axis (lube height) is from -1.2 to +1.2 nm.

Figure 5-13 shows the modulation profile associated with each of the subplots in Figure 5-12. This figure shows how the frequency band influences the lubricant

modulation profile. It is clear that the general shape of the modulation profile is maintained throughout all the frequency bands, but the magnitude strongly depends on the frequency band. Figure 5-14 shows the modulation profile associated with the same frequency bands, but after 10 minutes of relaxation time. It is clear that during the 10 minutes that elapsed between Figure 5-13 and Figure 5-14, the higher modulation frequencies relaxed away much quicker than the lower frequencies. It is worth noting that the change in lubricant modulation profile due to frequency band is similar to the change in lubricant modulation profile due to relaxation time. It is important to distinguish between these two trends as they explain different phenomena.

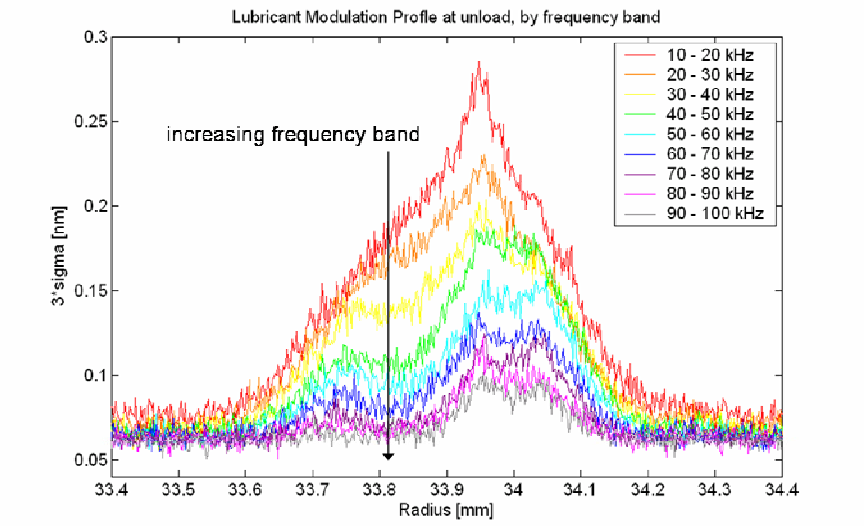

Figure 5-13. Lubricant Modulation Profile at slider unloading, by frequency band. Lower frequencies are associated with higher lubricant modulation.

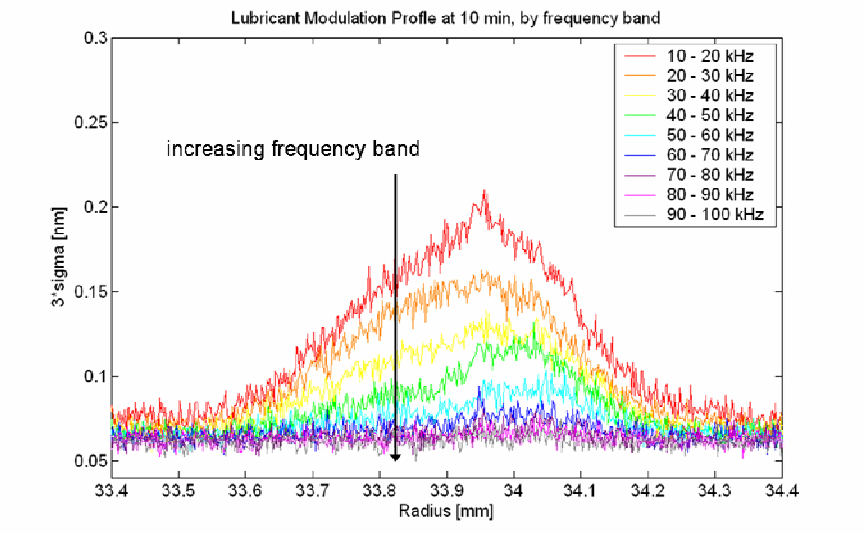

Figure 5-14. Lubricant Modulation Profile after 10 minutes of relaxation, by frequency band. Same y-scale as Figure 5-13.

With the experimental lubricant modulation data bandpass filtered into 10 kHz wide bands, the relaxation behavior of the lubricant can be analyzed in terms of modulation frequency. The change in modulation profile versus time associated with each frequency band is analyzed separately, similar to the analysis in Section 5.2.1. Again, seven experiments under similar experimental conditions are analyzed and averaged to find the average modulation area (after scaling and zeroing) versus time. Figure 5-15 shows the modulation area versus time for each frequency band, making it very obvious that the modulation associated with higher frequencies relaxes quicker than that associated with lower frequencies.

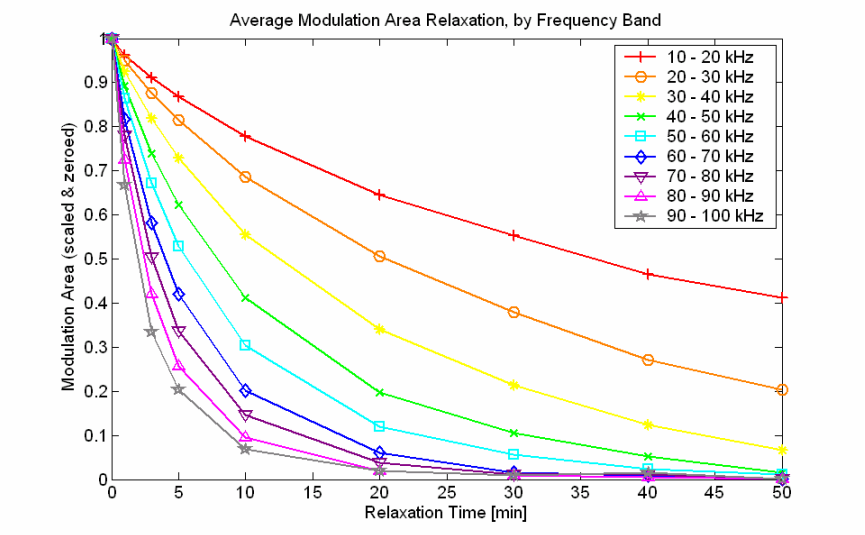

Figure 5-15. Average modulation area versus time, sorted by frequency band.

Having calculated these trends, best-fit curves can be found. Three equations were tried, a two-parameter logarithmic curve

$$\text{modarea} = a*\text{LN}(\text{time}_{relax}) + b, \tag{5.5}$$

a two-parameter exponential curve

$$\text{modarea} = a*\text{EXP}(b*\text{time}_{relax}), \tag{5.6}$$

and a one-parameter exponential curve

$$\text{modarea} = \text{EXP}(a*\text{time}_{relax}). \tag{5.7}$$

An example of how these three different equations describe the data to varying degrees is given in Figure 5-16.

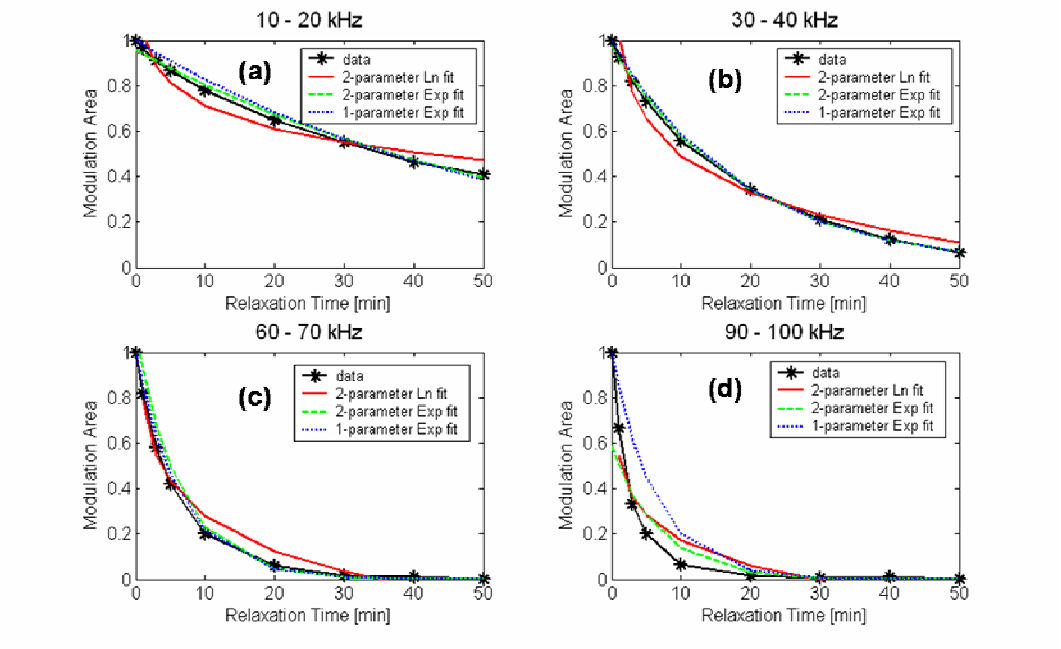

Figure 5-16. Example of three best-fit equations, as fitted to (a) 10 – 20 kHz band, (b) 30 – 40 kHz band, (c) 60 – 70 kHz band, (d) 90 – 100 kHz band. Experimental data (solid, asterisks), 2-parameter Ln fit (solid), 2-parameter Exp fit (dashed), 1-parameter Exp fit (dotted).

In the 10 – 20 kHz band (Figure 5-16(a)), the Ln fit curve under predicts at short relaxation times and over predicts at long relaxation times. This contrasts to the Exp fit curves which over predict at short times and under predict at long times. In the 30 – 40 kHz band (Figure 5-16(b)), the Exp fit curves describe the data very well. In the 90 – 100 kHz band (Figure 5-16(d)), all three curves begin to not be able to capture the characteristics of the relaxation trend. The R^2 "degree of fitness" of these three curves is plotted versus frequency band in Figure 5-17. The R^2 value comes from a standard root-mean-squared calculation.

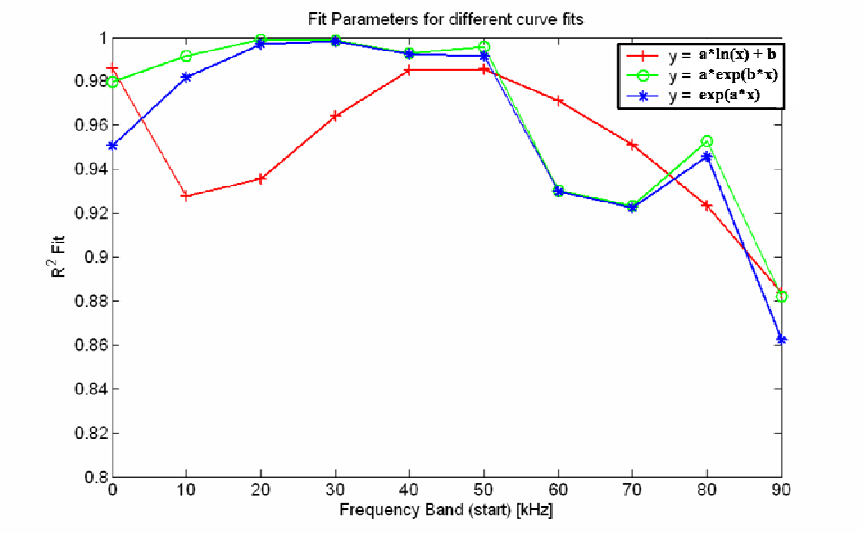

Figure 5-17. R^2 fit value for three curve fit equations versus frequency band.

The R^2 values are plotted using the start of the frequency band of interest as the x-coordinate and the R^2 value as the y-coordinate. For example, the data points located at 30 kHz on the x-axis represent the R^2 fit values for the three fit equations when applied to the lubricant modulation that occurs between 30 and 40 kHz. The data points located at 0 kHz represent how well the equations describe all the variation data (above 10 kHz) as described in Section 5.2.1. In contrast to the logarithmic trend used to describe the 10 kHz and above relaxation (Equation 5.2), it was found that, based on the R^2 value, the two-parameter exponential trend (Equation 5.6) describes the data in Figure 5-15 best.

However, the one-parameter exponential trend is worth considering based on another criteria. In Section 5.2.1, the scaling and zeroing procedure is described. Because of the scaling part of the procedure, the adjusted modulation area at slider unload (0 minutes) will always be exactly equal to one. Additionally, the adjusted

modulation area will always asymptote to zero at long relaxation times because of the zeroing part of the procedure. These two considerations give some qualitative restrictions on the prediction equations that will be most useful in describing the relaxation of the modulation area. The logarithmic fit equation does not satisfy either of these two restrictions, even though it has superior descriptive power when all frequencies of the lubricant modulation are considered together. Both exponential fit equations have the characteristic of asymptoting to zero at long relaxation times. However, only the one-parameter equation always gives adjusted modulation area of one unit at zero relaxation time. Finally, the R^2 values of the two exponential equations are generally comparable, especially at the sub-50 kHz frequencies where most lubricant modulation occurs. For reasons of qualitative characteristics (starting at unity, asymptoting to zero) and good R^2 fit to the data, the one-parameter exponential equation is chosen as the best descriptor of the frequency-based lubricant relaxation data.

Having established that the one-parameter exponential equation describes the data best, the variation of that one parameter can be plotted versus frequency band. Figure 5-18 shows how the exponential parameter changes with different frequency bands.

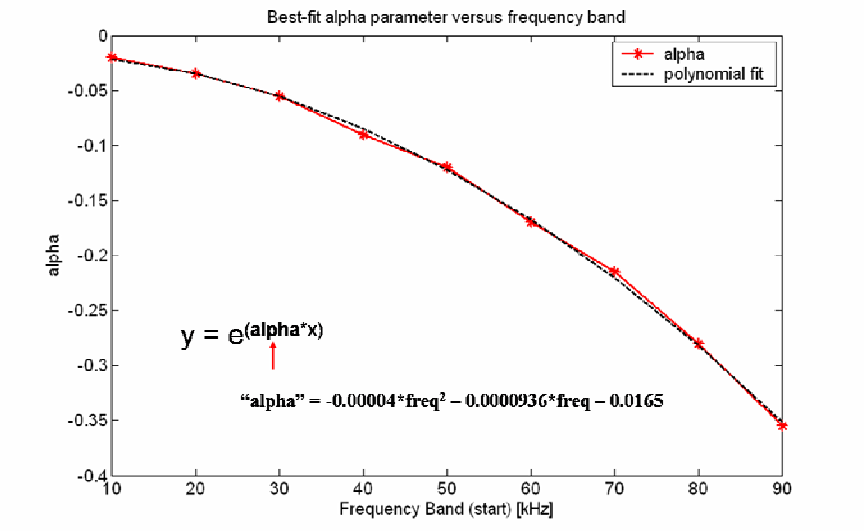

Figure 5-18. Variation of the exponential parameter "a" versus frequency band (solid red line with asterisks) and linear trendline of this variation (black dotted line).

The exponential parameter "alpha" varies in a quadratic trend with frequency band. The equation given in the figure is a best fit trendline describing how increasing the frequency band changes the exponential parameter. With this exponential parameter determined by the frequency band of interest using the equation, the relaxation of the lubricant modulation area with time can be predicted. For example, if the relaxation rate at 35 kHz is of interest, the exponential parameter is predicted to be "alpha" = -0.0655.

$$\text{alpha}_{\_35\text{kHz}} = (-0.00004)*(35^2) - (0.000093)*(35) - (0.0165)$$

$$= -0.0655$$

After substituting this value of alpha into Eqn 5.6, the prediction equation is found. The "relaxation factor", $e^{(-0.0655*\text{time})}$, is the fraction of the unload modulation area that will remain after the specified amount of lubricant relaxation time.

Table 3-2. Predicted Relaxation Factors for 35 kHz modulation

time	Relaxation Factor
0 min	1.0000
1 min	0.9366
3 min	0.8216
5 min	0.7207
10 min	0.5194
20 min	0.2698
30 min	0.1402
40 min	0.0728
50 min	0.0378
60 min	0.0196

5.3 Experimental Estimation of Lubricant Diffusion Constant

The approximate diffusion rate, D, for Zdol has been reported by previous researchers in the range of 0.3×10^{-12} to 7.5×10^{-12} m^2/s. Zhao et al. [6] reported D = 0.3×10^{-12} m^2/s for Zdol of about 3000 g/mol and 2.3 nm thickness. Dai et al. [7] reported D = 2.37×10^{-12} m^2/s for Zdol of 4000 g/mol and 1.0 nm thickness. Ma et al. [5] showed variation of the thickness-dependent diffusion constant for 1860 g/mol Zdol between 1 to 2 nm to range between 3×10^{-12} m^2/s and 7.5×10^{-12} m^2/s. Considering these differing reported values of Zdol's diffusion constant, a method of estimating the lubricant's diffusion constant from normal slider-induced lubrication results is useful.

The usual method of measuring the diffusion constant of a lubricated disk is by tracking a half-delubed step as it spreads across a disk, the "Matano interface method" [3-5]. While this method introduces a very distinct starting condition, it is only loosely similar to the type of lubricant modulation actually observed in operating hard drives. The half-delubed step is often a few to ten nanometers high while slider-induced lubricant modulation peaks are more often in the sub-nanometer height range. Expected uses of the experimentally determined diffusion constant are related to lubricant depletion/buildup or lubricant modulation/relaxation. Since lubricant modulation is a normal phenomenon in operating hard drives, diffusion constants estimated from relaxation of experimental modulation profiles are more true to the intended use of the parameter. Also, experimental modulation profiles can be easily measured without ruining a disk, as is necessary for a half-delubed step measurement.

5.3.1 Finite-Difference Simulations of Point-by-Point Lubricant Relaxation

In Section 5.2, the relaxation rate of the slider-induced lubricant modulation was analyzed in terms of the modulation profile and modulation area, both global measurements of the lubricant modulation. Another method of analyzing the relaxation of the slider-induced lubricant modulation is based on the conventional diffusion equation [8].

$$dh/dt = \Delta \cdot (D \Delta h) \tag{5.8}$$

The two-dimensional form of this equation, assuming constant D, is

$$dh/dt = D[d^2h/dx^2 + d^2h/dy^2] \tag{5.9}$$

Analysis of the OSA lubricant thickness relaxation scans shows clear spreading in both the angular and radial directions. Thus, we are using the two-dimensional form of this equation because our lubricant thickness data is two-dimensional. Taking the lubricant distribution after slider unloading as the initial condition, the diffusion equation can be used to simulate the relaxation of the slider-induced lubricant modulation.

5.3.2 Numerical Implementation

Numerical implementation of the 2D diffusion equation is as follows. The initial conditions for the simulation were the experimental lubricant thickness measurements taken just after slider unloading after a 20-minute on-track flyability test. These lubricant thickness measurements were stored as a matrix in Matlab (see Section 2.7). A simple finite-difference method (central difference) was used to calculate the second derivatives of lubricant height (d^2h/dx^2 and d^2h/dy^2) from the lubricant height matrix.

$$d^2h/dx^2(i,j) = [h(i+1,j) - 2*h(i,j) + h(i-1,j)] / delx^2 \qquad (5.10)$$

$$d^2h/dy^2(i,j) = [h(i,j+1) - 2*h(i,j) + h(i,j-1)] / dely^2 \qquad (5.11)$$

Where h(i,j) is the lubricant height at measurement point (i,j), delx is the radial step-size, and dely is the angular step-size. Both step sizes are determined by the resolution of the experimental data. The lubricant height matrix is updated in time using

$$h\_new = h\_old + (dh/dt)*delt \qquad (5.12)$$

Where h_new is the height matrix after the current time step, h_old is the height matrix at the previous time step, dh/dt is the change in height due to diffusion, and delt

is the simulation time step. A series of nested loops is used to find the point-wise dh/dt values and to evolve the height matrix in time. For the experimental data used here, delx = 2×10^{-6} m, dely = 2.6×10^{-5} m, and delt = 0.01 sec. The diffusion constant, D, was varied to match the experimental relaxation data. See Appendix B for the associated Matlab code.

5.3.2.1 Initial and Boundary Conditions

The initial conditions for the numerical simulation were based on the experimental "unload" OSA scan, taken just after the end of a twenty-minute flyability test (1mm x 22 deg). The data was bandpass filtered in Matlab from 10 to 100 kHz in the angular direction and low-pass filtered at ~40 um in the radial direction to minimize measurement noise. Figure 5-19 shows that the application of radial low-pass filtering at ~40 um only removes the noise in the data, not significantly affecting the shape or magnitude of the modulation.

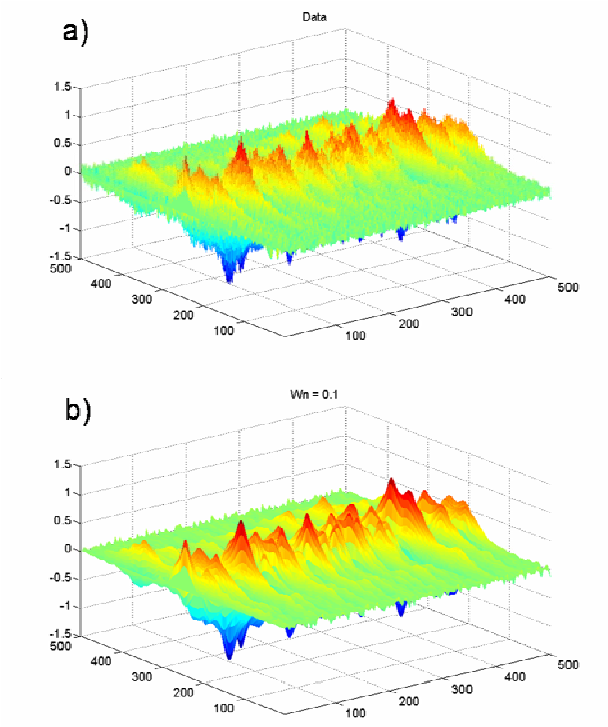

Figure 5-19. Lubricant Height for Experimental data, (a) before radial filtering and (b) after radial filtering at ~40 um. X-axis is the angular data point (0 to 600), Y-axis is the radial data point (0 to 500), and Z-axis is lubricant thickness [nm] (-1.5 to 1.5).

Analysis of the actual modulation profiles before and after radial filtering shows very little change in the modulation profile under the slider's path, and some change in the modulation profile outside the slider's path (Figure 5-20). Since we are mainly interested in the slider-induced modulation, the radial filtering method described here is effective in reducing the noise in the data without significantly affecting the data. The most obvious change is that the modulation outside the slider's path (near the edges of the profiles) is closer to zero. Analysis of the modulation area (Section 2.8.2) will ignore these areas, so the difference is not important.

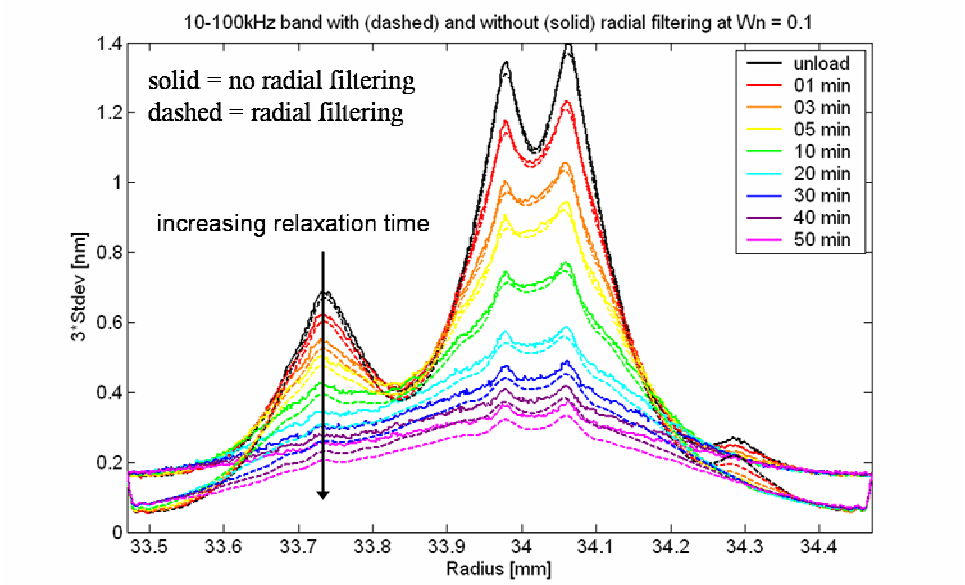

Figure 5-20. Modulation Profiles for Experimental data, without radial filtering (solid) and with radial filtering at ~40 um (dashed).

Only the first 22 degrees of angular data (500 data points) were used to reduce the size of the simulation. The modulation profile in this 22 degree section matched very well with the 360 degree modulation profile, ensuring that the simulation

captured the important experimental features. The angular boundary condition was periodic, a simplification since the 22 degree data set is not actually periodic (as the 360 degree data set would be). Ignoring the first and last degree of simulated data effectively eliminates this inaccuracy. Because there was negligible lubricant disturbance outside the slider's width, the radial boundary condition was also periodic (1 mm wide data and a 0.8 mm wide slider). As the radial boundary data showed artificial noise with application of this periodic condition, the first and last 100 um of simulated data was ignored.

5.3.3 Simulation Results

After implementing the finite-difference diffusion simulation described, lubricant modulation profiles at increasing relaxation times are produced. The results presented here are from a 1 mm x 22 deg section of one experimental data set, with simulated relaxation time of 50 minutes (300,000 time steps). Direct comparison between the experimental height matrix and modulation profiles is possible.

Pointwise comparison of the lubricant height matrices shows how well the simulation captures the point-by-point features of the relaxing lubricant modulation. Figure 5-21 compares the experimental and simulated lubricant height matrices at 20 minutes of relaxation time. Subplot (a) shows the actual lubricant height matrix at 20 minutes of relaxation time (from the experimental data). Subplot (b) shows the simulated lubricant height matrix at 20 minutes of simulated relaxation. Subplot (c) shows the difference between the simulated and actual lubricant height, with the

colorbar from -0.15 nm to 0.2 nm. Subplot (d) shows the modulation profiles for the actual (solid) and simulated (dashed) data.

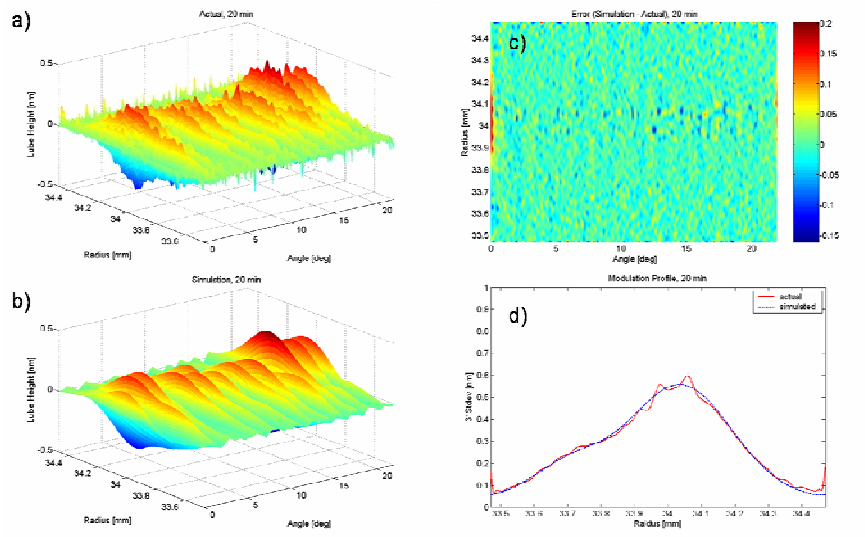

Figure 5-21. Comparison of actual and simulated relaxation of lubricant modulation at 20 minutes: a) actual lubricant height data b) simulated lubricant height data c) error (simulated – actual) d) modulation profiles for actual (red, solid) and simulated (blue, dashed) lubricant modulation.

After 20 minutes (120,000 time steps) of simulated relaxation, the simulated lubricant height remains very close to the actual lubricant height. The error plot (Figure 5-21c) shows errors scattered over the entire simulation area. These errors could be reduced by lowering the radial low-pass filter cutoff from ~40 um to something lower. However, the main modulation features remain well captured, and the simulated modulation profile matches the experimental modulation profile very closely (Figure 5-21d).

This type of comparison can be done between the experimental relaxation measurements and simulated data at 1, 3, 5, 10, 20, 30, 40, and 50 minutes of relaxation. Figure 5-22 shows the modulation profiles of the experimental measurement and simulated data.

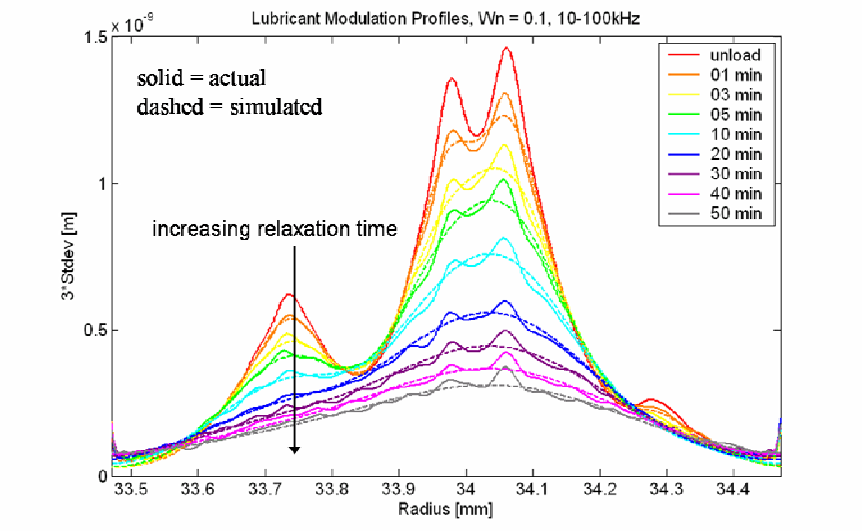

Figure 5-22. Modulation profile comparison between experiments (solid) and simulation (dashed).

From Figure 5-22 it appears that the simulations are accurately capturing the relaxation of the modulation profile. This simulation used a diffusion constant of D = 5.5×10^{-12} m^2/s. Other simulations were run with diffusion constants of 5.0 and 6.0×10^{-12} m^2/s. Analysis of the modulation areas for these three different diffusion constants can be used to see which simulation most closely matches the experimental modulation areas. Figure 5-23 shows the relaxation of the modulation area for the experimental data and these three simulations. While all three simulations follow the general trend of relaxing modulation area, the simulation at D = 5.5×10^{-12} m^2/s matches the experimental data the best.

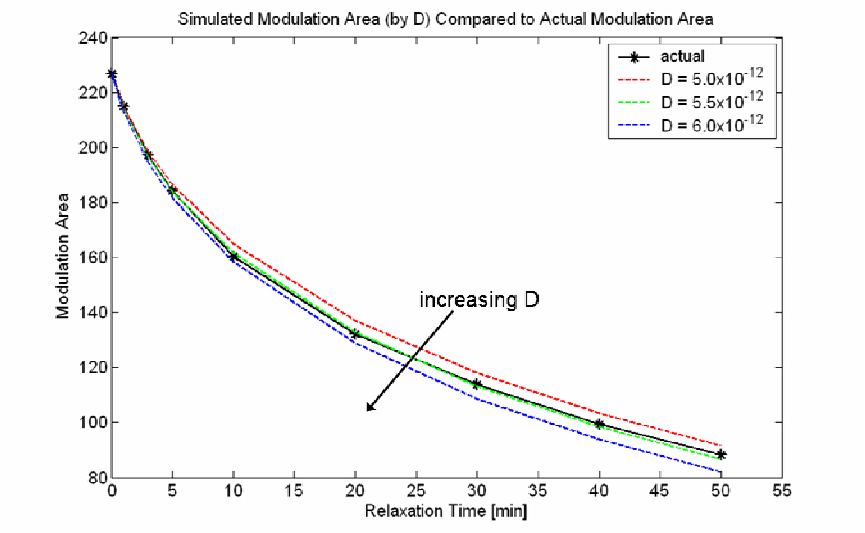

Figure 5-23. Comparison of actual modulation area (black, asterisks) and three simulated modulation areas (dashed) for D = 5.0x10^{-12} (red), 5.5x10^{-12} (green), and 6.0x10^{-12} (blue) m^2/s.

For this lubricant (Zdol+X1P 2000g/mol 2nm), the best-fit diffusion constant from numerical simulations was 5.5x10^{-12} m^2/s. While not exactly the same type of lubricant, other researchers have reported values for the diffusion constant of Zdol that are near this value; 2.37x10^{-12} m^2/s [7] and ~3x10^{-12} m^2/s [5]. Those reported values were for Zdol without additives. X1P is known to increase the lubricant mobility, and thus the diffusion constant [9]. Thus, the simulation-based estimate of diffusion constant is reasonable when considering that the lubricant types are not exactly identical.

The above described finite-difference simulation method was used to simulate the relaxation of a second lubricant (Zdol, 10.7 Å, 10,000 g/mol) after 20 minutes of slider-induced modulation. Again, the initial condition for the simulation was the experimental measurement of the lubricant modulation after unloading of the slider.

The results of the series of simulations are given below, expressed through the relaxation of modulation area (actual vs. simulated) for different simulated diffusion constants.

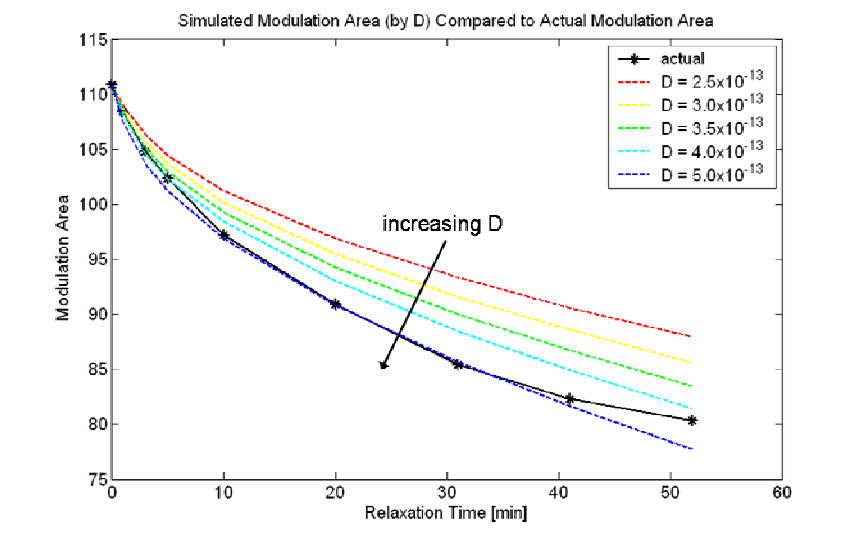

Figure 5-24. Comparison of actual modulation area (black, asterisks) and simulated modulation area for five different diffusion constants, D = 2.5 through 5.0x10^{-13} m^2/s.

Based on the modulation area relaxation curve, it appears that the simulations suggest a diffusion constant of 4-5x10^{-13} m^2/s for this lubricant. Examination of Ma et al.'s plots for the diffusion constant of Zdol at 1 nm thickness suggests a diffusion constant less than 1.0x10^{-12} m^2/s. Their data (ref. Figure 3) plots the diffusion constant for Zdol of 1860 g/mol up to 5560 g/mol. The trend is towards smaller diffusion constant for higher molecular weight, so the result of approximately 0.5x10^{-12} m^2/s is within the expected range of values.

5.4 Conclusion

In Section 5.2, experimental studies of the lubricant relaxation are presented. First, a zeroing and scaling method is introduced to allow comparison of results with different initial lubricant modulation levels. Then, this method is used to collapse a set of data into a tighter grouping for averaging. For the disk used in this example, ten minutes of relaxation gives a reduction of modulation area by 50% of the original value. Clearly, the lubricant relaxation occurs quickly after slider unloading and any systematic delay between the end of a test and scanning of the disk will introduce errors in any analysis. Next, the predictive ability of the lubricant relaxation trend is shown by using the average relaxation trend (two-parameter logarithmic curve) to predict the relaxation of another experimental result. While the prediction error is around 20%, the prediction is useful for ballpark estimations of lubricant relaxation based solely on modulation at slider unload. The effect of lubricant properties on lubricant relaxation rate is explored by comparing Zdol + X1P to Ztetraol after disturbance by the same slider. The resulting average relaxation trends were fitted using a two-parameter logarithmic curve. The offset parameters are similar between Zdol + X1P and Ztetraol, but the logarithmic parameter is very different between the two lubricants. A slightly modified form of the fit equation was used with a similar comparison between different molecular weights of Zdol, showing that higher molecular weight relaxes slower than lower molecular weight. Both of these comparisons show that changes in lubricant properties change the relaxation rate of slider-induced modulation. Finally, the effect of modulation frequency on the

lubricant relaxation rate is explored. The results indicate that higher modulation frequencies relax much faster than lower modulation frequencies. The relaxation was modeled with a one-parameter exponential curve, with the exponential parameter varying smoothly with modulation frequency. Thus, the relaxation rate can be predicted knowing only the frequency band of interest.

In Section 5.3, the experimental measurements of lubricant modulation relaxation were simulated using the 2D diffusion equation and a simple finite-difference method. This simple simulation scheme relied on the experimental measurement for an initial condition. The only parameter not experimentally determined was the diffusion constant. Conducting repeated relaxation simulations for different diffusion constants allowed one to find which diffusion constant most closely matched the experimental relaxation data. In the first case (Zdol+X1P, 2 nm, 2000g/mol), the best-fit diffusion constant was 5.5×10^{-12} m^2/s and compared favorably with previously reported values, when considering that the lubricant types are not exactly identical. The second simulation case (Zdol, 10.7 Å, 10,000 g/mol) again showed good agreement between the best-fit diffusion constant of approximately 0.5×10^{-12} m^2/s and previously reported values.

This method of experimentally determining the diffusion constant of a lubricant is unique because it involves only adding minor additional steps to existing flyability tests. Also, the relaxation of slider-induced modulation is a more realistic condition than a half-delubed disk that is used in the Matano interface method. A half-delubed step is essentially a step impulse, which can be viewed in frequency space as a collection of many frequencies. In Section 4.5, it was shown that the slider-

induced lubricant modulation consists of modulation at specific frequency ranges, with very little high-frequency content. Thus, a step-change in lubricant is only an approximation of the lubricant behavior in a slider-disk interface. Using the actual slider-induced lubricant modulation to determine the diffusion constant of the lubricant involves only those frequencies that are expected to exist in the interface. Thus, the alternative method presented here is easier to implement in the lab as well as more accurately captures the actual relaxation that occurs in the slider-disk interface. Such a technique would be useful in evaluating the properties of a new type of lubricant [10, 11].

6 Lubricant Droplets

6.1 Introduction

At a fundamental level, hard drive areal density is tied to magnetic spacing in that higher areal density necessitates smaller magnetic spacing. With current industry goals in mind, the magnetic spacing for 3.1 Tbit/in2 is about 2.8 nm. This drives a physical spacing of 1.1 nm between the slider and the disk surface, including the lubricant layer. With a physical spacing this small, anything that disturbs this spacing has potentially catastrophic consequences for hard drive design. Traditionally, a lubricant layer has been used in hard drives to lower friction in the case of contact-start-stop designs as well as to protect the interface against intermittent slider-disk contacts and corrosion. The behavior of lubricants has been studied extensively by previous researchers who reported the appearance of lubricant moguls [1] and ripples [2] as a slider flies above a particular disk track. These phenomena are ascribed to slider-induced air shear by Marchon et al. [3]. These phenomena are important in designing the interface, as they can contribute to magnetic spacing loss.

During investigations into the behavior of lubricants as applied to thermally-activated slider (TFC) designs, a new phenomenon was discovered. Sudden lubricant drop-off was observed when an un-actuated TFC slider was flown over a relatively thick Zdol + X1P lubricant disk. After a few minutes of flight a sudden spike in acoustic emission (AE) and/or laser doppler velocimeter (LDV) sensor signal was seen to correspond to the sudden appearance of a thick lubricant drop as measured by a

Candela optical surface analyzer (OSA). This thick lubricant drop was subsequently "smeared out" with continuing passes of the slider (on the order of a few seconds to minutes). The relatively large height of these lubricant drops (on the order of a few nm) suggests that understanding and controlling the drops is necessary to achieve a stable magnetic spacing. Such a degradation of magnetic signal was reported previously by Pit et al. [4] in response to a nominal fly-height change of 15 nm caused by a lubricant droplet intentionally introduced into the interface.

These recent experimental results are different from the moguls and ripples previously reported in that these lubricant droplets are discrete events occurring at specific times instead of features developing continuously in time over the entire disk circumference. In addition, the experiments in [4] were the result of a lubricant obstacle artificially introduced into the interface while the results presented here occurred spontaneously with no initialization or external influence required.

6.2 Experimental Setup

For these experiments, a current-generation femto form-factor ABS design was used with simulated nominal and minimum fly-height around 14 and 17 nm respectively. Figure 6-1 shows the ABS geometry. The disk was coated with Zdol + X1P, 2000 g/mol, 7% bonded ratio, total thickness 20.1 angstroms with the additive volume fraction contributing 0.6 angstroms. The pre-test lubricant roughness (three sigma) was around 0.45 nm. The disk was 0.050" thick with an outer diameter of 95 mm.

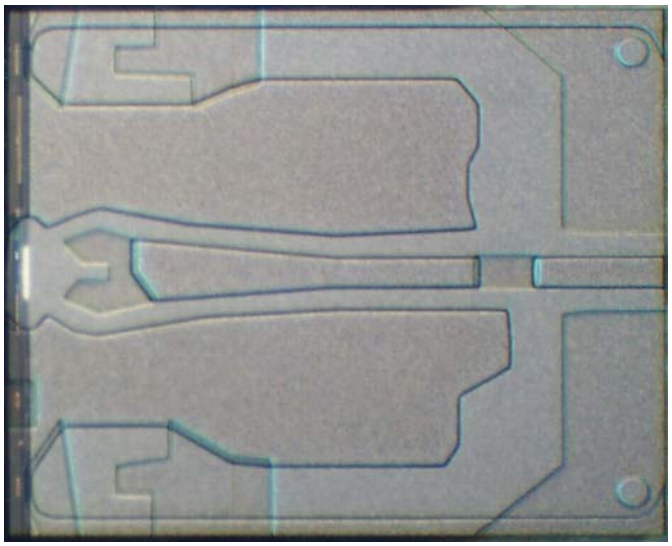

Figure 6-1. ABS geometry.

Experiments were performed using the spinstand described in Section 2.1 and data analysis was as described in Section 2.8. At the beginning of each test, the slider was loaded manually at the load radius and then moved inward by 1mm to the test radius. The LDV was focused on the flexure above the slider after movement to the test radius. Once loaded this way, the slider remained on-track at the test radius for approximately 20 minutes. At one minute intervals OSA scans were taken over the entire disk circumference and a radial range of 2 mm (test radius +/- 1 mm). The resolution of the OSA scan was 2 μm in the radial direction and approximately 0.044 degrees (20 to 30 μm) circumferentially. At the end of the test, the slider was unloaded manually and then inspected using a microscope for lubricant pick-up.

Prior to the tests, the disks were stored in standard 25-disk plastic cassettes wrapped in anti-static bags. As each disk was needed, it was transferred to a single-disk plastic cassette where it was returned immediately after each test. Immediately

before the slider was flown on the disk, an OSA scan of the flying track was taken and verified to be free of contamination. All storage and test operations except the after-test microscope examination and ABS cleaning were conducted under a laminar flow hood.

6.3 Experimental Results

The different measurement systems were correlated through the stopwatch measurements taken at each OSA scan and at the end of the AE/LDV data capture. Through these time measurements the events captured by the AE and LDV sensors can be correlated to the OSA lubricant thickness data.

6.3.1 AE/LDV sensor

During a standard on-track flying test, the AE/LDV data capture looks like the example shown in Figure 6-2. The data capture length was usually two minutes longer than the flying time to allow for loading and unloading the slider. Since the AE and LDV sensor captures were started before the slider was loaded and continued after the slider was unloaded, the severe spikes seen at the beginning and end of the data set represent those loading events. In this example at 30 m/s linear speed, spikes are clearly seen in both the AE (top) and LDV (bottom) sensor data. Close inspection of the timing of the spikes in both sensors supports the conclusion that the sensors are capturing the same event. The delay between spikes varies widely between tens of seconds and minutes. The region after the first set of spike events is interesting in that it shows that once the events begin, they may end abruptly only to re-start later.

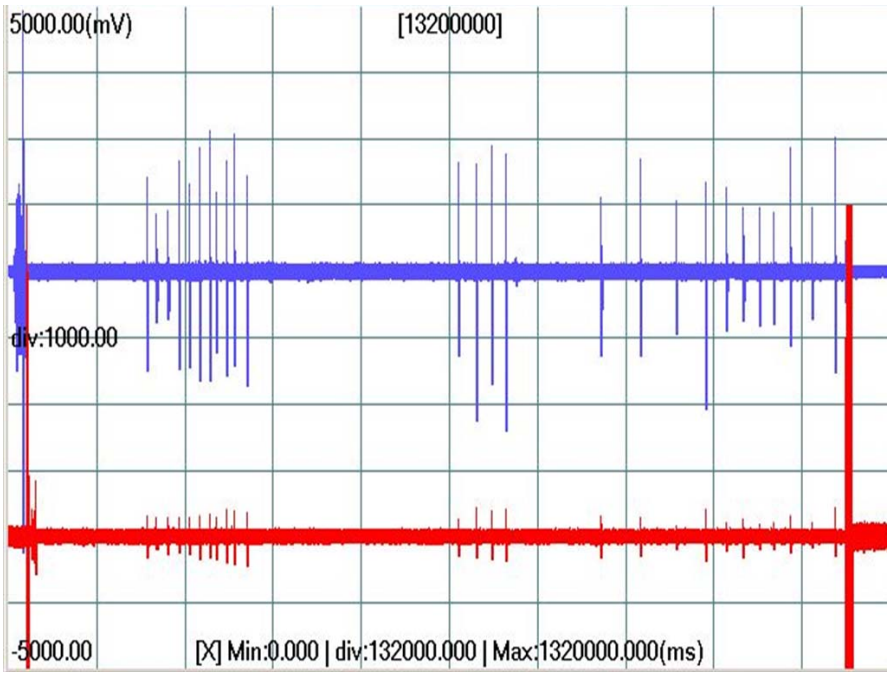

Figure 6-2. AE (top) and LDV (bottom) data showing intermittent spikes during a 20-minute flying test at approximately 30m/s linear speed.

The shape of a single spike event as recorded by the AE sensor is shown in Figure 6-3. This Fig. reveals that each spike event is not a single spike, but a region of higher signal within a decay envelope. The region has duration of around 700 micro-seconds (on the order of 100 revolutions). The decay envelope appears to be roughly exponential as expected from a spring-mass-damper type response. This supports the interpretation that the slider is encountering an obstacle in its path and flying over it; with every pass reducing the size of the obstacle. The magnitude of the AE spike is as much as 15 times larger than the non-spike AE magnitude. A similar figure for the LDV spike shows a magnitude about three times larger than the non-spike LDV magnitude (Fig. not shown). This indicates that during the spike event the fly-height modulation (FHM) velocity is three times higher than usual, or either the slider is

moving enough to de-focus the LDV spot. Either interpretation suggests a severe change in FHM.

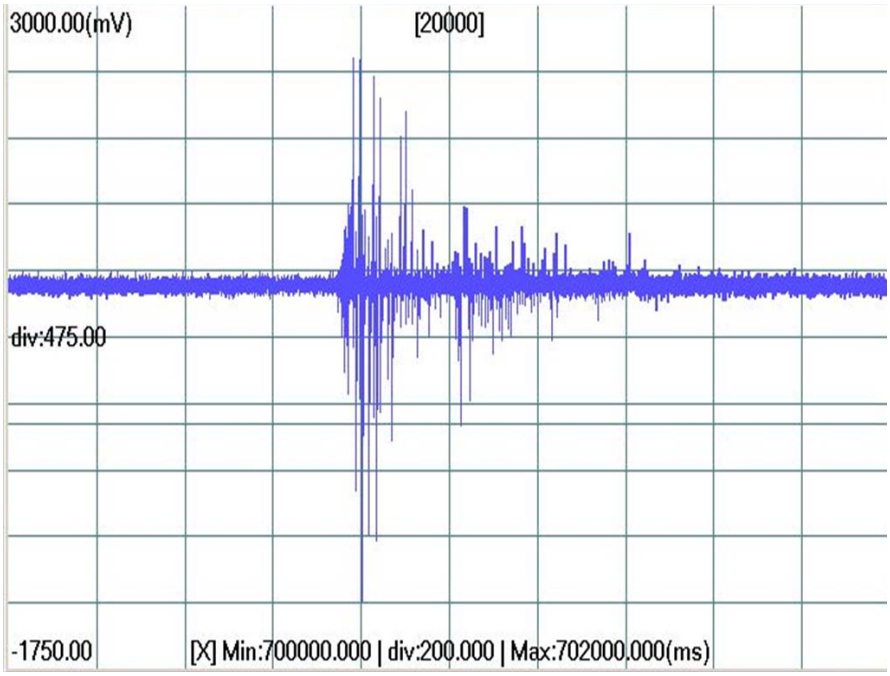

Figure 6-3. Example AE sensor spike (x-axis length is 2 seconds).

Later experiments were conducted with a much higher sampling rate (1 MHz compared to 10 kHz) and identical experimental conditions. While an experiment-long capture of the AE and LDV sensors is not possible at such a high sampling rate due to limitations of the data acquisition system, short but high-resolution views of the "spike" events were captured. Figure 6-4 shows the AE capture of one such spike.

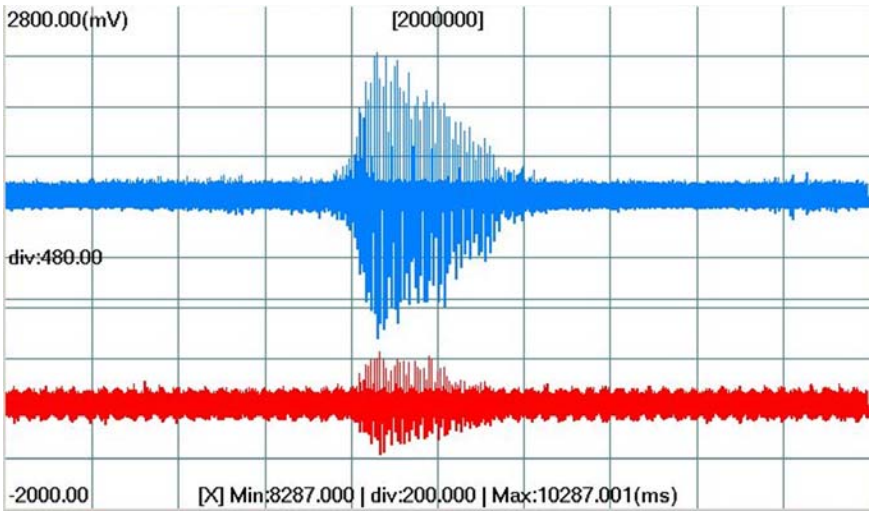

Figure 6-4. Example AE and LDV sensor spike (x-axis length is 2 seconds).

At a higher sampling rate, the shape of the "spike" is more obvious as compared to Figure 6-3. Closer examination of the "spike" shape reveals that it is not a solid event, but instead a series of smaller events grouped tightly together. Figure 6-5 through Figure 6-7 reveals these "sub-spikes" in ever smaller time windows.

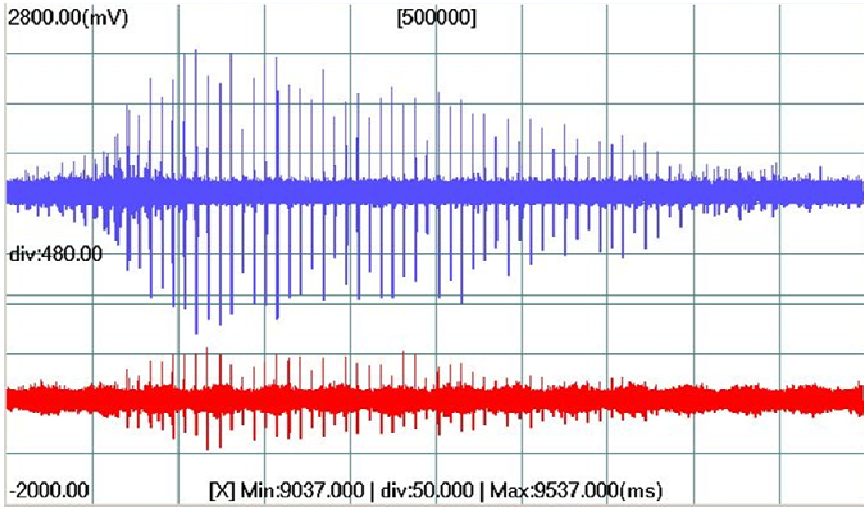

Figure 6-5. Example AE and LDV sensor spike (x-axis length is 0.5 seconds). Same data as in Figure 6-4.

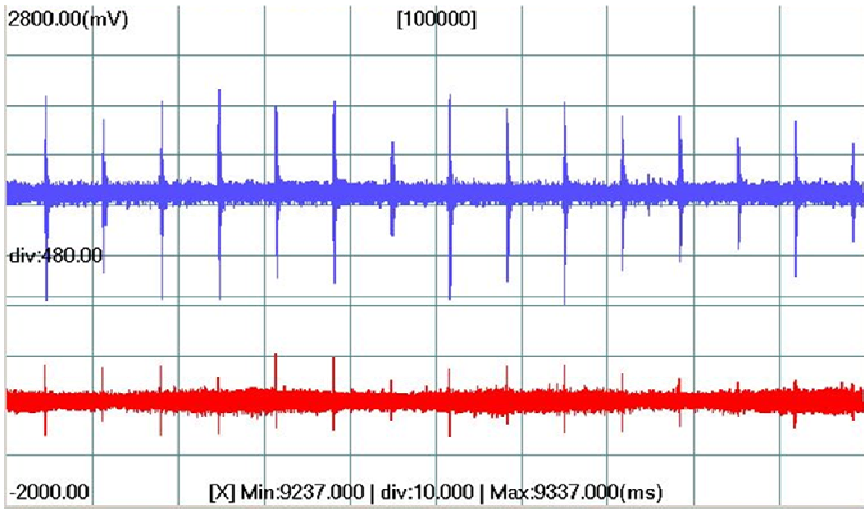

Figure 6-6 Example AE and LDV sensor spike (x-axis length is 0.1 seconds). Same data as in Figure 6-4.

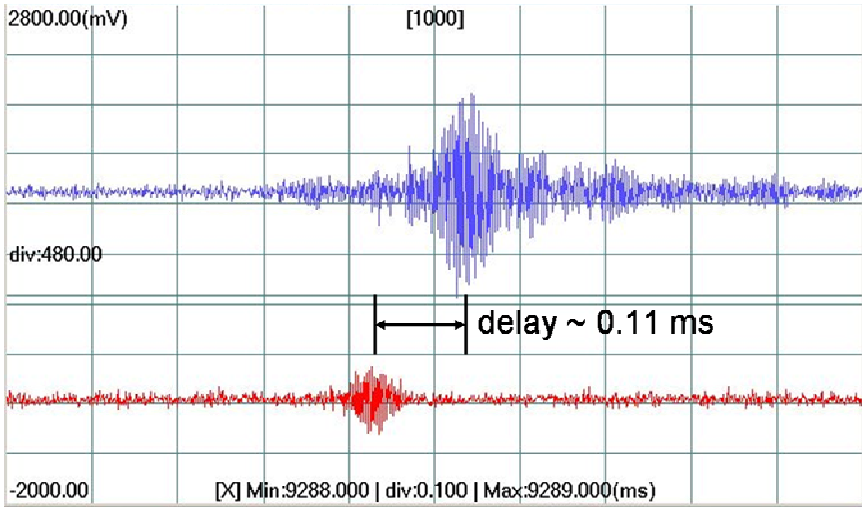

Figure 6-7 Example AE and LDV sensor spike (x-axis length is 1 millisecond). Same data as in Figure 6-4.

In Figure 6-6 it is clear that these sub-spikes are occurring at a specific frequency. Analysis of the time delay between ten successive sub-spikes gives the sub-spike frequency 149 Hz, corresponding to 8940 rpm. Unexpectedly, the disk rpm for this experiment was 9610 rpm, corresponding to 160 Hz. This discrepancy was

never repeated as all other results show sub-spike frequency corresponding to the disk rotation rate. A possible explanation for this mis-match between frequencies is that continuous lubricant pick-up and drop-off at slightly different locations on the disk cause the disturbance to occur at a slightly retarded frequency.

In Figure 6-7, the delay between AE and LDV spikes of 0.11 ms is highlighted. This delay is not necessarily related to any inherent difference between the two sensing mechanisms, but is most likely a systematic delay related to the specific setup of the AE and LDV sensor capture circuits. Some of this delay can be attributed to the time it takes for a disturbed slider's wave to travel up the suspension, through the baseplate, into the mounting arm, and to the AE sensor.

6.3.2 OSA scans

Sample OSA measurements taken during the test depicted in Figure 6-2 are shown in Figure 6-8 and Figure 6-9. Figure 6-8 shows typical OSA scans during time intervals where there are no AE/LDV spikes. The images shown in Figure 6-8(a) and (b) are typical lubricant modulation patterns found by subtracting the before-test scan of the disk surface from the in-situ scans at 9 and 8 minutes, respectively. Of interest here is the result found by subtracting successive OSA scans to illuminate the changes in lubricant thickness during the 60 seconds between scans (Figure 6-8(c)). The relative uniformity of Figure 6-8(c) as compared to Figure 6-8(a) and Figure 6-8(b) shows that while the lubricant modulation pattern is strong, it is not changing very rapidly in the minute between scans. This slow change in lubricant modulation is typical of most experiments. The OSA images in Figure 6-9 are taken from the same

area of the disk as the images from Figure 6-8, but later in the test. At first glance, the images shown in Figure 6-9(a) and Figure 6-9(b), taken at 16 and 15 minutes, seem very similar to the images in Figure 6-8(a) and Figure 6-8(b). However, when the successive scans are subtracted, Figure 6-9(c) shows a major change in lubricant occurred between the 15 and 16 minute scans. The dark line in the middle of Figure 6-9(c) represents a region were the lubricant thickness at 16 minutes is much thicker than it was at 15 minutes. The relative uniformity of the rest of the image shows that this is an isolated region of higher thickness. It is clear from Figure 6-9(a) and Figure 6-9(b) that the sudden thickness increase in lubricant may not be easily visible in the standard "measurement – base" screen capture. A "measurement – previous measurement" difference may be required to see the change. Thus, in-situ OSA scans are required to observe the phenomena described here.

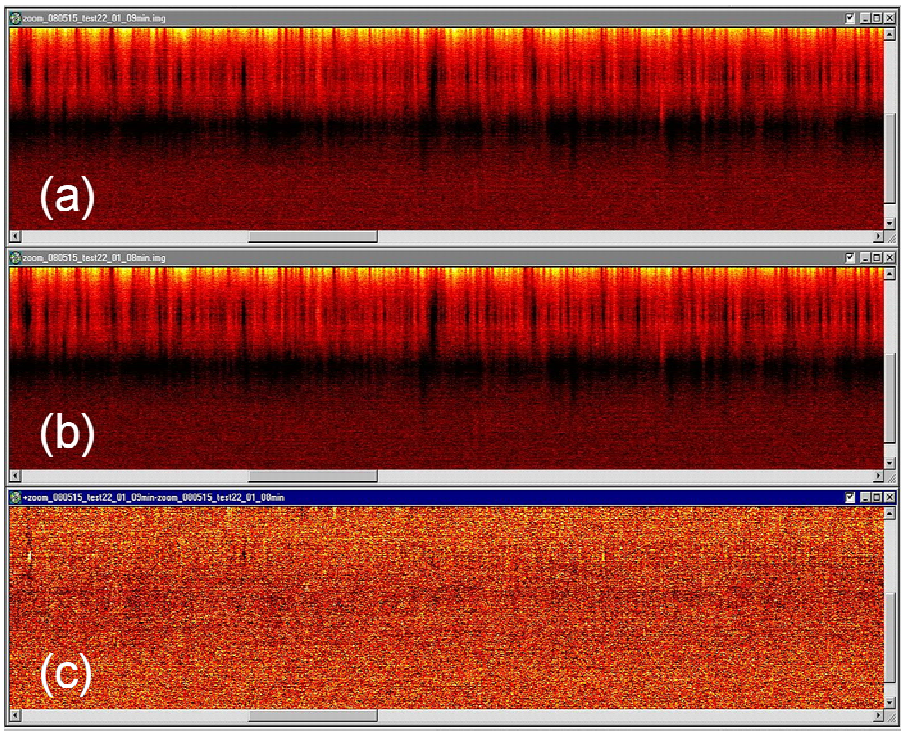

Figure 6-8. OSA screenshot showing lubricant thickness over 500 µm x 54 degree area (darker = thicker) showing an interval with no lubricant droplets or AE/LDV spikes (a) 9 minute – base (b) 8 minute – base (c) 9 minute – 8 minute.

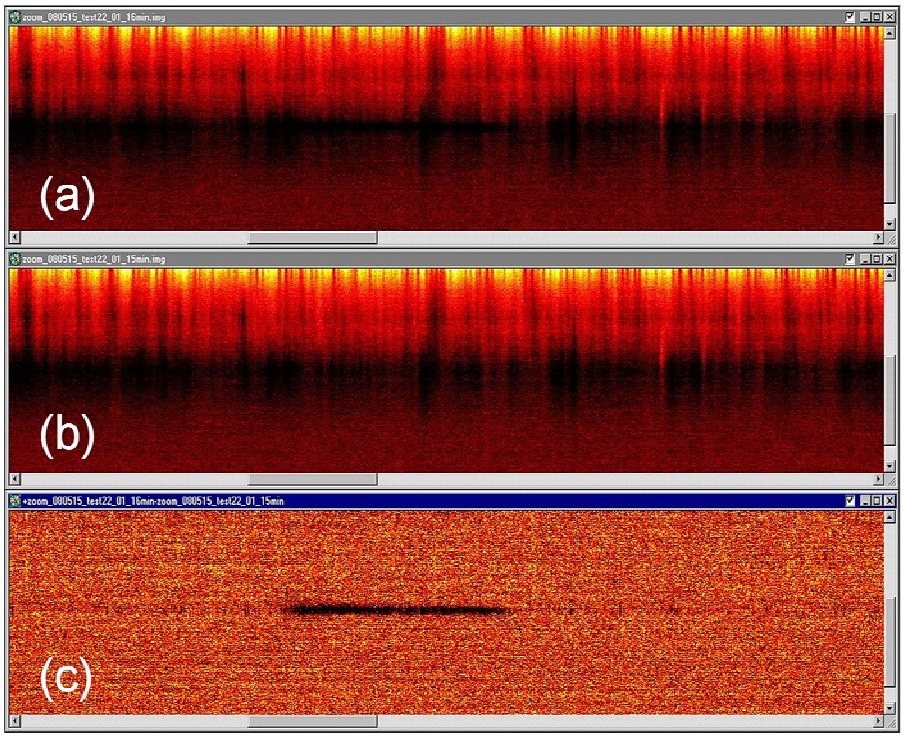

Figure 6-9. OSA screenshot showing lubricant thickness over 500 µm x 54 degree area (darker = thicker) showing a lubricant droplet (a) 15 minute – base (b) 16 minute – base (c) 16 minute – 15 minute.

Figure 6-10 and Figure 6-11 present the lubricant height data for Figure 6-9(c) in oblique and angular views. Examination of the OSA data shows that these thicker lubricant regions can easily be on the order of 1 nm thicker than the surrounding area. Considering that the thickness measured by the OSA is the thickness after the end of the spike event, it is expected that the thickness during the spike event will be higher than the 1 nm measured here. As the lubricant thickness for this particular disk is only 2 nm, this region of thicker lubricant represents a significant change in the lubricant profile to which the slider must adapt to maintain constant slider-disk spacing.

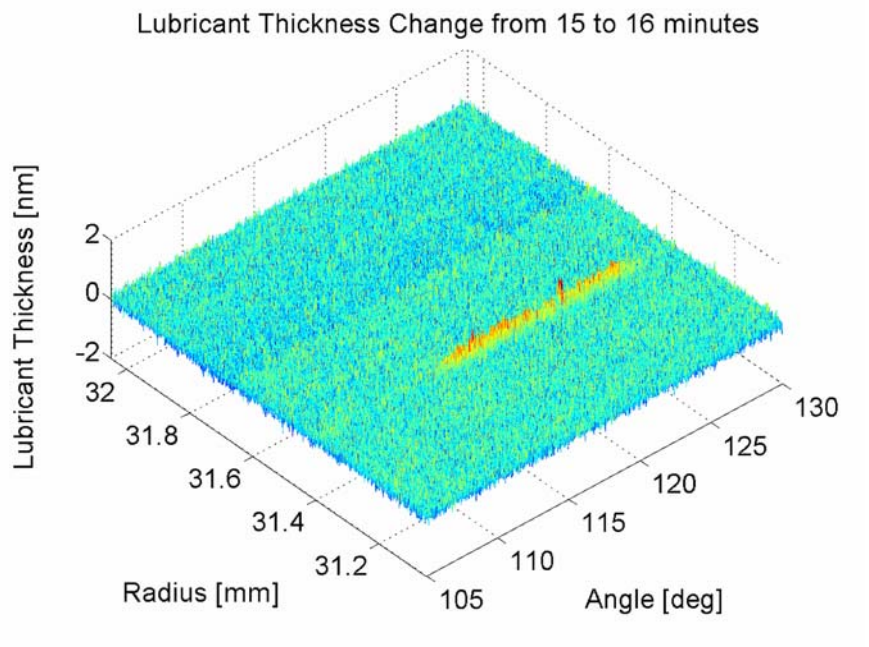

Figure 6-10. Lubricant height from 16 minute – 15 minute data showing 1 mm x 25 degree area around lubricant droplet (oblique view).

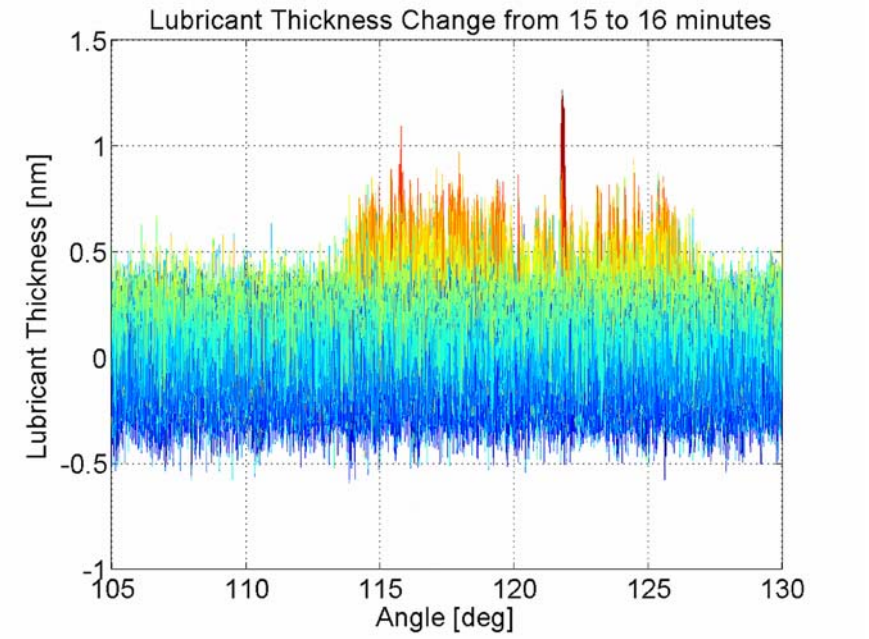

Figure 6-11. Lubricant height from 16 minute – 15 minute data showing 1 mm x 25 degree area around lubricant droplet (angular view).

During repeated testing, time intervals that include AE/LDV spike events, such as seen in Figure 6-2, also show some amount of sudden lubricant thickness increase as measured by the OSA. Only one example is given here, but the result has been observed in multiple experiments. AE/LDV spike events and OSA regions of suddenly thicker lubricant were observed during a later test using a disk coated with 20.8 angstroms of Zdol, spinning at approximately 30 m/s. This result suggests that lubricant droplets do not appear to require the additive X1P. After all tests, some lubricant pickup was observed at the trailing edge center (TEC) of the slider (near the sensors). However, the lubricant was easily removed through dipping the ABS surface in an HFE ultrasonic bath as seen in Figure 6-12.

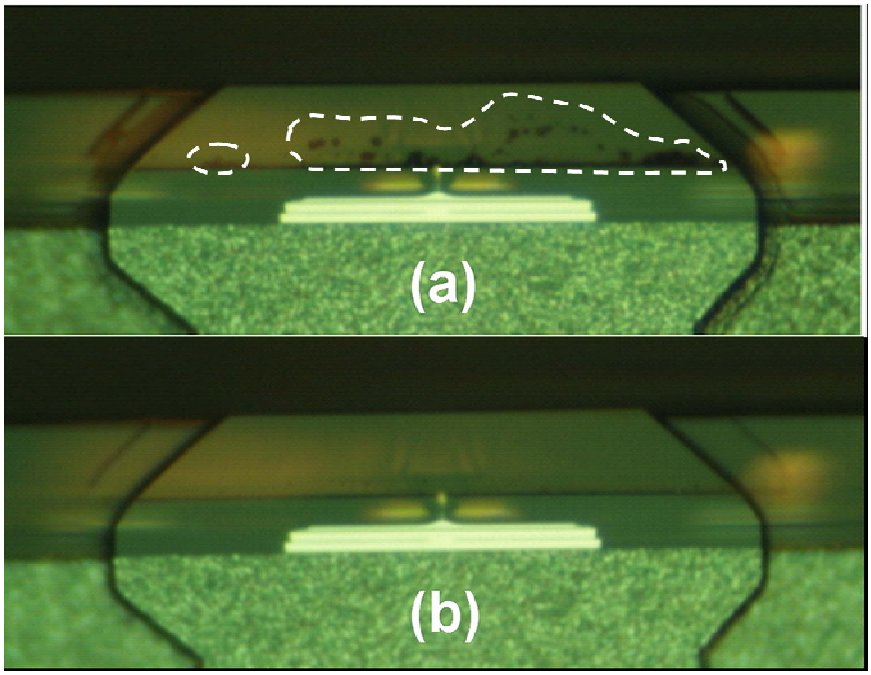

Figure 6-12. Microscope pictures of lubricant pickup at TEC (a) after a 20 minute on-track flying test with lubricant pickup area outlined (b) after cleaning with HFE ultrasonic bath. The width of the TEC rail is approximately 0.15 mm.

6.3.3 Lubricant dragging

During another test using the same disk of Zdol + X1P, at a linear speed of 30 m/s, intermittent LDV spikes were seen during the first seven minutes of the test (with corresponding sudden changes in lubricant thickness as measured by the OSA). After about seven minutes of flying time, the LDV signal broadened noticeably until about 11.5 minutes after which there were no more events. The LDV data captured is shown in Figure 6-13. While the magnitude of the broadened region is less than the adjacent spike event, the continuous nature implies a somewhat different origin.

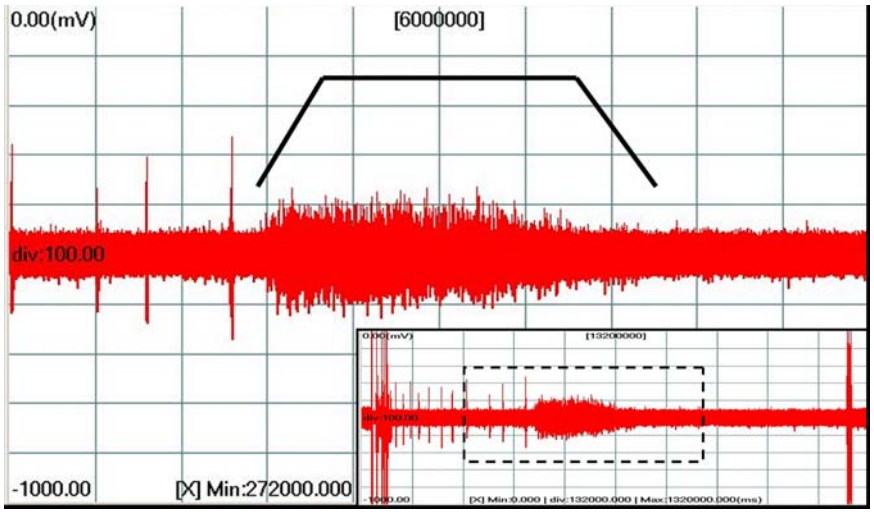

Figure 6-13. LDV sensor data from lubricant dragging result, zoomed view of 4 to 14 minutes with broadened region bracketed. Inset shows the entire 20 minute test data with the 4 to 14 minute region outlined.

In investigating the corresponding OSA scans, some difference images were obtained and are shown in Figure 6-14. In Figure 6-14, the difference images are presented in sequential order, from bottom right moving upwards and then bottom left moving upwards. At 5 minutes (not shown), a long region of thicker lubricant

appeared, similar to that seen in Figure 6-11(c). By the 6 minute scan, that region was gone (producing the light band in the middle) and replaced by a very short region of thicker lubricant, near the left of the 6 minute minus 5 minute image. From 6 minutes through 12 minutes, the short region moved in the down-track direction about 4 degrees (2 mm) every minute which corresponds to approximately 0.2 microns/revolution. Finally at 13 minutes, the feature was gone.

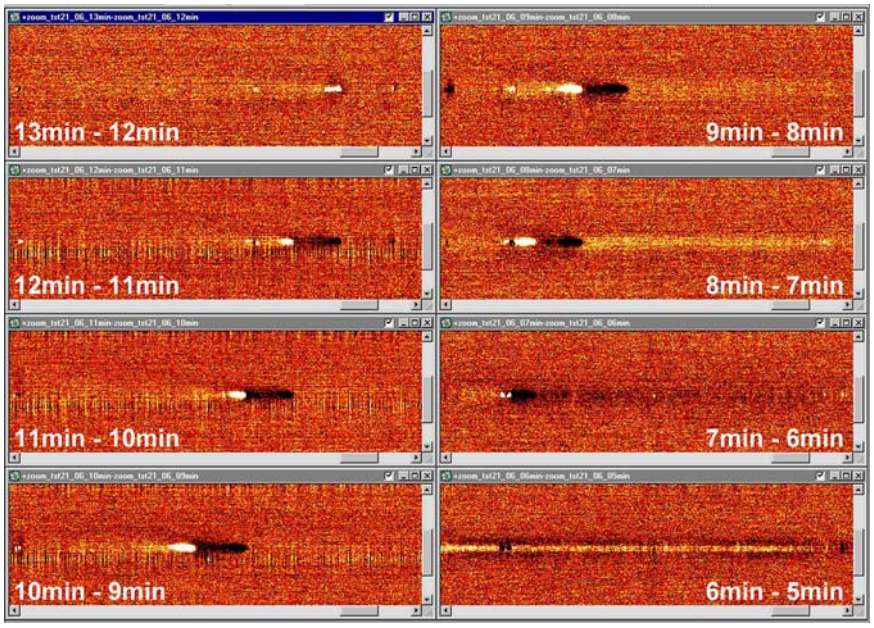

Figure 6-14. OSA screenshot of changes in lubricant thickness between scans over 350 µm x 27 degree area (darker = thicker) showing down-track motion of a large lubricant droplet (down-track is to the right of each frame).

Figure 6-15 shows the height of this lubricant droplet from each OSA scan in a combined image. Notice that the peak height of this lubricant droplet is around 45 nm while the thickness of the disk lubricant layer is approximately 2 nm. The height of the lubricant droplet drops smoothly with time. The broadened LDV sensor data from Figure 6-14 returned to the baseline level at approximately 11.5 minutes which

corresponds to a peak droplet height of between 26 and 14 nm. The CMLAir simulation results of this slider and experimental conditions show a minimum fly-height of about 17 nm. The obvious interpretation of this data is that during the time period where the lubricant droplet height was larger than the nominal fly-height, the flight of the slider was disturbed by the lubricant droplet, resulting in the broadening of the LDV sensor data. A similar lubricant dragging result was found in a later experiment, indicating repeatability. It is not immediately clear why these lubricant droplets remained on the disk for several minutes while other droplets did not.

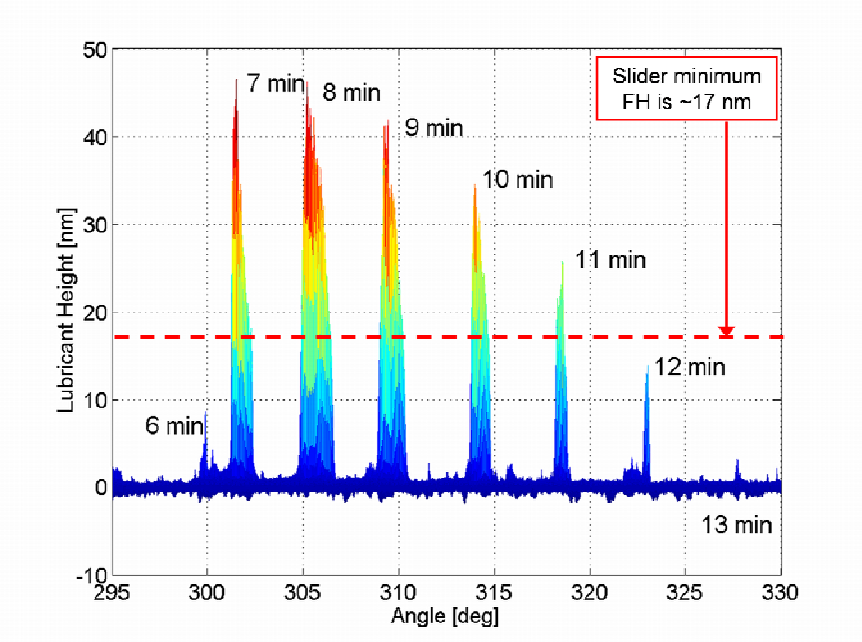

Figure 6-15. Angular view of lubricant droplet height data as it moves down-track with successive OSA scans (6 min to 13 min) with CMLAir simulation minimum FH marked.

6.4 Repeatability of droplets

The repeatability of these results is presented in Table 1. Of the 23 experiments performed, eight showed definite AE/LDV sensor spikes. Seven of these cases

corresponded to obvious lubricant droplets on the incremental OSA images. Twelve experiments showed no indication of lubricant droplets, with ten of these results corresponding to the absence of AE/LDV sensor spikes. Finally, no tests showed the definite appearance of one indicator in combination with the definite absence of the other indicator. These 23 experiments were performed on disks with the following properties: disk A (Zdol + X1P 2000 g/mol, 20.1 Å thickness, 7% bonded ratio, 0.6 Å additive), disk B (Zdol + X1P 2000 g/mol, 15.0 Å thickness, 9% bonded ratio, 0.6 Å additive), and disk C (Zdol 3500 g/mol, 20.8 Å thickness) with similar results seen on all three disks.

Table 1. Repeatability Data

	Definite lube droplets	Possible lube droplets	Definitely no lube droplets	Total:
Definite AE/LDV Spikes	7	1	0	8
Possible AE/LDV Spikes	0	1	2	3
Definitely no AE/LDV Spikes	0	2	10	12
Total:	7	4	12	(23)

6.5 Radial repeatability of location

The radial location of the lubricant droplets is usually at or near the trailing edge center (TEC) air-bearing rail. Some modulation patterns are as wide as the slider body, so specifying the location of the TEC during the experiment is simple. Other modulation patterns show a smaller pattern that reflects the modulation from the inner diameter (ID) side rail and TEC, but not from the OD side rail. In these cases,

knowledge of the radial accuracy of the positioning method combined with examination of the modulation pattern can sometimes help locate the exact position of the slider in reference to the modulation pattern. In cases where the location can be determined, the relationship between the slider ABS and the lubricant modulation patterns and droplets can be examined.

Figure 6-16 shows the lubricant modulation pattern that occurred after 20 minutes of on-track flying of a WD Femto #1 slider design. Other experimental parameters are as follows. The disk was perpendicular media, coated with Ztetraol lubricant, 15 angstroms, 3000 g/mol molecular weight. The disk rpm and radius combined to give 20 m/s linear speed under the slider. The slider was loaded on one track and the radius was reduced by 1 mm to reach the test track. No TFC power was applied. Two lubricant droplets are visible near the center of the image, aligned with a depletion band (light color).

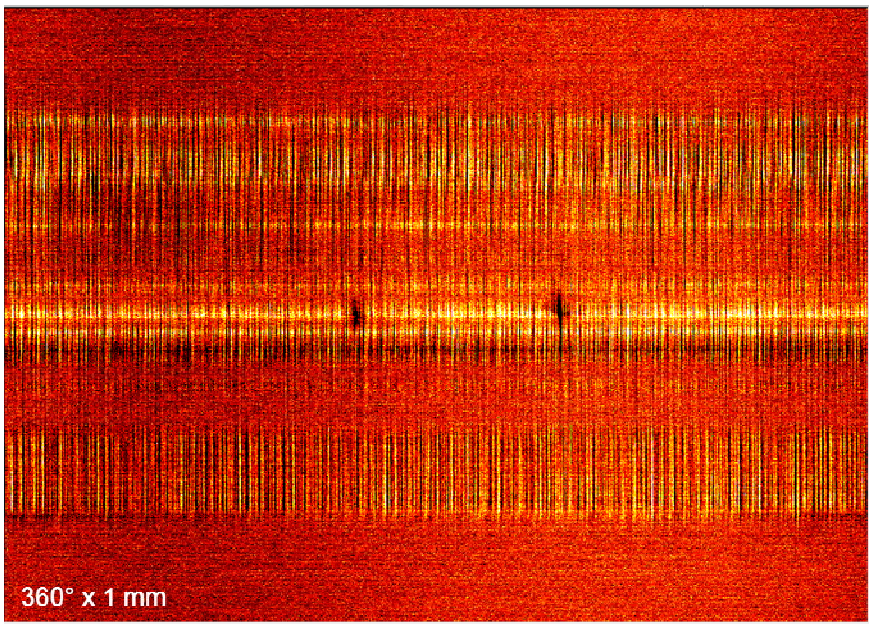

Figure 6-16. Lubricant net change at 20 minutes of on-track flying (20min – base). Dark regions represent thicker lubricant and light regions represent thinner lubricant. The entire image is 360 degrees in the x-axis and 1 mm in the y-axis.

Knowing that the width of this image corresponds to 1mm, it is clear that the modulation pattern width is approximately 0.7 mm, corresponding to the width of the slider body. With this knowledge, a microscope picture of the ABS can be superimposed on the lubricant modulation image above to show how the radial location of the lubricant droplets corresponds to the slider TEC rail. Figure 6-17 shows this superimposed image, with a different angular scaling of the OSA scan (37 degrees instead of 360 degrees seen in Figure 6-16.)

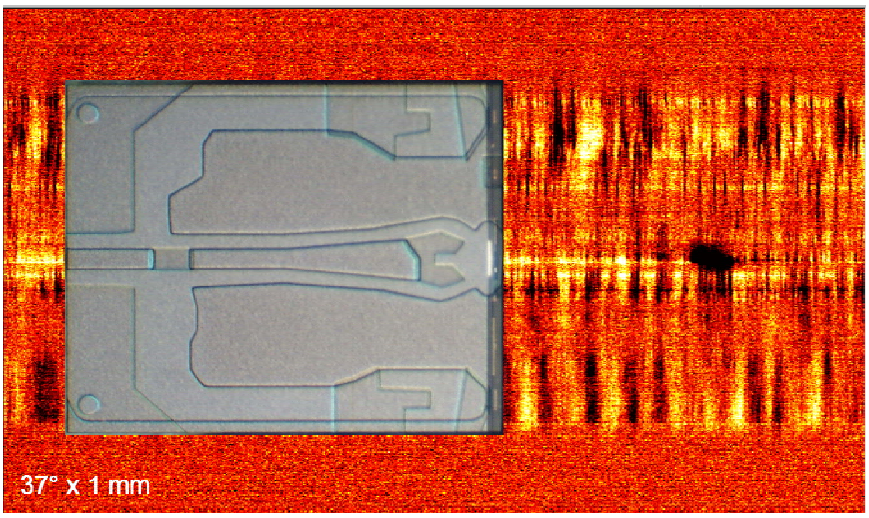

Figure 6-17. Lubricant net change at 20 minutes of on-track flying (20min – base). Dark regions represent thicker lubricant and light regions represent thinner lubricant. The entire image is 37 degrees in the x-axis and 1 mm in the y-axis. The superimposed ABS picture is scaled correctly in the radial direction (y-axis), but the circumferential length (x-axis) is exaggerated by a factor of 21.

The lubricant droplet visible near the right side of Figure 6-17 corresponds with the TEC ABS rail. This region is identified as a lubricant droplet by examining the incremental lubricant change image that results from subtracting the 19 minute scan from the 20 minute scan. In this image (Figure 6-18) the strong side-rail modulation features are not visible, as they change very slowly during one minute of slider flight.

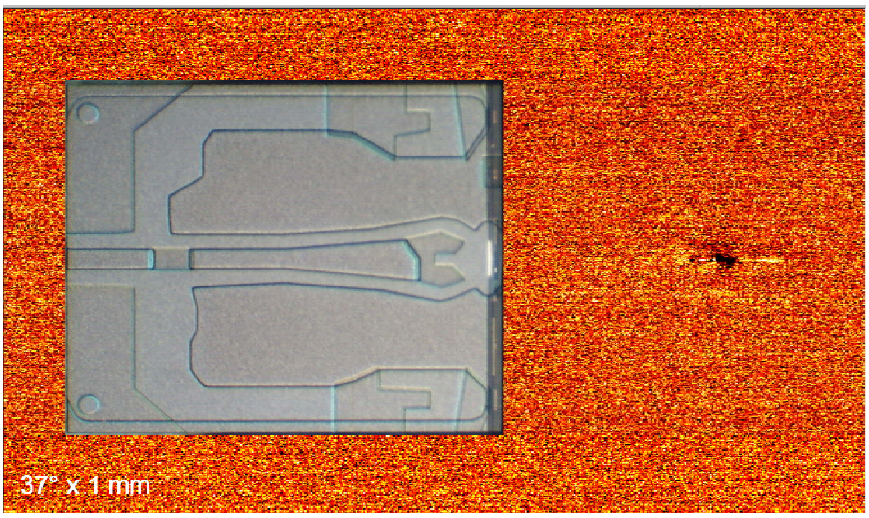

Figure 6-18. Lubricant incremental change image (20 min – 19 min) of the same OSA data as Figure 6-17. The dark region on the right of the image is a lubricant droplet.

Of results where the relationship between the slider body and lubricant modulation could be established, any lubricant droplets that occurred fell in the region under or near the slider's TEC rail.

6.6 Circumferential repeatability of location

To investigate the circumferential repeatability of lubricant droplets, a series of experiments were conducted in which a slider was repeatedly flown on the exact same track of a disk for 20 minutes. Recovery time was given between successive experiments so that each time the slider flew, the lubricant profile was relatively undisturbed. Of the experiments conducted in this way, three experiments showed lubricant droplets. Figure 6-19 presents the location of the lubricant droplets, with each color representing a different experiment. The size of the boxes represents the approximate 2D size of the lubricant droplets.

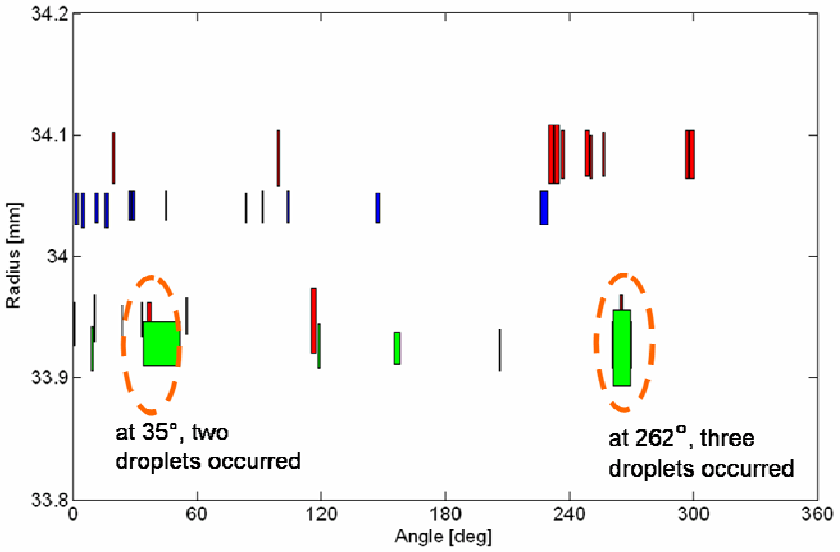

Figure 6-19. Location repeatability of lubricant droplets. The colored boxes (red, blue, and green) represent separate successive tests on the same track. Note that the y-axis is 0.4 mm wide.

From these three experiments, approximately 35-40 droplets were observed. Of this number, the droplets overlapped in location only twice. It appears that the droplets are occurring at random angular locations on the disk, suggesting that the disk substrate or carbon layer are not a driving force in the phenomenon.

6.7 Explanation

While the exact physical process responsible for these lubricant drops is currently being investigated, the experimental data presented here shows unequivocally that such lubricant drops can occur naturally in some slider-disk interfaces. The following physical process is hypothesized: First, the slider gathers lubricant over the entire flying track through evaporation, shear effects, corrugation instabilities, and/or intermolecular force-induced dewetting as suggested by Ambekar

et al. [5]. As it continues to fly, the lubricant on the ABS surface migrates towards the trailing edge as reported by Kubotera and Bogy [6]. Next, due to some physical process, the lubricant gathered near the trailing edge forms a droplet and is deposited on the disk, possibly due to an intermittent contact event or intermolecular forces. During the next revolution, the slider encounters the lubricant droplet as an obstacle in its path and the vibration of the slider is what is picked up by the AE and LDV sensors. After tens to hundreds of revolutions, the physical slider-droplet encounter and slider-induced air-shear spreads out the lubricant droplet enough so that the flying path is not severely affected and the AE and LDV sensor data return to their baseline values.

For the lubricant dragging result, it is hypothesized that the original lubricant droplet 1) may be so large as to cause a significant increase in fly-height with associated decrease in air shear and thus may remain on the disk far longer than smaller droplets or 2) may fall at a location between the slider pads with minimal air shear and thus less dispersive force. Experiments are currently being conducted to investigate under what conditions formation of these lubricant drops is likely to occur.

6.8 Analytical prediction

The proposed lubricant droplet mechanism is initiated by lubricant transfer from the disk to the slider during normal flight. The air shear field that exists on the ABS surface could cause the lubricant to migrate towards the trailing edge of the slider, where the lubricant could gather into pools or puddles. This pooling effect has been observed using an optical microscope after a flying experiment, with lubricant pooling

visible at both the deep etch and TEC ABS pad. The visibility of lubricant puddles to a relatively insensitive optical microscope suggests large lubricant thickness in these areas. If the lubricant thickness in these puddles exceeded the dewetting thickness, a lubricant droplet could form on the slider and transfer to the disk during slider flight. The theoretical feasibility of this mechanism is explored more fully here.

It has been established by other researchers that a thin layer of lubricant exists on the slider surface when the slider flies over a lubricated disk [7-16]. This thin lubricant layer has been experimentally determined to be between 0.5 and almost 3 nm, depending on the location of the measurement, for Ztetraol lubricant [7]. Zhao et al. experimentally determined that Zdol lubricant tends to transfer more lubricant to the slider than Ztetraol [8, table 2]. Thus, the Zdol+X1P lubricant studied here should have lubricant pick-up even higher than Guo's results [7]. Zhao found ABS lubricant pick-up on the trailing edge pads of a slider to be on the order of 4 to 6 nm for Zdol+X1P after flying for 18 or 60 hours. The experiments here were conducted for 20 minutes, so the lubricant pick-up will be lower at shorter times.

Taken together, these published results provide the basis for establishing the existence of a lubricant layer of some thickness on the ABS surface for the present experimental conditions. Simulations by Kubotera and Bogy [6] show that the air-shear in the slider-disk interface is sufficient to drive migration of the lubricant layer on the ABS surface towards the deep etch and trailing edge. Their simulation began with 2.0 nm of lubricant on the ABS rails closest to the disk (shallowest etch) and resulted in peak lubricant accumulation in the deep etch of 3.5 nm in as little as 100 seconds. Even though the ABS geometry in Kubotera and Bogy's simulation is

substantially different from the ABS geometry used in these experiments, the qualitative result of lubricant accumulation and migration should hold for any ABS design.

Based on work by previous researchers who established the existence of a lubricant layer on the ABS surface and migration of this lubricant layer due to air shear, the next step is to estimate the likelihood of formation of lubricant droplets on the slider surface. The proposed method of lubricant droplet formation is through dewetting thickness. The idea of dewetting thickness has been explored by Waltman, Khurshudov, and Tyndall [17] among others. While the dewetting thickness for the specific lubricant studied here, Zdol + X1P 2000 g/mol 2.0 nm, is not readily available, it can be estimated based on their results.

Waltman et al. found a dewetting thickness around 1.5 nm for Zdol 2000 g/mol. They also showed that the additive X1P tends to reduce the dewetting thickness, depending on the amount of the additive. The lubricant used here was 20.1 angstroms of 2000 g/mol Zdol with 0.6 angstroms of additive X1P (e.g. 3% additive), corresponding to a very minor drop in dewetting thickness. Thus, Waltman's results suggest a dewetting thickness around 1.5 nm for the lubricant used in these experiments. Despite this prediction of dewetting for lubricant thicknesses above 1.5 nm, no dewetting was observed for these 2.0 nm disks even after months of storage. This suggests that the disk substrate/carbon overcoat layer may be substantially different from that of the disks studied by Waltman et al. Waltman showed a dewetting thickness increase by 1 nm due to a change in nitrogenated carbon content

from 0 to 15%. A higher nitrogen content in the CNx layer could help explain the lack of dewetting for this 20.1 angstrom lubricant layer.

With all these previous results taken together, a lubricant dewetting thickness of a few nanometers is a reasonable estimate for the slider surface. If the lubricant that is picked up by the slider migrates on the slider surface into puddles as Kubotera and Bogy showed, it may reach thicknesses larger than the dewetting thickness. If these lubricant puddles occur on the TEC pad, they could dewet into lubricant droplets and transfer to the disk surface. Thus, dewetting into lubricant droplets is theoretically possible on the slider surface.

6.9 Simulation results of slider-droplet interaction

Taking the previous explanation of the slider-drop interaction as the true physical process under observation, it is instructive to conduct simulations of said interaction. The OSA scans taken during the lubricant dragging result (see Section 6.3.3) can be used as a basis to model the size and geometry of a single lubricant droplet. The CMLAir dynamic simulator software has a feature called “point-by-point disk track profile” where the user can specify point-by-point features on the disk. This is useful to specify laser textured zones as well as unusual disk roughness and waviness patterns. It is used here to simulate the size and geometry of a single lubricant droplet, allowing simulations to be run to investigate how a slider would react to encountering such a droplet during steady flight.

The simulation procedure is as follows. First, the OSA scan data is analyzed in Matlab and the height of a single lubricant droplet is extracted. This single lubricant

droplet is numerically isolated into a .txt file depicting a short region of flat disk with the droplet in the middle. This file is used as a user-defined disk profile for dynamic simulation. Figure 6-20 depicts the file used as the "point-by-point disk track profile".

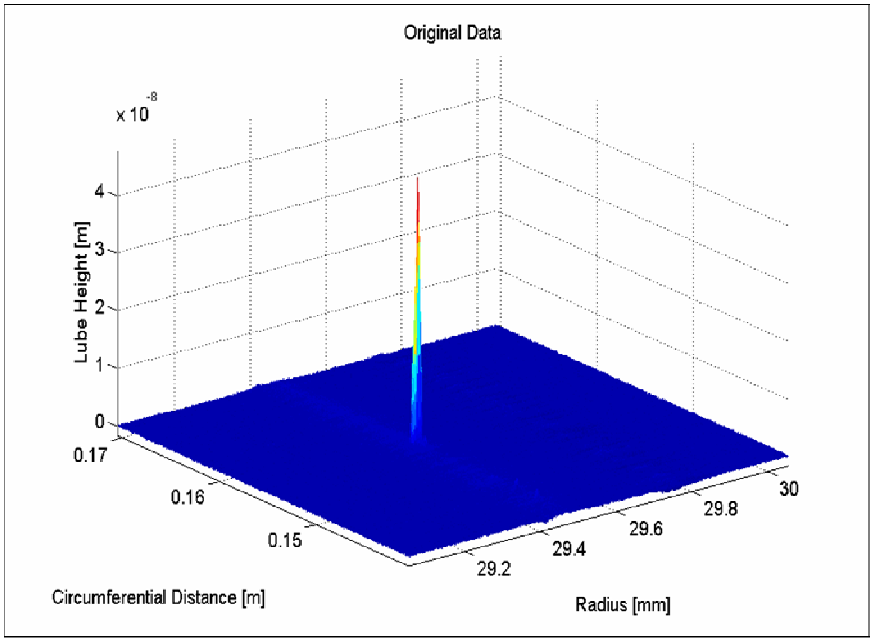

Figure 6-20. Point-by-point disk track profile used in the CMLAir dynamic simulator to model the effect of a large lubricant droplet on the flyability of the slider.

The spike in the middle of Figure 6-20 is the actual lube droplet data extracted from the OSA scan at 7 minutes (see Section 6.3.3). This actual lube droplet is numerically shifted in the radial direction to simulate the droplet falling at a different radial location in the path of the slider. Steps of 0.025 mm are used to shift the location of the droplet between extremes of +/- 0.4 mm from the slider centerline. Since the slider's width is 0.7 mm, this range covers the entire width of the slider. In this way, the influence of the lubricant droplet radial location on the flyability of the slider can be investigated.

To characterize the flyability of the slider as it encounters this lubricant droplet, the variation in the minimum FH is used. Figure 6-21 depicts a standard dynamic simulation result where the slider encountered the lubricant droplet at 0.5 ms. The minimum FH is around 17 nm before the interaction and the disturbance gives a peak-to-peak disturbance of approximately 40 nm. This value of 40 nm quantifies the flyability (or lack thereof) of the slider encountering the lubricant droplet at this location.

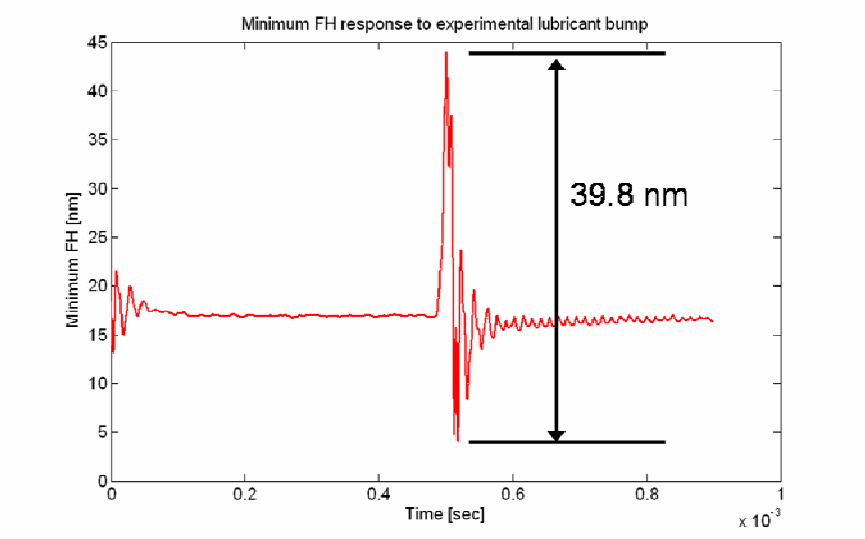

Figure 6-21. Dynamic simulation result (minimum FH vs. time) from slider encountering the lubricant droplet.

When all simulations are finished, a plot of the peak-to-peak minimum FH disturbance versus droplet location can be constructed. Figure 6-22 shows such a figure resulting from simulating the slider's response to the droplet height and geometry at 7 minutes.

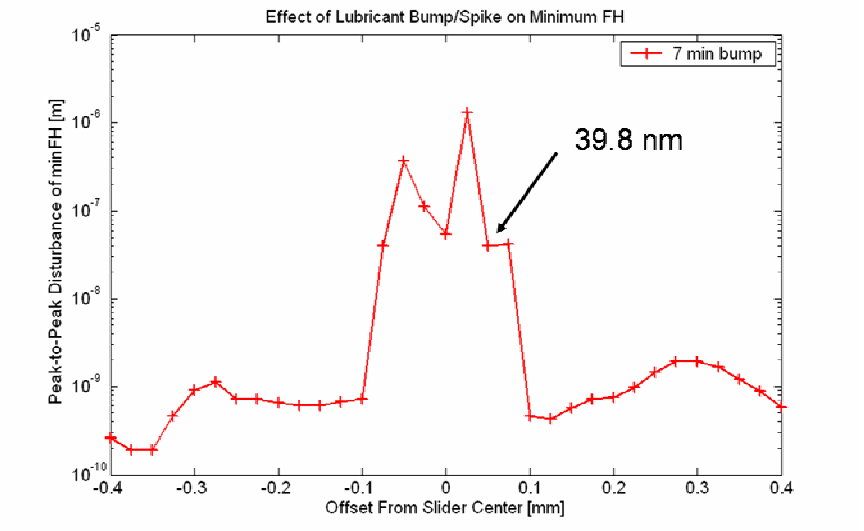

Figure 6-22. Disturbance profile (peak-to-peak disturbance [nm] vs. offset from center [mm]) of slider's response to the 7 minute lubricant droplet. Note the log scale on the y-axis.

In this figure, the 40 nm disturbance shown in Figure 6-21 is depicted as a single point. From this figure it is clear that the disturbance is much more severe when it occurs at the slider centerline. More detailed analysis of the location effect is given later. A series of simulations can be conducted using the experimental droplet data as the basis for the disturbance. As the droplet height reduces in time, the disturbance in the minimum FH also reduces. Figure 6-23 shows a series of disturbance profiles based on the 7 to 12 minute droplet data.

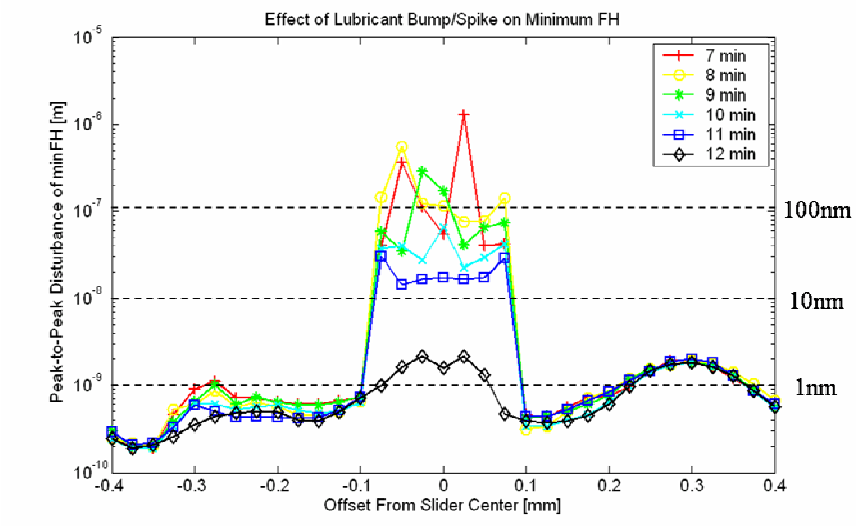

Figure 6-23. Disturbance profiles for droplet height data taken from 7 through 12 minutes. Note the log scale on the y-axis.

The biggest change in disturbance occurs between the 11 and 12 minute results. At 11 minutes, the lubricant droplet induces a minimum FH variation of around 11 nm. At 12 minutes, the minimum FH variation is around 2 nm. Thus it is clear that a lubricant droplet with height less than the slider's minimum FH disturbs the slider an order of magnitude less than a droplet with height larger than the slider's minimum FH.

Now that we have investigated the effect of the size of the lubricant droplet on the disturbance, the same data can be used to investigate the effect of the lubricant droplet radial location. Figure 6-24 presents the same data in combination with a scaled picture of the trailing edge slider rails.

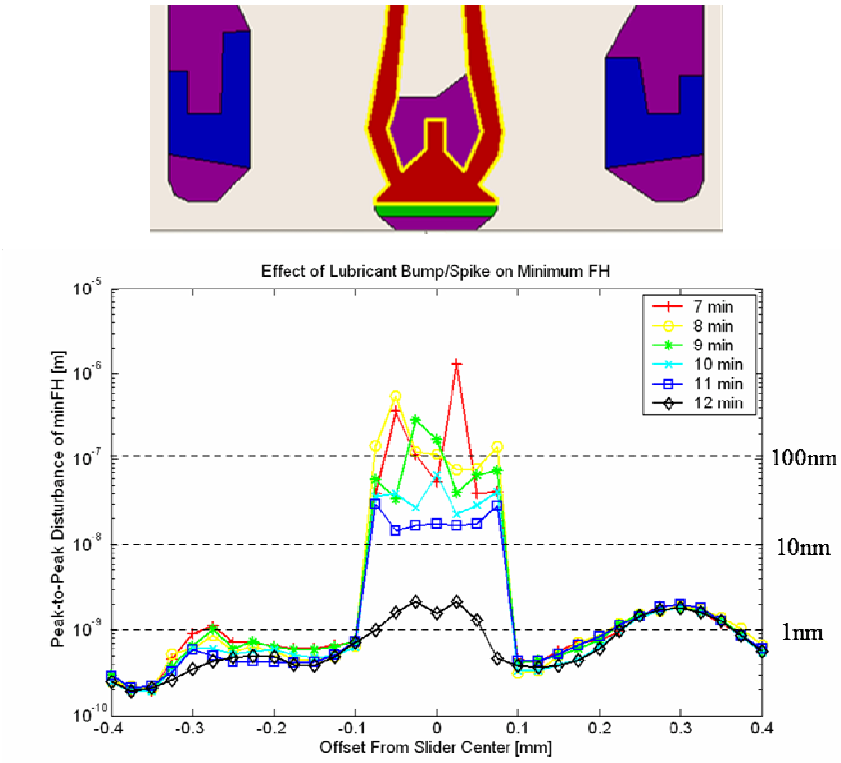

Figure 6-24. Comparison between droplet radial location, size of minimum FH disturbance, and slider rail geometry.

This figure makes it abundantly clear that the most severe disturbance of the slider occurs when the lubricant droplet occurs directly underneath the TEC rail. Interestingly enough, when the droplet falls between rails, the disturbance is less than 1 nm. When the droplet falls under a side rail, the disturbance is still a significant 1 or 2 nm, but an order of magnitude less than when the droplet falls under the center rail. While a 1 or 2 nm disturbance is probably not very significant for a slider that flies at about 17 nm, next generation sliders that fly at a few nanometers at most will see such a disturbance as a failure-inducing disturbance in magnetic spacing.

6.10 Conclusion

In this Chapter, a new experimental phenomenon of lubricant droplets was detailed. This phenomenon is different from the lubricant moguls and ripples reported by other researchers in that the lubricant droplets occurred as discrete events and not developing continuously in time. The indicators of this event are a sudden spike in AE or LDV sensors, corresponding to the sudden appearance of a thicker lubricant region as observed by in-situ OSA. Each AE spike actually consists of sub-spikes at a frequency at or near the disk rotation rate. The disturbance is usually gone in 700 microseconds and OSA scans taken after the droplets show a thicker lubricant region of around 1 nm thick. Other disturbances remain for minutes at a time and correspond to thicker lubricant regions of tens of nanometers. These lubricant thickness changes are not detectable without an in-situ OSA that can scan the disk while the slider is flying. Inspection of the ABS surface shows lubricant pickup at the trailing edge center pad.

Repeatability of the sensors was studied and no results were seen with definite appearance of one indicator (AE/LDV spikes and OSA thickness changes) without the appearance of the other indicator. Radial repeatability was investigated and showed that the lubricant droplets appeared on the disk at the slider centerline (i.e. under the trailing edge pad). Angular repeatability of the lubricant droplets showed that most droplets occurred over the entire disk circumference, not being repeated at a particular disk location. This is evidence for the lack of influence of the disk substrate or carbon layer on the location of lubricant droplets.

A physical explanation of this phenomenon is given, based on lubricant pick-up by the slider, migration and pooling towards the trailing edge, and dewetting instability causing the droplet to transfer from the slider to the disk. The feasibility of each of these steps has been demonstrated by other researchers and combined here. Simulations of the slider encountering a lubricant droplet were conducted, with the droplet size taken from experimental results. Simulations show that a lubricant droplet with height larger than the slider's minimum FH disturb the slider an order of magnitude more than a droplet with height below the slider's minimum FH. Also, the location of the droplet influences the severity of the slider disturbance. If the droplet occurs under the trailing edge center pad of the slider, the disturbance of the FH is two orders of magnitude more severe than if the droplet occurs at the side pads (100 nm vs 1 nm). These simulations show that lubricant droplets on the order of those seen experimentally here will challenge the current slider-disk interface. Future industry goals that rely on even closer slider-disk spacing will make this type of disturbance even more critical to control.

7 Effect of Thermal Fly-height Control on Lubricant

7.1 Introduction

One common solution to the problem of reducing slider-disk spacing is the concept of thermal fly-height control (TFC). This solution uses localized thermal expansion to move the read/write sensors closer to the disk while keeping the main body of the slider at larger fly-heights, first described in a US patent by Meyer et al. [1]. A small heater element is embedded in the slider body during manufacture and is powered by a special heater circuit controlled by the disk drive itself. By changing the amount of power delivered to the heater, the sensor-disk spacing can be controlled. This adjustment is useful in adjusting for manufacturing tolerances, "write-induced" protrusion, and changes in ambient pressure or temperature, all of which can affect the fly-height.

Suk et al. experimentally demonstrated the idea of a TFC design by using the writing element of a traditional slider as a surrogate heater [2]. They showed a substantial change in magnetic spacing caused by thermal expansion of the writing element while reading a pre-written data track. Juang et al. simulated the effect of a heating element on the intermolecular forces present at the slider-disk interface [3]. They concluded that the small protrusion area as compared to a traditional slider design reduced the intermolecular forces present. Other work by Miyake et al. [4] and Liu et al. [5] investigate the effect of heater size and location, and air-bearing design

on efficiency and performance of the slider. Shiramatsu et al. [6] investigate the ability of a TFC system to dynamically follow disk modulation in the kHz regime.

While there is work available discussing these aspects of TFC designs, the author is not aware of any experimental studies showing how the TFC actuation affects the modulation of the lubricant layer. Marchon et al. [7] used a single TFC actuation scheme as a tool to evaluate a new type of lubricant, but did not systematically investigate various TFC actuation levels on the lubricant. Ambekar et al. [8] used a TFC slider to investigate the effect of TFC actuation on lubricant loss in the flying track, but did not investigate changes in lubricant modulation brought about by this actuation. Specifically, it is desirable to investigate how closely the thermal protrusion may approach the disk without significant change in the modulation of the lubricant layer.

7.2 Repeatability of touchdown

One of the difficulties in evaluating TFC actuation is reliably determining the heater power required for touchdown. Actuation levels are often described in reference to the touchdown power (TDP) at which slider-disk contact occurs. Many contact detection schemes are available: read-back signal, thermal asperities, friction force, motor torque, LDV, and acoustic emission (AE) [9-12]. In these tests, an AE detection scheme is chosen. Some tests use an LDV detection scheme to corroborate the AE results.

To demonstrate the repeatability of TDP of a particular slider design at a particular radius and disk rpm, a series of tests was performed with identical

experimental parameters. The slider was loaded onto the disk and moved to the test track. Once on the test track, the power to the heater circuit was increased in 5 mW steps until the AE sensor showed a sudden change in signal response. This sudden change could be a “spike” appearing in the middle of the signal, associated with a particular spot on the disk, or a sudden change in the peak-to-peak signal over an entire disk revolution. Figure 7-1 shows examples of these changes in the AE signal. The heater power was recorded whenever these events occurred and tabulated.

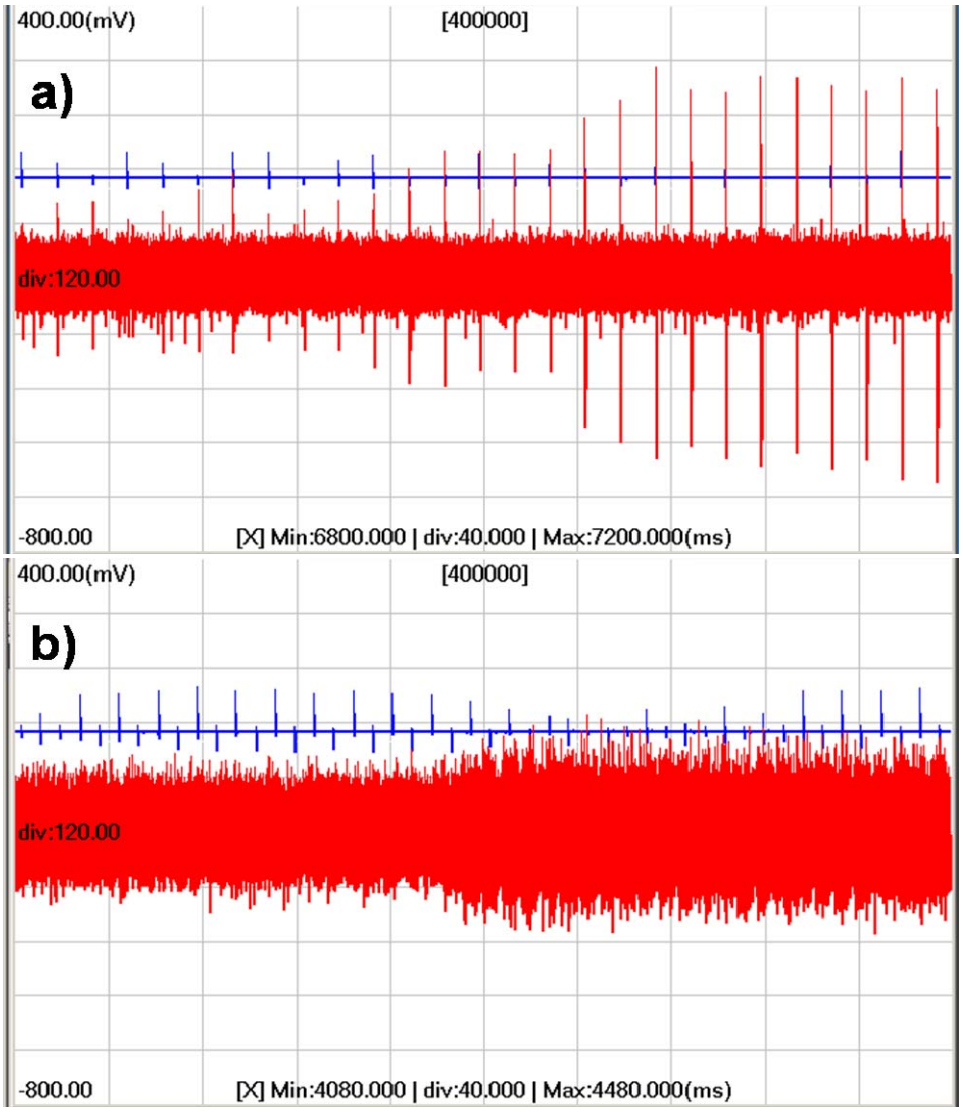

Figure 7-1. Examples of indication of slider touch-down. A) Sudden AE spike corresponding to a particular location on the disk. B) Sudden change in peak-to-peak AE signal. In both plots, the top trace is the once-around trigger signal, showing the disk rotation rate.

Over a series of tests, the TDP versus test number was recorded. At each radius and disk speed, three touchdown tests were performed consecutively within two minutes of each other. Between these three tests, the only thing that changed was the heater power. This was done to investigate the variation in TDP that occurs because of the touch-down test. If a touch-down test does not dramatically affect the lubricant

layer, consecutive touch-down tests should give the same (or very similar) touch-down powers. Figure 7-2 shows the variation in TDP across the three touch-down tests of 22 separate slider radius/disk rpm combinations as compared to the first TDP value seen. It is clear that the majority of radius/rpm combinations yield consistent touch-down powers. The resolution of the touch-down test (5 mW) is reflected in the bar graph bins. Variations of 5 mW might be explained as borderline cases where the actual TDP fell between two power increments. The 10 or 15 mW variations might be cases of slight modification of the lubricant layer during a touch-down test, causing the next touch-down test to give a different value. The number of these results is less than 10% of the total. Results where the TDP remained within 5 mW of the first TDP value consist of 91% of the total. In this way, the TDP repeatability is established. Later analyses that use a "back-off" criterion are based on this kind of TDP determination.

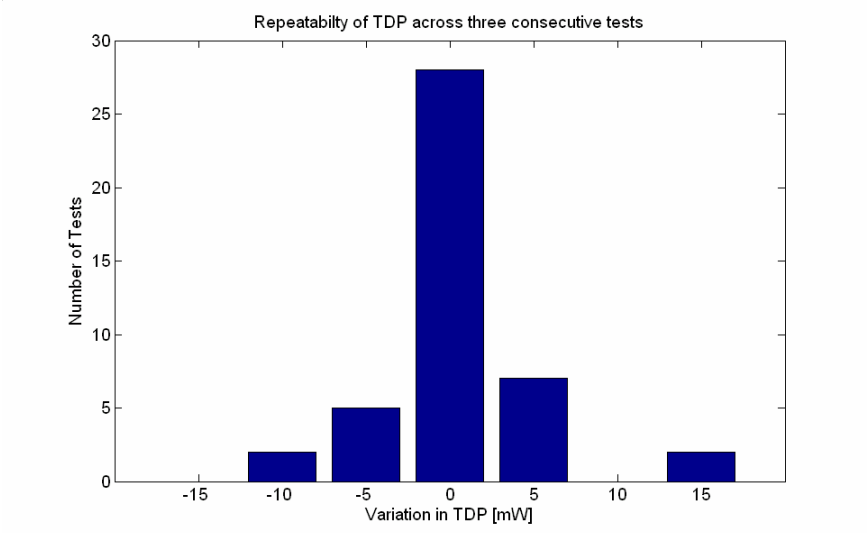

Figure 7-2. Variation of experimental TDP versus test number.

7.3 Effect of TFC on lubricant

Since TFC slider designs fundamentally change the slider-lubricant interface, it is expected that the lubricant behavior will therefore change. Various methods of investigating these changes are pursued in the following sections.

7.3.1 Lubricant buildup/depletion

One of the simplest slider-lubricant effects to measure is lubricant buildup/depletion. As a slider flies over the disk at a particular track, the strong air shear field below the slider causes the lubricant to move over the disk. In some locations, the lubricant becomes thicker (buildup) and in others it becomes thinner (depletion). By comparing the lubricant thickness during the slider flight to the lubricant thickness before the slider was flown, it is possible to quantify the buildup/depletion occurring under the slider during flight.

In this series of experiments, the lubricant buildup/depletion variation across the slider width (depletion profile) was tracked. Experiments of a TFC slider design flying without heater actuation were compared to those with heater actuation at touch-down. In these experiments, the heater circuit was driven very coarsely with a DC power supply connected directly to the HGA pads. Since precise control of the heater actuation was not desired, finer control was not necessary. More detailed examination under precise heater control is explored in Section 7.4.

Figure 7-3 shows the lubricant buildup/depletion profiles under a TFC slider during both un-actuated and fully-actuated flight. During this test, the un-actuated slider was flown for 5 minutes on track, taking OSA scans every minute. After 5:30

of flight, the heater circuit was actuated at approximately 400 mW of power. The slider remained flying at this power for 5 additional minutes, taking OSA scans every minute. The OSA data from each scan was analyzed in Matlab to determine the mean lubricant thickness at each measurement radius in 2 um steps. The profiles associated with un-actuated flight are given in solid lines while the actuated profiles are given in dashed lines.

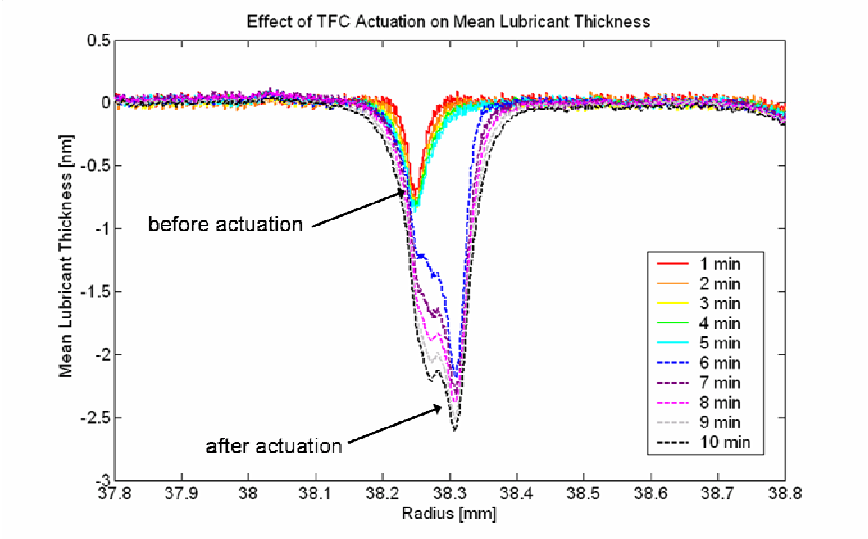

Figure 7-3. Example of lubricant buildup/depletion profiles for un-actuated (1-5 min) and fully-actuated (6-10 min) TFC slider flight.

During the un-actuated portion of the slider's flight (the first 5 minutes), the lubricant depletion profile does not change much. There is a region near the center of the slider's path where the average lubricant thickness was less than before the slider was flown, giving negative values. After the heater circuit was actuated at 5.5 minutes, the resulting lubricant depletion profile changes immediately. Beginning at the 6 minute profile, there has been an almost three-fold increase in the depth of the

depletion region as well as a slight shifting of the maximum depletion of about 0.5 mm towards the OD. The basic observation to make is that a strongly actuated TFC circuit will dramatically increase the lubricant depletion on the flying track. The high heater power applied of 400 mW is likely to be over the actual TDP. Thus, the results in Figure 7-3 are likely to be a worst-case scenario of extreme touchdown with the slider driven into the disk. It is clear from this figure that a severe touch-down event only a few tens of seconds long dramatically changes the lubricant buildup/depletion profile. To prevent such dramatic changes in lubricant thickness from occurring in a consumer hard drive, the touch-down test should be as sensitive and as short as possible.

7.3.2 Lubricant modulation profile

Besides the mean lubricant buildup/depletion profile, another method of investigating the slider-lubricant interaction is the lubricant modulation profile. The details of this type of analysis was presented earlier in Section 2.8.1. Here, a comparison is made between the lubricant modulation profiles of un-actuated and fully actuated TFC slider designs. The lubricant modulation profile was measured by OSA scan at one minute intervals throughout the test. Figure 7-4 presents the lubricant modulation profiles of un-actuated and fully actuated TFC slider flight.

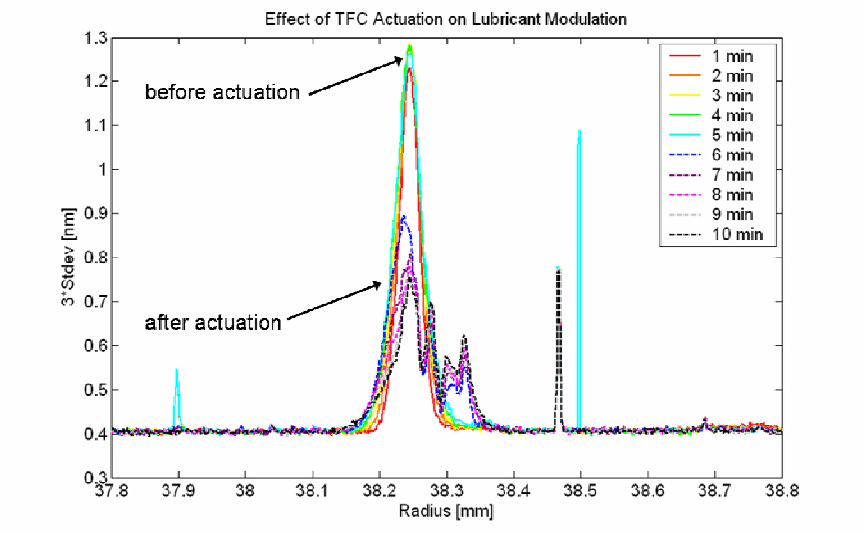

Figure 7-4. Lubricant modulation profiles for un-actuated (1-5 min) and fully-actuated (6-10 min) TFC slider flight.

The lubricant modulation profile that existed under the un-actuated TFC design was very strong at the center of the slider's path, and very weak otherwise. This high center modulation level was established by 5 minutes of flying on-track without heater actuation. After heater actuation, the lubricant modulation profiles were also strong in the center of the slider's path, but noticeably different from the profiles that existed before heater actuation. The smoothness in the un-actuated profile is replaced with some "jaggedness" in the fully-actuated modulation profile. Thus it is established that strong heater actuation changes the lubricant modulation profile in both general shape as well as strength, producing lower lubricant modulation than un-actuated flight.

7.3.3 Lubricant modulation frequencies

One final method of comparing un-actuated TFC flight to fully-actuated TFC flight is to consider the modulation frequencies of the lubricant layer. In Section 7.3.2, the lubricant modulation profile was discussed. Here, that data is analyzed in frequency space to see what changes are induced by high-power TFC actuation.

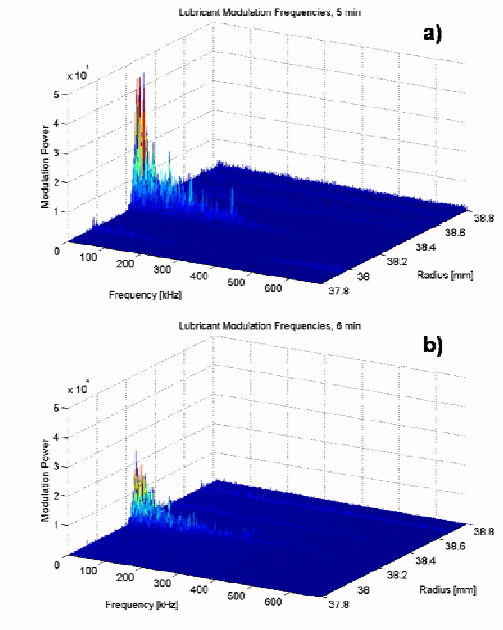

Figure 7-5. Lubricant modulation frequencies for a) un-actuated (5 min) TFC slider flight and b) actuated (6 min) TFC slider flight.

In the interval between 5 and 6 minutes, the heater circuit was turned on at high power. In comparing Figure 7-5 a) and b), it is clear that the modulation power drops dramatically after TFC actuation. In addition, no obvious frequency peaks appear during heater actuation that did not exist before heater actuation. Thus, it is shown that high-power TFC actuation causes a dramatic drop on lubricant modulation power as compared to non-actuated flight. Recalling the large lubricant depletion seen in

Figure 7-3, the drop in lubricant modulation can be explained by the large depletion track (caused by the high power actuation) removing the modulated lubricant that existed there before high power actuation.

7.4 Back-off studies

Having established that full TFC touch-down at high power introduces sudden changes in the lubricant layer, further investigation of exactly when these changes occur is pursued. Specifically, the heater power is systematically changed and OSA scans are taken. The previous analyses of the buildup/depletion profiles, modulation profiles, and modulation frequencies can be analyzed in terms of the heater actuation power at smaller discrete steps.

The trend in slider designs is towards closer slider-disk spacing. For TFC designs, this is accomplished by driving the heater with higher powers. Section 7.3 established that driving the heater to, and possibly past, full touch-down dramatically changes the mean thickness, modulation profile, and modulation frequencies of the lubricant layer. An important parameter to establish is how close to full touch-down can the slider be driven before these dramatic changes take place.

Since the actual TDP of slider designs varies across radius and disk rpm, the analysis is performed in terms of the "back-off" power. Having established the TDP through the touch-down method from Section 7.2, the "back-off" power is defined as the heater power difference as compared to the TDP. Thus, a back-off power of 0 mW corresponds to TDP. A back-off power of 20 mW corresponds to 20 mW below TDP.

To investigate the minimum back-off before dramatic change in lubricant distribution, sliders were flown on-track for a few minutes at a time at various back-off levels. The experimental procedure was as follows. First, the slider was loaded onto the load track. Then the slider was moved to the test track and allowed to fly for one minute to establish a non-actuated modulation profile. An OSA scan was taken to capture the lubricant thickness. Next, a touch-down test was performed, using 5 mW steps. Details of the touch-down test are explained in Section 7.2. After the TDP was established, the heater power was reduced to a pre-determined back-off level. This back-off level was maintained for three minutes, with OSA scans being taken at one-minute intervals. The heater circuit was then unpowered and a final OSA scan was taken. Throughout this entire sequence, the AE sensor was sampled at 10 kHz, along with the heater voltage.

The heater power can be determined from the resistance of the heater circuit and the applied voltage. The touch-down powers for these slider/disk/rpm/radius combinations were around 150 – 200 mW and the simulated minimum FH was approximately 14 nm without TFC power. A simplistic linear assumption between heater power and FH reduction gives an actuation efficiency on the order of 10 mW/nm. This is admittedly a simplification of the complex heat-transfer problem, but should give an approximate range of FH. Previous work by Liu et al. [5] has shown that near touch-down, the system stiffens and it takes more power to actuate into contact, called “push-back”. Thus, a 10 mW back-off is likely to be less than the 1 nm back-off assumed here.

7.4.1 Minimum back-off for negligible change to mean lubricant thickness

In direct analogy to Section 7.3.1, the mean lubricant thickness can be analyzed at various back-off levels. The mean lubricant thickness vs. radius for various back-off levels is presented in Figure 7-6. Each subplot contains two profiles, the profile taken after approximately one minute of un-actuated on-track flying (red) and the profile taken after the touch-down test and back-off level was set (blue). By comparing the profiles, the effect of various back-off levels on the mean lubricant thickness can be analyzed. Any differences between these two profiles of the same subplot are attributable to the touch-down test or back-off level. As the touch-down test was conducted the same way for all back-off levels, any differences between the subplots is attributable to the different back-off levels.

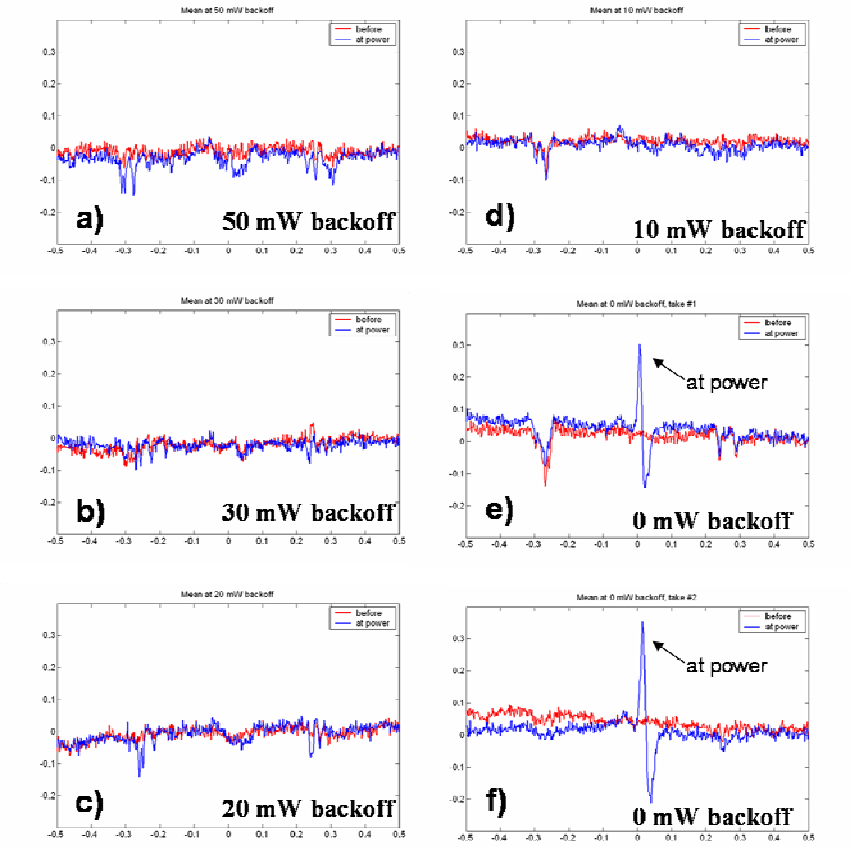

Figure 7-6. Mean lubricant thickness vs. radius before heater actuation (red) and after back-off (blue) for a) 50 mW back-off, b) 30 mW back-off, c) 20 mW back-off, d) 10 mW back-off, e) 0 mW back-off, and f) 0 mW back-off.

At back-off levels of 50, 30, 20, and 10 mW (a-d), the mean lubricant thickness does not change significantly after heater actuation. The small increases in depletion are attributable to the influence of increased flying time. The two cases of zero back-off (e and f), i.e. flying at the TDP, show dramatic changes in the mean lubricant thickness after heater actuation. As the touch-down test for each subplot was conducted the same way, these dramatic changes in mean lubricant thickness are attributable to the different back-off levels. Of interest is that there appears to be both a buildup and depletion zone. This seems to be evidence of a "snowplow"

phenomenon while flying at TDP. In the same way that a snowplow pushes snow from the street onto the curb, a TFC slider flying at TDP could be pushing the lubricant around. Thus, it is shown that flying at TDP seems to induce dramatic changes in the mean lubricant thickness that do not appear at back-off levels as small as 10 mW. Thus, the minimum back-off for negligible change to mean lubricant thickess is certainly below 10 mW in the time scale studied here.

7.4.2 Minimum back-off for negligible change to lubricant modulation

In direct analogy to Section 7.3.2, the lubricant modulation profile can be analyzed at various back-off levels. Figure 7-7 presents the lubricant modulation profiles based on the same experimental results as seen in Figure 7-6. Again, the red curve represents the lubricant modulation profile after one minute of on-track flight before the heater was actuated. The blue curve represents the lubricant modulation profile after the touch-down test and back-off level was set. The horizontal axis of the plots represent radius (1 mm wide, as compared to the 0.7 mm width of the slider.) Subplots a) through d) show that the side-pad modulation increases after heater actuation. A small drop in the center modulation can also be observed for these non-zero back-offs. The general shape of the modulation profile tends to remain the same after heater actuation at these levels. Subplots e) and f) show a different trend regarding the side-pad modulation. Zero back-offs appear to reduce the side-pad modulation in contrast to the non-zero back-offs that showed an increase. The qualitative change in lubricant modulation occurs between zero and ten mW back-off. Thus, the minimum back-off for negligible change to lubricant modulation is certainly

below 10 mW in the time scale studied here. While there is evidence of the center modulation generally decreasing after heater actuation at these levels, there is one location in subplot e) where a modulation peak appears where there was not one in the before-actuation profile. Examination of the frequency data shows a very strong frequency peak appearing in this location, which will be examined in Section 7.4.3.

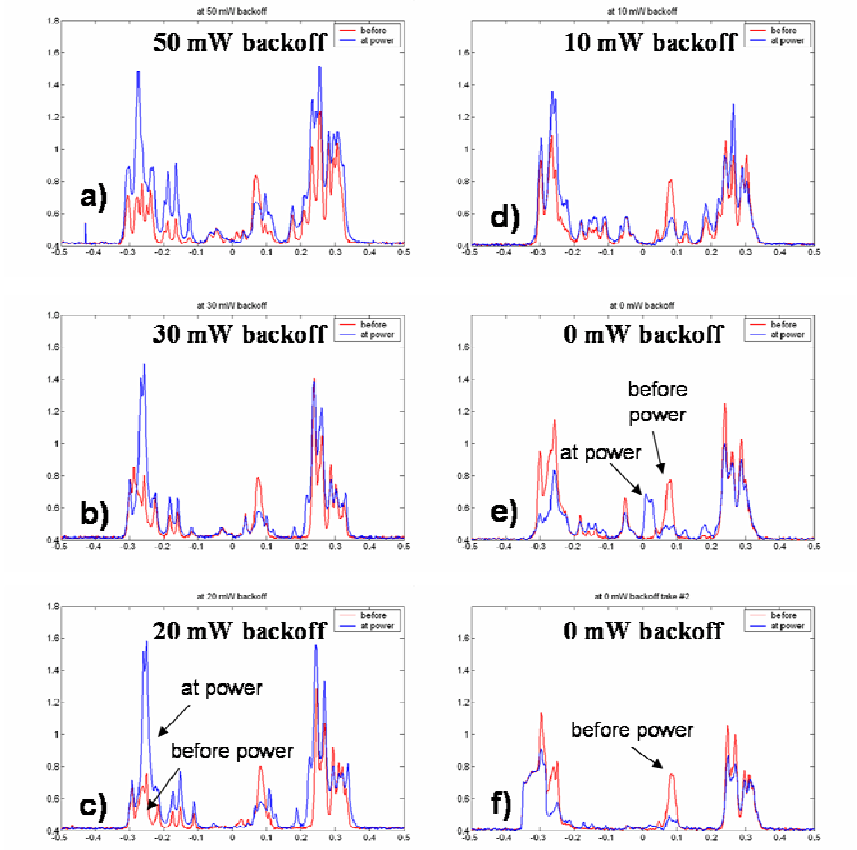

Figure 7-7. Lubricant modulation profile vs. radius before heater actuation (red) and after back-off (blue) for a) 50 mW back-off, b) 30 mW back-off, c) 20 mW back-off, d) 10 mW back-off, e) 0 mW back-off, and f) 0 mW back-off.

7.4.3 Minimum back-off for negligible change to modulation frequency

In direct analogy to Section 7.3.3, the lubricant modulation frequencies can be analyzed at various back-off levels. Figure 7-8 presents the average before and after actuation modulation frequencies across the entire 1 mm measurement width for 10 mW (a) and 0 mW (b) backoff. Subplot a) shows that the modulation power increases after heater actuation (blue) as compared to before heater actuation (red). Most of the modulation power occurs in the range below 100 kHz, with the strongest band occurring below 50 kHz. A back-off of 10 mW introduces negligible change in the lubricant modulation above 100 kHz. Similar results are seen for the 50 mW, 30 mW, and 20 mW backoff data.

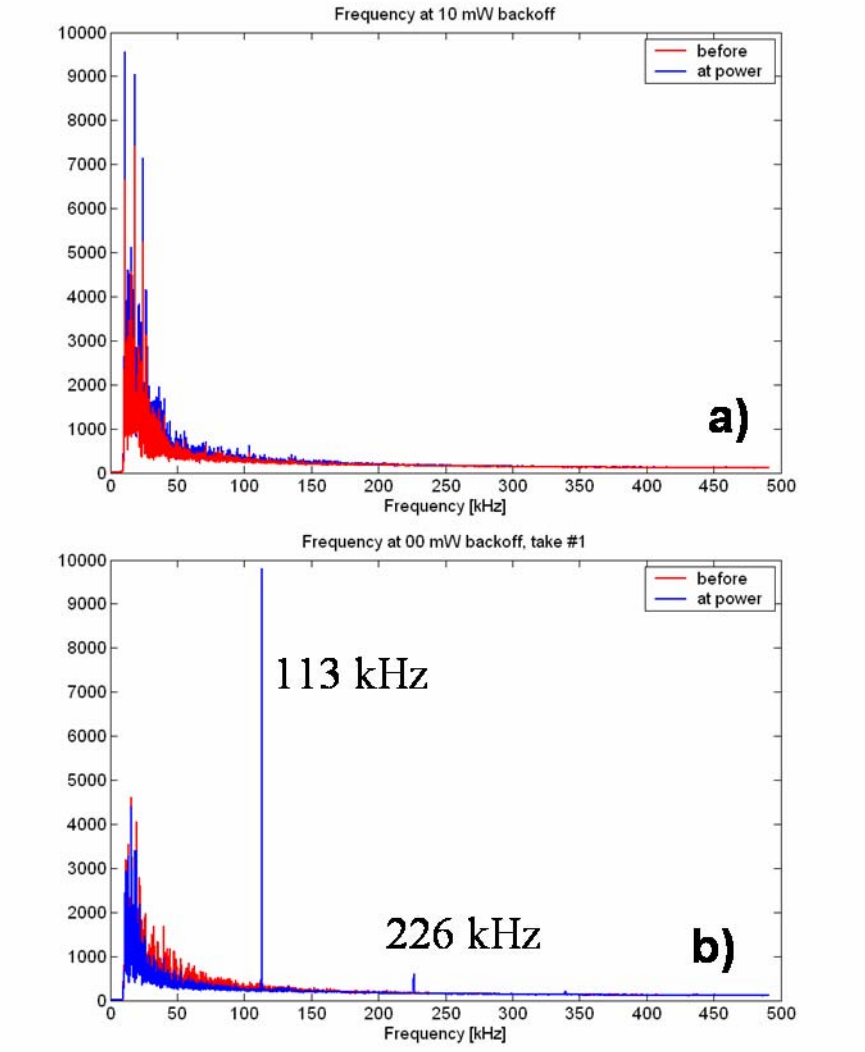

Figure 7-8. Lubricant modulation frequencies before heater actuation (red) and after back-off (blue) for a) 10 mW back-off and b) 0 mW back-off.

Subplot b) shows that the modulation power below 100 kHz drops after heater actuation. However, for 0 mW back-off, very strong modulation peaks appear at 113 kHz and its first harmonic of 226 kHz. These strong modulation peaks did not exist before the heater actuation. The 113 kHz peak appears in the second 0 mW back-off result, but the 226 kHz peak does not appear. More detailed analysis of the 113 kHz peak is possible by examining the distribution of the frequency peaks in the direction

of the slider width. Figure 7-9 presents the lubricant modulation data before and immediately after heater actuation at 0 mW back-off. Subplots a) and b) correspond to the red and blue curves in Figure 7-8(b), respectively.

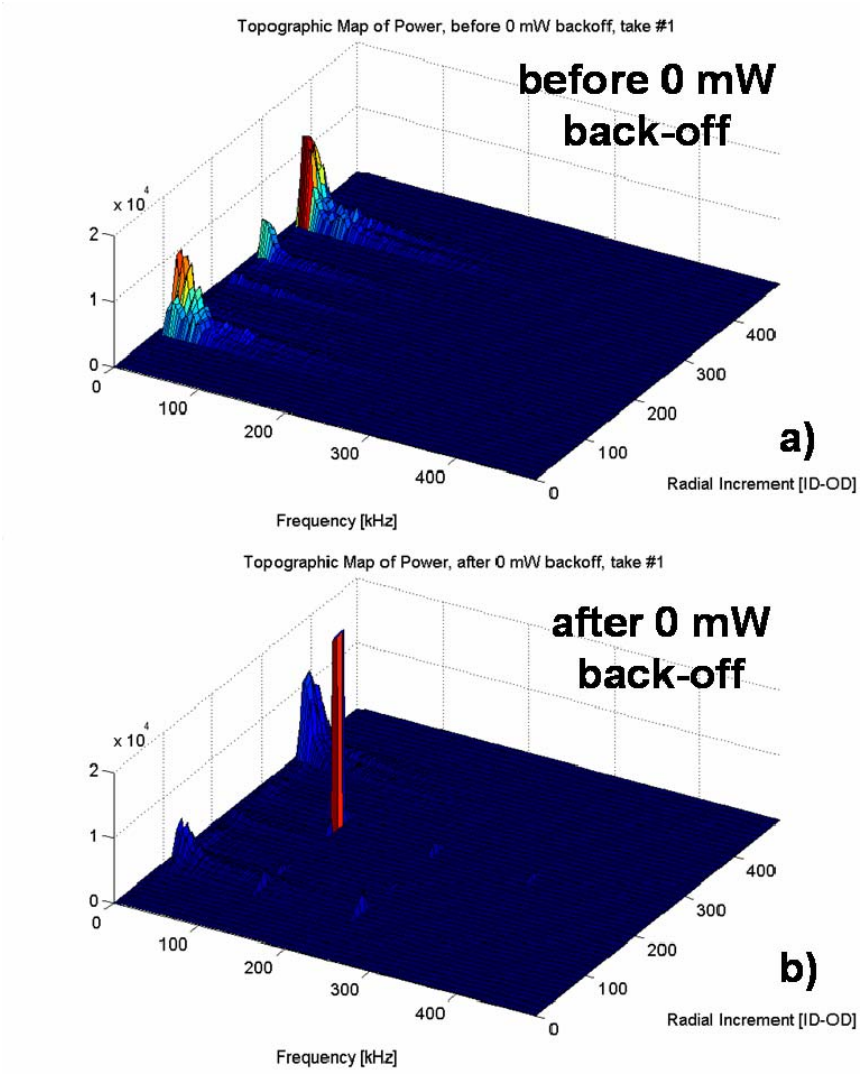

Figure 7-9. Variation of lubricant modulation frequency across slider width a) before heater actuation and b) after 0 mW back-off. X-axis is the radial increment in 2 μm steps, Y-axis is the modulation frequency [kHz], and Z-axis is the arbitrary modulation power, with both subplots using the same scaling.

From this figure, the reduction in side-modulation at low frequencies is visible (see Section 7.4.2) as well as the location of the 113 kHz peak and its harmonics.

Close inspection of subplot b) shows the 113 kHz peak and its harmonics showing up in two locations—at the center of the profile as well as at the ID side pad. The second 0 mW back-off test (not shown) shows a 113 kHz peak at the center, not at the ID side pad. Thus, while the center 113 kHz peak is repeatable, the ID side peak is not. As the heater protrusion is localized at the center pad, the ID side pad geometry is not changed during heater actuation. However, it is known that on the un-actuated slider the ID/trailing edge corner is the closest point to the disk. During heater actuation, the center pad protrudes towards the disk, becoming the new closest point to the disk. The identical frequency peaks at the center and ID side pad at 113 and 226 kHz suggest that the slider is either vibrating in a roll mode with axis between the center and ID side pad, or in a pitch mode with two locations approaching very close to the disk. Considering that the modulation frequency did not significantly change until zero mW back-off, it has been shown that the minimum back-off for negligible change to lubricant modulation frequency is certainly below 10 mW in the time scale studied here. Flying at zero back-off obviously can introduce very strong lubricant modulation frequencies that do not exist at 10 mW and above back-off.

7.4.4 Relationship of lubricant changes to slider features

The changes in the lubricant discussed above are all related to the mechanics of the touch-down test and setting the back-off level. It is interesting to evaluate the relationship between these lubricant features and the geometry of the ABS surface. The slider used in these tests is a femto form-factor of 1 mm long and 0.7 mm wide. The OSA data collected was analyzed in a 1 mm wide band to ensure that the entire

slider width was included in the analysis. In the results where the lubricant changed substantially across a 0.7 mm wide band, it becomes simple to relate the lubricant features to the ABS geometry.

Figure 7-10 shows the ABS geometry overlaid on top of the changes in lubricant thickness after flying at 0 mW backoff. The left side of the OSA image was taken after one minute of on-track flying, before heater actuation. The right side of the OSA image was taken after flying at 0 mW back-off for about one minute. It is possible to combine these two measurement images because the measurements were made in-situ while the slider was flying. As the slider location was not moved during heater actuation, the relationship between the slider location and OSA scan did not change. This composite image corresponds to the second 0 mW back-off test, seen in Figure 7-6(f) and Figure 7-7(f). The OSA image has been numerically transformed from a ring-shaped scan into a rectangular data set, with the horizontal axis representing the circumferential direction (angle) and the vertical axis representing the radial direction. The data has been "fitted" in a way that allows viewing of the entire ~200 mm x 1 mm scan in a single window, so the horizontal axis is substantially compressed in this image. Knowing that the OSA data is exactly 1 mm wide, a microscope picture of the ABS surface has been scaled to its correct width of 0.7 mm and centered over the OSA data. Because of the horizontal axis scaling, the slider appears to occupy one-third of the horizontal axis, when in fact its length corresponds to only one two-hundredth of the horizontal axis. This figure shows how well the changes in the lubricant layer correspond to the dimensions of the slider, with negligible change in the lubricant outside the slider's path.

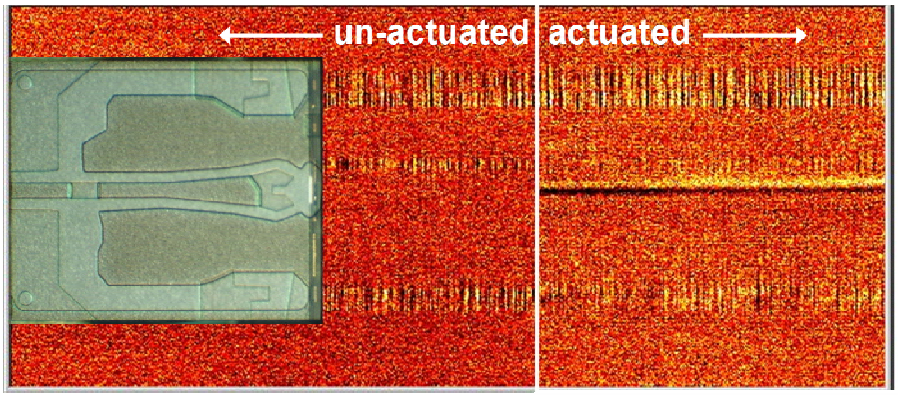

Figure 7-10. Relationship of lubricant features to ABS geometry at 0 mW back-off.

One important observation to make is that the buildup/depletion (dark/light) band in the center of the actuated image corresponds to the slider's trailing edge center pad. This makes sense, as the TFC actuation occurs in a very localized area on the slider's TEC pad. Also of note is that the side modulation does not change in character after heater actuation. This shows that the TFC actuation introduces the most dramatic changes under the slider's TEC pad.

7.4.5 Lubricant recovery after back-off tests and conclusion

In the previous discussions, the changes in the lubricant layer induced by touch-down tests and various back-off levels were explored. The most extreme back-off interface exists at a back-off of 0 mW. While the previous discussions have focused on the changes immediately apparent in the lubricant layer, the long-term changes in the lubricant layer are worth investigating. Specifically, it is of interest to see if the dramatic changes induced by 0 mW back-off are short-lived or permanent.

Figure 7-11 shows a small section of the 0 mW back-off OSA scans a) after power off and b) after approximately 20 hours of non-spinning recovery time. Both scans cover a section 27° long and 0.8 mm wide. Image a) was taken immediately after the heater power was turned off after flying at 0 mW for approximately one minute. Image b) was taken after 20 hours of recovery time. The disk was removed from the spindle during the recovery time, so the data points coincide only in radius.

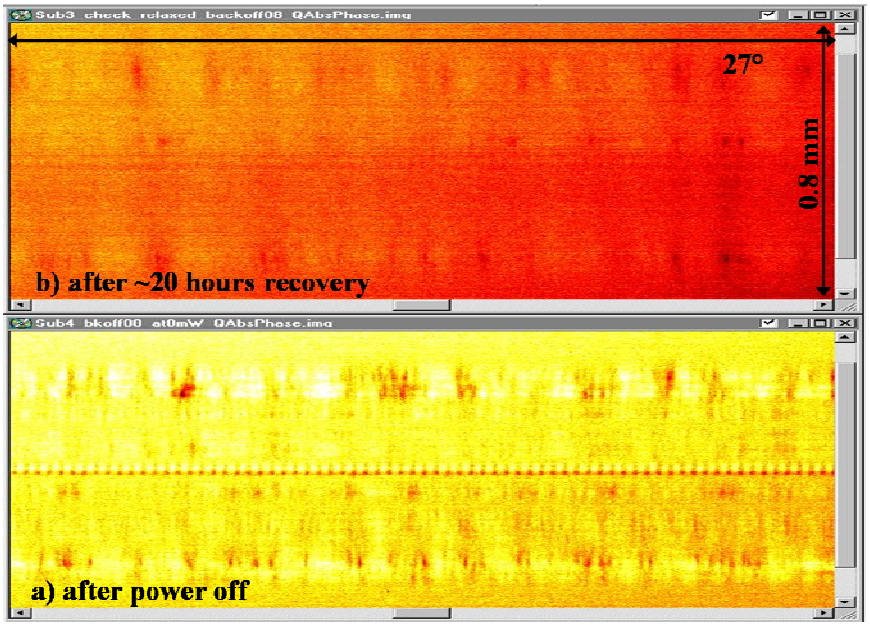

Figure 7-11. Lubricant thickness a) after 3 minutes of 0 mW back-off flight and b) after ~20 hours of recovery time.

This figure shows how the strong modulation at the center of the slider's path (corresponding to the 113 kHz peak from Section 7.4.3) has fully relaxed away after 20 hours of recovery. In addition, the side modulation has decreased noticeably in this time and is expected to fully recover with longer recovery time. Thus, even the extreme depletion/buildup track caused by flying at the TDP for minutes at a time has

not permanently damaged the ability of the lubricant to recover after the test. Different lubricant parameters (thickness, molecular weight, lubricant type, etc.) are expected to influence the recovery of the depletion/buildup track in a similar way to how they influence the non-TFC modulation and recovery.

7.5 Conclusion

As TFC slider designs represent a solution to the current and next generation of hard disk drives, understanding what happens during TFC actuation to touch-down is important for the industry. In Section 7.2 a touch-down test method was introduced and used to establish the general stability of TDP at specific slider/disk parameters. In Section 7.3 high-power TFC actuation was used to show that TFC actuation could dramatically affect the lubricant layer of a hard disk drive. The changes seen included sharp increase in the lubricant depletion, decrease in lubricant modulation, and decrease in lubricant modulation power.

In Section 7.4.1 finer TFC power control was used to show that flying at TDP caused sharp buildup/depletion bands in the lubricant, while back-off levels of 50, 30, 20, and 10 mW showed very little change in the mean lubricant thickness. In Section 7.4.2 non-zero back-off levels were seen to cause an increase in side pad lubricant modulation as compared to non-actuated flight. In contrast, flying at TDP reduced the side pad lubricant modulation. Section 7.4.3 examined the modulation frequencies of the lubricant, showing that back-off levels of 10 mW and above introduced negligible change in the lubricant frequency above 100 kHz and an increase in lubricant modulation below 100 kHz. Flying at TDP introduced a drop in modulation power

below 100 kHz but a very strong modulation peak appeared at 113 kHz. This 113 kHz peak was not apparent before the heater was actuated, nor did it appear in any of the non-zero back-off tests. This frequency peak likely corresponds to a pitch mode or a combined pitch plus roll mode, based on the frequency peaks seen in the side and center pads. Taken together, the results from Section 7.4.1 through 7.4.3 show that the critical back-off level at which sudden changes in the lubricant modulation and mean thickness occur is between 10 and zero mW.

Other TFC-related results were that the changes in the lubricant layer correspond very strongly with the width of the ABS geometry (Section 7.4.4). The strong buildup/depletion bands seen in the 0 mW back-off tests correspond very closely to the slider's TEC pad. Finally, Section 7.4.5 showed that even after minutes of flying at 0 mW back-off, the lubricant layer recovered almost completely after resting for approximately 20 hours. Thus, it was shown that precise control of the heater circuit allows flying at touch-down power for minutes at a time without permanent damage to the lubricant layer.

As discussed earlier, the 10 mW back-off setting corresponds to approximately one nm "cushion" between the heater protrusion and strong interaction with the disk. Industry targets for the future make reference to slider-disk spacings in the sub-nanometer level. Thus, industry targets may well be approaching the critical back-off level. Even better control of the heater circuit will be necessary to investigate these sub-nanometer back-offs. Improvements in the heater control circuit from a resolution of 5 mW to a resolution of 1 or 2 mW would make this possible. Additionally, more

sensitive AE sensors could improve the touch-down test by detecting more subtle slider-disk interactions in the sub-nanometer clearance regime.

8 Conclusion and Future Work

8.1 Summary

The computer hard drive has improved in storage capacity, access speed, durability, and cost since it was first introduced in 1956. The fundamental idea of a hard drive is based on the idea of storing information as magnetic "bits" in a rotating medium, or disk. The magnetic spacing between the read/write sensors and the bits is related to the storage capacity. One of the layers of the disk between the magnetic bits and the read/write sensors is the lubricant layer, so any disturbance of the lubricant can affect the magnetic spacing in the drive. This dissertation focuses on the behavior of the lubricant occurring in the slider-disk interface *while the slider is flying*.

The experimental apparatus used in these experiments is important in that the details of the apparatus determine the types of data that can be collected. The multi-instrument test stand was detailed in Chapter 2, showing the location of the measurement systems and reviewing their basic operation. The general experiment workflow was given along with the data processing workflow in Matlab. The standard "net change" analysis was detailed along with the more advanced "incremental change" analysis of the changes in the lubricant layer. These analysis methods are only possible with the disk spindle shared between the flying setup and OSA scanning setup. Some of the basic analytical tools of the lubricant modulation profile and lubricant modulation area were detailed. This experimental setup and test/analysis procedure was used throughout the remainder of this dissertation.

Some general experimental observations that apply to most experimental tests, regardless of the specific slider-lubricant interface, are given in Chapter 3. These general observations allow better appreciation of the influence of different slider-lubricant parameters on the results, as they provide a backdrop against which comparisons are made. The general observations include: the shape of the modulation profile and depletion profile remaining qualitatively the same and increasing in magnitude with increased flying time; the plot of modulation area versus time follows a logarithmic shape, with larger changes at early times and smaller changes at later times; and relaxation of the modulation profile occurring rapidly after removal of the slider. A zeroing and scaling method to analyze this modulation profile relaxation was given so that comparisons can be easily made between results of different initial modulation levels. It was shown that the unloading of a slider can significantly affect the lubricant modulation and depletion profiles. Local lubricant peaks were shown to grow in magnitude in a logarithmic trend with time, helping to explain the logarithmic trend of modulation area with time. Local repeatability of lubricant modulation was shown to be strongly affected by the exact slider radial positioning and weakly affected by disk substrate and carbon layer, with only some regions of repeated peaks or troughs upon repeated testing on the same track. However, the modulation area was shown to be repeatable, despite the shifting of the modulation profile according to slider radius. Having established some of the common experimental observations, the next chapters focused on how changes in the slider-lubricant interface affect such observations.

Studies of the effect of various interface parameters on the lubricant modulation area were undertaken in Chapter 4. Using 45 minute flyability experiments on identically lubricated disks, it was shown that modulation area was larger for pico sized sliders as compared to femto sized sliders. The higher modulation area was attributed to the larger size of the pico sliders. Lubricant thickness studies using the same slider showed that thicker lubricant increases the modulation area. Similar studies of lubricant molecular weight showed that higher molecular weight increased modulation area. Finally, additive studies showed that the modulation area was increased for Zdol + A20H as compared to Zdol + X1P. Studies of the modulation frequencies during this series of tests showed strong modulation at frequencies under 100 kHz with only the 10,000 g/mol molecular weight result showing strong modulation at 50 and 265 kHz.

In the previous chapters, the slider-induced lubricant modulation was studied. After the slider was removed, the lubricant modulation was observed to relax away towards the original undisturbed state. Chapter 5 studied this lubricant relaxation. A series of experiments showed that while the relaxation of modulation area can vary between tests, a logical zeroing and scaling method can be used to show that the relaxation results tend to follow a similar trend. This trend shows strong lubricant relaxation during the first few minutes after slider unloading. Thus, any experiments that intend to study the slider-induced lubricant modulation should take care to standardize the delay between the end of the experiment and the measurement of the lubricant by OSA. An in-situ OSA system eliminates this problem. An average trend of lubricant relaxation was used to predict the relaxation of another experiment, with

accuracy around 20% of the measured value. Studies of the effect of lubricant properties on the modulation relaxation showed that changing the lubricant type from Zdol + X1P to Ztetraol strongly affected the pre-logarithmic parameter of a two-parameter logarithmic fit equation. A study of the effect of lubricant molecular weight on modulation relaxation showed that higher molecular weight lubricant relaxes slower than lower molecular weight lubricant. The effect of modulation frequency was studied, showing that higher modulation frequencies relax faster than lower modulation frequencies. Fitting a one-parameter exponential curve to the data showed reasonable explanatory ability and satisfied logical constraints on the trend based on the zeroing and scaling method used. The usefulness of the frequency-based relaxation results in predicting lubricant modulation relaxation was demonstrated.

Chapter 5 continued by exploring finite-difference simulations of the lubricant relaxation based on a simple 2D diffusion equation. A central difference method based on the lubricant modulation after slider unloading was implemented in a simple Matlab code. Simulation results closely matched experimental results in modulation profile and modulation area. Simulations with different diffusion coefficients were conducted and the coefficient that best matched the experimental results fell within the previously reported experimental diffusion constants for two different lubricants. Thus, using numerical simulations to find the diffusion constant of a lubricant based on the experimental relaxation of slider-induced lubricant modulation was demonstrated. This method is preferable to the traditional Matano interface method in that it can easily be incorporated into standard flyability tests and more closely approximates the kind of modulation seen in hard disk drives.

During investigations into the behavior of thermal fly-height control sliders (detailed later in Chapter 7), a new slider-lubricant interaction was discovered. This interaction involves a lubricant droplet forming on the slider and transferring to the disk, where it is encountered as an obstacle to the slider's flight. Evidence of the interaction was presented, including intermittent spikes of around 700 microseconds in length occurring in both AE and LDV sensors occurring randomly throughout a twenty minute flyability test. Each spike consists of "sub-spikes" occurring at or near the disk rotation rate that rise and fall in magnitude. In time intervals that include an AE/LDV spike, a sudden increase in lubricant thickness is seen in the OSA scan of the disk. This sudden increase in lubricant thickness is on the order of one or two nanometers and is attributed to a lubricant droplet falling to the disk. However, because of the time required to scan the disk with the OSA, the actual droplet height could be much higher than a few nanometers. Some experimental results show AE/LDV disturbance of a few minutes in length. OSA scans during this interval show lubricant droplets with height in the tens of nanometers range. The time in which the AE/LDV disturbance is detected correspond exactly to the time in which the measured lubricant droplet height is larger than the slider's minimum fly-height. Repeatability of these droplets is shown in occurrence (no AE/LDV spikes without OSA droplets) and radial location (near the slider centerline), but circumferential location is seemingly random (repeatability is `weak at best). The physical explanation involves lubricant transferring to the slider during normal flight. The lubricant on the slider migrates to the trailing edge due to shear forces. Once at the trailing edge, the lubricant could easily surpass the dewetting thickness and form an unstable droplet

that transfers to the disk. Simulations of the slider's response to a lubricant droplet show that the fly-height disturbance is strongest when the lubricant droplet height is larger than the slider's minimum fly-height. When the droplet height is less than the minimum fly-height, the disturbance is an order of magnitude smaller. Further simulations show that a droplet occurring near the center of the slider disturbs the flight an order of magnitude more than when a droplet occurs between rails or at the side rails. Given the industry targets of sub-nanometer physical clearance between slider and disk, any lubricant droplets of the kind described here will present severe challenges to the interface.

One of the newest technologies to allow higher capacity hard drives is thermal fly-height control (TFC), where a small resistive heating element is incorporated into the design of the slider. This technology is studied in an effort to understand how TFC actuation affects the lubricant layer, with specific focus of studying how closely the thermal protrusion can approach the disk without significant change in the lubricant layer. To begin, the repeatability of the touch-down power (TDP) was established. Then, high-power TFC actuation (around 400 mW) was used to show that the TFC circuit was capable of significantly changing the lubricant depletion and modulation profiles. More precise studies were undertaken using 5 mW steps of power. These studies showed that flying at TDP can cause a "snowplow" effect by introducing a depletion and buildup band near the slider centerline. Flying 10 mW less than TDP (on the order of 1 nm back-off) is sufficient to eliminate this snowplow effect. Similarly, 10 mW back-off was sufficient to eliminate the strong changes in lubricant modulation profile that occur when flying at TDP. In these two ways, back-offs of 10

mW through 50 mW were very similar in slider-lubricant interaction. The interface at these back-offs was shown to be significantly different from the interface at TDP (0 mW back-off). Thus, strong changes in slider-lubricant interaction were shown to occur somewhere between TDP and 10 mW back-off for this slider design. The changes in lubricant attributed to TFC actuation were shown to be strongest near the slider centerline, where the thermal expansion is greatest. Finally, even after minutes of flying at TDP, the lubricant layer was shown to recover well after tens of hours of recovery time. Thus, TFC slider designs can be used to approach the disk closely without strong lubricant interactions.

8.2 Future Work

The experimental methods and analysis techniques in this dissertation can be easily extended to evaluate the performance of any new lubricant type or slider design. Extending the time of the flyability portion of the tests could be used to evaluate long-term (hours or days) durability and performance of lubricants. Many of the experimental results presented here are only possible to measure using an in-situ OSA system. While the system described here is very useful, improvements could be imagined. The modulation and recovery of lubricants during ramp loading/unloading could be studied by modifying the existing experimental apparatus with a rotary actuator and installing the necessary ramp system. Improvements in the scanning speed of the OSA system could be implemented to help understand the lubricant droplet and other high-speed phenomena. Finally, a more detailed study of different lubricants in the realm of TFC back-off studies could be undertaken to further explore

this new type of slider-lubricant interface. Clearly, there are many outstanding issues and further clarifications that could be pursued in the future, using this work as a stepping stone.

References

Chapter 1

[1] Hitachi Global Storage Technology's Technology Timeline. Retrieved 3/2009. http://www.hitachigst.com/media/timeline/hitachi_main_final01.html

[2] B. Tomcik, T. Osipowicz, J.Y. Lee, "Diamond-like film as a corrosion protective layer on the hard disk", Thin Solid Films, vol 360, issues 1-2, p. 173-180, February 2000.

[3] J. Choi, T. Kato, "Development of the Mixed Nanolubricant System by FDTS Islands and PFPE Mobile Phase", IEEE Trans Mag., vol 39, no 5, p. 2444-2446, September 2003.

[4] A. Khurshudov, R. J. Waltman, "Tribology challenges of modern magnetic hard disk drives" Wear, vol. 251, p.1124-1132, 2001.

[5] J. Gui, "Tribology Challenges for Head-Disk Interface Toward 1 Tb/in^2", IEEE Trans Mag, vol. 39, no. 2, p. 716-721, March 2003.

[6] C. M. Mate, Q. Dai, R. N. Payne, B. E. Knigge, P. Baumgart, "Will the Numbers Add Up for Sub-7-nm Magnetic Spacings? Future Metrology Issues for Disk Drive Lubricants, Overcoats, and Topographies", IEEE Trans Mag, Vol. 41, no. 2, p. 626-631, February 2005.

[7] X.-C. Guo, B. Knigge, B. Marchon, R. J. Waltman, M. Carter, J. Burns, "Multidentate functionalized lubricant for ultralow head/disk spacing in a disk drive", Journal of Applied Physics, Vol. 1000, 044306, 2006.

[8] P.H. Kasai, V. Raman, “Z-dol versus Z-tetraol: Bonding and durability in magnetic hard disk application”, Tribology Letters, vol. 16, nos. 1-2, p. 29-36, February 2004.

[9] J. Ruhe, G. Blackman, V. J. Novotny, T. Clarke, G. B. Street, S. Kuan, “Terminal Attachment of Perfluorinated Polymers to Solid Surfaces”, Journal of Applied Polymer Science, Vol. 53, p. 825-836, 1994.

[10] N. Tagawa, A. Mori, K. Senoue, “Effects of Molecularly Thin Liquid Lubricant Films on Slider Hysteresis Behavior in Hard Disk Drives”, Journal of Tribology, vol. 129, p. 579-585, July 2007.

[11] N. Tagawa, N. Yoshioka, A. Mori, “Interactions between nano-spacing flying head sliders and ultra-thin liquid lubricant films with non-uniform distribution in hard disk drives”, Microsyst Technol, Vol. 11, p. 867-874, 2005.

[12] A. Khurshudov, P. Baumgart, R. J. Waltman, “In situ quantitative analysis of nano-scale lubricant migration at the slider-disk interface”, Wear, Vol. 225, p. 690-699, 1999.

Chapter 2

[1] S. W. Meeks and H. P. Nguyen, Multiple Spot Size Optical Profilometer, Ellipsometer, Reflectometer and Scatterometer. US Patent 6,930,765 B2. August 16, 2005.

[2] S. W. Meeks, “A Combined Ellipsometer, Reflectometer, Scatterometer and Kerr Effect Microscope for Thin Film Disk Characterization”. Machine Vision

Applications in Industrial Inspection VIII, Proceedings of SPIE, Vol. 3966, 2000.

[3] "Vibrometry Basics" http://www.polytec.com/int/158_942.asp. Accessed January 30, 2009.

[4] A. Khurshudov and P. Ivett, "Head-disk contact detection in the hard-disk drives", Wear vol.255, pt.2, pp. 1314-1322, Aug.-Sept. 2003.

[5] P.H. Kasai and C. Spiese, "Interaction between disk lubricants and solvents in the dip-coating process", Tribology Letters, Vol. 17, no. 4, Nov. 2004.

Chapter 3

[1] R. Pit, B. Marchon, S. Meeks, V. Velidandla, "Formation of lubricant "moguls" at the head/disk interface", Tribology Letters vol. 10, no. 3, pp. 133-142, 2001.

Chapter 4

[1] B. Marchon, Q. Dai, V. Nayak, R. Pit, "The Physics of Disk Lubricant in the Continuum Picture", IEEE Trans. Magn., vol. 41, no. 2, pp. 616-620, 2005.

[2] Q. Dai, C. Saint-Olive, R. Pit, B. Marchon, "Genesis and Evolution of Lubricant Moguls", IEEE Trans. Magn., vol. 38, no. 5, pp. 2111-2113, 2002.

[3] C. M. Mate, P. H. Kasai, G. W. Tyndall, "Investigation of Phosphazene Additive for Magnetic Recording Lubrication", IEEE Trans. Magn., vol. 34, no. 4, pp.1744-1746, 1998.

[4] R. J. Waltman, N. Kobayashi, K. Shirai, A. Khurshudov, H. Deng, “The tribological properties of a new cyclotriphosphazene-terminated perfluoropolyether lubricant”, Tribology Letters, vol. 16, no. 1-2, pp. 151-162, 2004.

[5] R. Ambekar, Dynamic Stability and Slider-Lubricant Interactions in Hard-Disk Drives, Ph. D. Dissertation, University of California Berkeley, 2007.

Chapter 5

[1] X. Ma, H. Tang, M. Stirniman, J. Gui, “Lubricant Thickness Modulation Induced by Head-Disk Dynamic Interactions”, IEEE Trans Mag, vol 38, no. 1, p. 112-117, January 2002.

[2] T. Watanabe and D. Bogy, “A Study of the Air Bearing Effect on the Lubricant Displacement Using an Optical Surface Analyzer”, IEEE Trans Mag, vol. 38, no. 5, p. 2138-2140, September 2002.

[3] J. Choi, M. Kawaguchi, T. Kato, “Spreading of Perfluoropolyethers on FDTS-Coated Amorphous Carbon Surfaces”, IEEE Trans Mag, Vol. 40, No. 4, p. 3189-3191, July 2004.

[4] M. C. Kim, D. M. Phillips, X. Ma. M. S. Jhon, “The Molecular Spreading of Nonpolar Perflroropolyether Films on Amorphous Carbon Surfaces”, Journal of Colloid and Interface Science, Vol. 228, p. 405-409, 2000.

[5] X. Ma, J. Gui, L. Smoliar, K. Grannen, B. Marchon, M. S. Jhon, C. L. Bauer, ”Spreading of perfluoropolyalkylether films on amorphous carbon surfaces”, Journal of Chemical Physics, vol. 110, no. 6, p. 3129-3137, February 1999.

[6] Z. Zhao, E. R. Karazic, Q. Zhao, M. J. Embree, P. H. Trinh, T. Lam, "Lubricant bonding, chemical structure, and additive effects on tribological performances at head-disk interfaces", Microsystem Technologies, Vol. 9, p. 48-54, 2002.

[7] Q. Dai, F. Hendriks, B. Marchon, "Washboard Effect at Head-Disk Interface", IEEE Trans Mag, Vol. 40, no. 4, p. 3159-3161, July 2004.

[8] V. J. Novotny, "Migration of liquid polymers on solid surfaces", Journal of Chemical Physics, vol. 92, no. 5, p. 3189-3196, March 1990.

[9] Z. F. Li, C. Y. Chen, J. J. Liu, S. A. Pirzada, "Media tribology design to improve flyability at low flying height", Journal of Applied Physics, Vol. 93, no. 10, p. 8713-8715, May 2003.

[10] X.-C. Guo, B. Knigge, B. Marchon, R. J. Waltman, M. Carter, J. Burns, "Multidentate functionalized lubricant for ultralow head/disk spacing in a disk drive", Journal of Applied Physics, Vol. 100, issue 4, p. 044306, 2006.

[11] D. Shirakawa, K. Sonoda, K. Ohnishi, "A Study on Design and Synthesis of a New Lubricant for Near Contact Recording", IEEE Trans Mag, Vol. 43, no. 6, p. 2253-2255, June 2007.

Chapter 6

[1] R. Pit, B. Marchon, S. Meeks, V. Velidandla, "Formation of lubricant "moguls" at the head/disk interface", Tribology Letters vol. 10, no. 3, pp. 133-142, 2001.

[2] X. Ma, H. Tang, M. Stirniman, J. Gui, “Lubricant Thickness Modulation Induced by Head-Disk Dynamic Interactions”, IEEE Trans. Magn., vol. 38, no. 1, pp. 112-117, 2002.

[3] B. Marchon, Q. Dai, V. Nayak, R. Pit, “The Physics of Disk Lubricant in the Continuum Picture”, IEEE Trans. Magn., vol. 41, no. 2, pp. 616-620, 2005.

[4] R. Pit, Q. H. Zeng, Q. Dai, B. Marchon, “Experimental Study of Lubricant-Slider Interactions”, IEEE Trans. Magn., vol. 39, no. 2, pp. 740-742, 2003.

[5] R. Ambekar, D. B. Bogy, Q. Dai, B. Marchon, “Critical clearance and lubricant instability at the head-disk interface of a disk drive”, Applied Physics Letters, vol. 92, no. 3, pp. 033104-1-3, 2008.

[6] H. Kubotera and D. B. Bogy, “Effect of various physical factors on thin lubricant film migration on the flying head slider at the head-disk interface of hard disk drives”, Journal of Applied Physics, vol. 102, pp. 054309-1-6, 2007.

[7] X.-C. Guo, D.J. Pocker, V. Raman, A. Spool, Q. Dai, N. Bach, “Experimental Inquiries into the Lubricant Pickup in Hard Disk Drives”, ASME ISPS Conference, Santa Clara, CA, June 2008.

[8] Z. Zhao, E. R. Karazic, Q. Zhao, M. J. Embree, P. H. Trinh, T. Lam, ”Lubricant bonding, chemical structure, and additive effects on tribological performances at head-disk interfaces”, Microsystem Technologies, vol. 9, p. 48-54, 2002.

[9] Y. S. Ma and B. Liu, “Lubricant transfer from disk to slider in hard disk drives”, Applied Physics Letters, Vol. 90, issue 14, p. 143516, 2007.

[10] C. M. Mate, “Molecular tribology of disk drives”, Tribology Letters, Vol. 4, issue 2, p. 119-123, 1998.

[11] C. M. Mate, “Visualization of Mechanisms for Lubricant Transfer between Disk and Slider Surfaces”, ASME ISPS Conference, Santa Clara, CA, June 16-17, 2008.

[12] B. Marchon, T. Karis, Q. Dai, R. Pit, “A Model for Lubricant Flow From Disk to Slider”, IEEE Trans Mag, Vol. 39, no. 5, p. 2447-2449, September 2003.

[13] M. J. Smallen and H. W. Huang, “Effect of Disjoining Pressure on Disk-to-Head Lubricant Transfer”, IEEE Trans Mag, Vol. 39, no. 5, p. 2495-2497, September 2003.

[14] R. J. Waltman, D. J. Pocker, G. W. Tyndall, “Studies on the interactions between ZDOL perfluoropolyether lubricant and the carbon overcoat of rigid magnetic media”, Tribology Letters, Vol. 4, issue /4, p. 267-275, 1998.

[15] Z. F. Li, C. Y. Chen, J. J. Liu, S. A. Pirzada, “Media tribology design to improve flyability at low flying height”, Journal of Applied Physics, Vol. 93, no. 10, p. 8713-8715, May 2003.

[16] R. P. Ambekar and D. B. Bogy, “Effect of Slider Lubricant Pickup on Stability at the Head-Disk Iinterface”, IEEE Trans Mag, Vol. 41, no. 10, p. 3028-3030, October 2005.

[17] R. J. Waltman, A. Khurshudov, G. W. Tyndall, “Autophobic dewetting of perfluoropolyether films on amorphous-nitrogenated carbon surfaces”, Tribology Letters, vol. 12, no. 3, p. 163-169, April 2002.

Chapter 7

[1] D.W. Meyer, P.E. Kupinski, J.C. Liu, “Slider with temperature responsive transducer positioning”, U.S. Patent 5,991,113, Nov. 23, 1999.

[2] M. Suk, K. Miyake, M. Kurita, H. Tanaka, S. Saegusa, N. Robertson, “Verification of thermally induced nanometer actuation of magnetic recording transducer to overcome mechanical and magnetic spacing challenges”, IEEE Trans. Magn., vol. 41, no. 11, pp. 4350-4352, November 2005.

[3] J.Y. Juang, D. Chen, D.B. Bogy, “Alternate air bearing slider designs for areal density of 1 Tb/in^2”, IEEE Trans. Magn., vol. 42, no. 2, pp. 241-246, February 2006.

[4] K. Miyake, T. Shiramatsu, M. Kurita, H. Tanaka, M. Suk, S. Saegusa, “Optimized design of heaters for flying height adjustment to preserve performance and reliability”, IEEE Trans. Magn., vol. 43, no. 6, pp. 2235-2237, June 2007.

[5] B. Liu, S.K. Yu, W.D. Zhou, C.H. Wong, W. Hua, “Low flying-height slider with high thermal actuation efficiency and small flying-height modulation caused by disk waviness”, IEEE Trans Mag, vol. 44, no. 1, pp. 145-150, January 2008.

[6] T. Shiramatsu, T. Atsumi, M. Kurita, Y. Shimizu, H. Tanaka, “Dynamically controlled thermal flying-height control slider”, IEEE Trans Mag, vol. 44, no. 22, pp. 3695-3697, November 2008.

[7] B. Marchon, Q. Dai, B. Knigge, R. Pit, “Lubricant dynamics in the sub-nanometer clearance regime”, IEEE Trans Mag, vol. 43, no. 9, p. 3694-3698, September 2008.

[8] R.P. Ambekar, D.B. Bogy, Q. Dai, B. Marchon, “Critical clearance and lubricant instability at the head-disk interface of a disk drive”, Applied Physics Letters 92, 033104 (2008), DOI:10.1063/1.2837187

[9] Y. Tang, S.Y. Hong, N.Y. Kim, X. Che, “Overview of fly height control applications in perpendicular magnetic recording”, IEEE Trans. Magn., vol. 43, no. 2, pp. 709-714, February 2007.

[10] A. Khurshudov and P. Ivett, “Head-disk contact detection in the hard-disk drives”, Wear vol.255, pt.2, pp. 1314-1322, Aug.-Sept. 2003.

[11] B. Knigge, T. Suthar, P. Baumgart, “Friction, heat, and slider dynamics during thermal protrusion touchdown”, IEEE Trans. Magn., vol. 42, no. 10, pp. 2510-2512, October 2006.

[12] W.K. Banks, K.K. Chew, D.R. Gillis, G.J. Smith, “System and method for monitoring friction between head and disk to predict head disk interaction failure in direct access storage devices”, U.S. Patent 5,539,592, Jul. 23, 1996.

Appendix A

```
% OSA_analysis_convert_filter
% Written by Sean Moseley, last updated 2/27/2009
%
% This script processes the text data from an OSA scan by converting the
% lubricant height from [% reflectivity] into [nm].  The matrix of heights
% is called 'height' where (row,column) == (radius,angle).  It high-pass
% filters the data at a specified cutoff frequency into the matrix
% 'variation' (again, rows = radii, columns = angles). If
% desired, the Matlab workspace is saved in the current directory for
% further analysis.

clear angle height radius variation variationFFT myhighfilter power freqs
variation_mean variation_meanFFT power_mean

%%%%%%%%%%%%%%
%%% Input Parameters %%%
%%%%%%%%%%%%%%
filename = 'sld27_04_unload.txt;     % filename of the OSA text file you want to
                                      process
rpm = 7200;                          % rotational speed DURING THE
                                      EXPERIMENT [rev/min]
target_cutoff = 10000;               % cutoff for high-pass filter [Hz], set to '0' if no
                                      filtering is needed
convert = -0.067;                    %reflectivity/nm], this conversion is based on
                                      the OSA parameters
dosaveworkspace = 1;                 % set to '1' to save the processed workspace

%%%%%%%%%%%%%%%%%%%%%%%%%%%%%%%%%%%%
%%% Extract the angle vector from the first line of the text file %%%
%%%%%%%%%%%%%%%%%%%%%%%%%%%%%%%%%%%%
fprintf(['\nProcessing OSA data from the file ' filename '\n'])
fid = fopen(filename);               % open the file in memory for extraction
fprintf('   Extracting angle vector...')
line1 = fgetl(fid);                  % read first line
whereiscircle = find(line1 == '°');  % find degree symbols '°'
anglelength = length(whereiscircle); % define number of angular datapoints
line1(whereiscircle) = ' ';          % replace '°' with whitespace
angle = str2num(line1(14:end));      % define angle [deg] by converting from strings
                                      to numbers
fprintf('done. \n')
clear line1 whereiscircle;           % no longer needed
```

```
%%%%%%%%%%%%%%%%%%%%%%%%%%%
%%% Extract the height matrix, line-by-line %%%
%%%%%%%%%%%%%%%%%%%%%%%%%%%
refl = zeros(1000,anglelength);          % pre-allocate reflectivity matrix, will trim
                                         afterwords
i = 1;                                   % counter
fprintf('   Currently working on line 0\n')
nextline = fgetl(fid);                   % get second line of file
while length(nextline) ~= 1
   if rem(i,100)==0
      fprintf(['   Currently working on line ' num2str(i) '\n']);
                                         % display current line so you know Matlab
                                         hasn't frozen
      pause(.1)
   end
   radius(i) = str2num(nextline(1:8));             % radius is first 8 characters
   refl(i,:) = str2num(nextline(12:end));          % refl is the remainder of the line
   nextline = fgetl(fid);                          % get next line of file
   i = i+1;                                        % increment counter
end
refl = refl(1:i-1,:);                              % remove any extra rows if they
                                                   exist from the pre-allocation
                                                   above
height = refl./convert;                            % convert refl [%] into height
                                                   [nm]
fclose(fid);                                       % close the file, we're done with it
clear nextline refl;                               % no longer needed

%%%%%%%%%%%%%%%%%%%%%%%%%%%%%%%%%%%%%%%%%%%%%
%%% High-Pass filter the 'height' matrix to get the 'variation' matrix%%%
%%%%%%%%%%%%%%%%%%%%%%%%%%%%%%%%%%%%%%%%%%%%%
sampfreq = length(angle) * rpm/60;                 % sampling frequency based on
                                                   length of angle vector [Hz]
nyquistfreq = sampfreq/2;                          % Nyquist frequency [Hz]
filtfactor = target_cutoff/nyquistfreq;            % factor to use in filter function
                                                    togive desired cutoff freq
filtorder = floor((anglelength-2)/6)*2;             % order of high-pass filter
i = 1;
while 2^i < filtorder
   i = i + 1;
end
filtorder = 2^(i-1);                               % make the filter order a power
                                                   of 2
if filtfactor == 0                                 % i.e. don't filter, just subtract
                                                   the mean
```

```
   variation = height - mean(mean(height));
else                                                         % i.e. filter using given cutoff
   fprintf(['   High-pass filtering a ' num2str(size(height,1)) ' by '
num2str(size(height,2)) ' matrix (don''t hold your breath)...'])
   myhighfilter = fir1(filtorder,filtfactor,'high');        % define the high-pass filter
   variation = filtfilt(myhighfilter,1,height')';           % filter 'height' into 'variation'
                                                             using filtfilt function
   fprintf('done. \n')
end
sig3 = 3*std(variation')';                                    % create the 'sig3' vector with
3*sigma of each radius [nm]
sig3_raw = 3*std(height')';                                   % 3sigma of raw data [nm]

%%%%%%%%%%%%%%%%%%%%%%%%%%%%%%%%%%%%%%%
%%% Calculate the frequencies of the 'variation' matrix --> 'power' matrix %%
%%%%%%%%%%%%%%%%%%%%%%%%%%%%%%%%%%%%%%%
fprintf('   Finding power...')
variationFFT = fft(variation')';                             % perform the FFT on the
                                                             'variation' matrix
power = variationFFT.*conj(variationFFT);                    % calculate the 'power' matrix
power = power(:,1:floor(length(power)/2)+1);
freqs = ((nyquistfreq)*(0:length(angle)/2)) ./ (length(angle)/2);
                                                             % calculate the corresponding
                                                             frequencies of the FFT [Hz]
freqs = freqs(1:end)./1000;                                  % convert frequencies into [kHz]
fprintf('done. \n')


%%%%%%%%%%%%%%%%%%%%%
%%% Save the workspace if desired %%%
%%%%%%%%%%%%%%%%%%%%%
if dosaveworkspace == 1
   workspacename = ['workspace_' filename(1:end-4) '_' num2str(target_cutoff/1000)
'kHz'];
   fprintf(['   Saving workspace as ' workspacename '.mat ...'])
   eval(['save ' workspacename])
   fprintf('done. \n')
end
fprintf('OSA data processing complete.\n')
```

Appendix B

```
% Finite Difference Code to simulate lubricant relaxation
% by Sean Moseley

clear all
load workspace_relax10_unload_initialcondition.mat
D = 1.0e-12                 % simulated diffusion constant [m^2/sec]
fprintf(['Beginning simulation at  [Yr Mo Dy Hr Mn S] = ' num2str(fix(clock)) '\n'])

%%% band-pass filter the data %%%
%%% first pass is at constant radius, second pass is at constant angle %%%
[variation,power] = dobandpass(variation,10000,100000,angle,rpm);   % 10-100kHz
[variation,power] = dobandpassradial(variation,0,0.1,radius);       % below 40um

h_0  = variation(:,1:500).*1e-9;            % only take the first 500 data points to
                                            speed up simulation
h_0 = h_0 - mean(mean(h_0));
keep radius h_0 rpm angle D
delx = (radius(1)-radius(2))*1e-6;          % radial step [m]
dely = (mean(radius)*1e-6*2*pi)/8192;       % average angular step is based on 8192
                                            angular data points [m]
delt = 0.01;                                % timestep [sec]

%%% Take 'n' time steps
tic
n = 6000*52;                                % n = 6000 = 1 minute of simulated
                                            relaxation
h_last = getnext(h_0,delx,dely,D,delt);
profiles(1,:) = 3.*std(h_last');
nyquistfreq = rpm/60*8192/2;
[temp freqs] = findpower(h_0,nyquistfreq);
powers(1,:) = max(temp);
protime(1) = 0;
proi = 2;
for i = 2:n
   h_next = getnext(h_last,delx,dely,D,delt);
   h_last = h_next;
   if rem(i,6000) == 0                      % capture modulation profile at each
                                            minute of simulation
      profiles(proi,:) = 3.*std(h_next');
      [temp freq] = findpower(h_next,nyquistfreq);
      powers(proi,:) = max(temp);
      protime(proi) = i*delt;
```

```
      fprintf(['Simulation time is now ' num2str(protime(proi)/60) ' min\n'])
      proi = proi + 1;
   end
   if i/6000 == 1 | i/6000 == 3 | i/6000 == 5 | i/6000 == 10 | i/6000 == 20 | i/6000 ==
31 | i/6000 == 41 | i/6000 == 52 | i/6000 == 62
      eval(['h_' num2str(i/6000) 'min = h_last;'])
   end
end
h_end = h_last;
clear h_next h_last;

%%% Plot modulation profiles
figure;resizefig;hold on;box on;
title('Modulation Profile at Start and End')
plot(radius./1000,profiles);
xlabel('Radial Index');ylabel('3*stdev [nm]')
fprintf(['Avg time/step = ' num2str(toc/n) ' sec'])
save workspace_0415a
```

```
function [filteredmatrix,power] = dobandpass(matrix,cutoffA,cutoffB,angle,rpm)
%%% [filteredmatrix,power] = dobandpass(matrix,cutoffA,cutoffB,angle,rpm)
%%% Filter the variation matrices into small frequency windows %%%

anglelength = length(angle);
sampfreq = (360/(angle(2)-angle(1))) * rpm/60;      % sampling frequency based on
                                                    the first two entries of 'angle'
                                                    [Hz]
nyquistfreq = sampfreq/2;                           % Nyquist frequency [Hz]
filtfactorA = cutoffA/nyquistfreq;                  % factor to use in filter function
                                                    to give desired cutoff freq
filtfactorB = cutoffB/nyquistfreq;                  % factor to use in filter function to
                                                    give desired cutoff freq
filtorder = floor((anglelength-2)/6)*2;             % order of high-pass filter to get
                                                    variation
i = 1;
while 2^i < filtorder
   i = i + 1;
end
filtorder = 2^(i-1);
fprintf(['   High-pass filtering a ' num2str(size(matrix,1)) ' by ' num2str(size(matrix,2))
' matrix (don''t hold your breath)...'])
myfilter = fir1(filtorder,[filtfactorA filtfactorB],'bandpass');        % define the high-
                                                                        pass filter
filteredmatrix = filtfilt(myfilter,1,matrix')';     % filter 'height' into 'variation'
                                                    using filtfilt function
fprintf('done. \n')

%%% Do the FFT %%%
fprintf('   Finding power...')
variationFFT = fft(filteredmatrix')';               % perform the FFT on the
                                                    variation' matrix
power = variationFFT.*conj(variationFFT);           % calculate the 'power' matrix
power = power(:,1:floor(length(power)/2)+1);
fprintf('done. \n')
```

```
function [filteredmatrix,power] =
dobandpassradial(matrix,filtfactorA,filtfactorB,radius)
%%% [filteredmatrix,power] =
dobandpassradial(matrix,filtfactorA,filtfactorB,radius)
%%% Filter the matrix in the radial (colum) direction at the specified
%%% filter factors.  Use filtfactorA = 0 to have a low-pass, else it's
%%% band-pass between filtfactorA and filtfactorB.

radiuslength = length(radius);
filtorder = floor((radiuslength-2)/6)*2;          % order of high-pass filter to get
                                                   variation
i = 1;
while 2^i < filtorder
   i = i + 1;
end
filtorder = 2^(i-1);
if filtfactorA == 0
   fprintf(['   Low-pass filtering a ' num2str(size(matrix,1)) ' by '
num2str(size(matrix,2)) ' matrix (don''t hold your breath)...'])
   myfilter = fir1(filtorder,filtfactorB,'low');          % define the high-pass filter
else % it's band-pass
   fprintf(['   Band-pass filtering a ' num2str(size(matrix,1)) ' by '
num2str(size(matrix,2)) ' matrix (don''t hold your breath)...'])
   myfilter = fir1(filtorder,[filtfactorA filtfactorB],'bandpass');      % define the high-
                                                                          pass filter
end
filteredmatrix = filtfilt(myfilter,1,matrix);          % filter 'height' into 'variation'
                                                       using filtfilt function
fprintf('done. \n')

%%% Do the FFT %%%
fprintf('   Finding power...')
variationFFT = fft(filteredmatrix')';                  % perform the FFT on the
                                                       'variation' matrix
power = variationFFT.*conj(variationFFT);              % calculate the 'power' matrix
power = power(:,1:floor(length(power)/2)+1);
fprintf('done. \n')
```

```
function [h_next] = getnext(h,delx,dely,D,delt);
% Does the numerical diffusion based on central-difference method

% periodic boundary condition
bufferh = zeros(size(h)+2);
bufferh(2:end-1,2:end-1) = h;
bufferh(1,2:end-1) = h(end,:);
bufferh(end,2:end-1) = h(1,:);
bufferh(2:end-1,1) = h(:,end);
bufferh(2:end-1,end) = h(:,1);

%%% equation is dh/dt = D*d^2h/dx^2 + D*d^2h/dy^2
hppx = zeros(size(h));
hppy = zeros(size(h));
for i = 2:size(bufferh,1)-1
   for j = 2:size(bufferh,2)-1
      hppx(i-1,j-1) = (bufferh(i+1,j)-2*bufferh(i,j)+bufferh(i-1,j))/delx^2;
      hppy(i-1,j-1) = (bufferh(i,j+1)-2*bufferh(i,j)+bufferh(i,j-1))/dely^2;
   end
end

%%% update matrix %%%
h_next = h + (D*hppx + D*hppy).*delt;
```